(12) PATENT
(19) AUSTRALIAN PATENT OFFICE

(11) Application No. AU 199876927 B2
(10) Patent No. 754083

(54) Title
Analogs of duocarmycin and CC-1065

(51)[6] International Patent Classification(s)
C07D 223/32 C07D 487/04

(21) Application No: 199876927 (22) Application Date: 1998.05.22

(87) WIPO No: WO98/52925

(30) Priority Data

(31) Number	(32) Date	(33) Country
60/048505	1997.05.22	US

(43) Publication Date : 1998.12.11
(43) Publication Journal Date : 1999.02.04
(44) Accepted Journal Date : 2002.11.07

(71) Applicant(s)
The Scripps Research Institute

(72) Inventor(s)
Dale L Boger

(74) Agent/Attorney
DAVIES COLLISON CAVE,1 Little Collins Street,MELBOURNE VIC 3000

CT)

(51) International Patent Classification 6 :
C07D 223/32, 487/04

A1

(11) International Publication Number: WO 98/52925

(43) International Publication Date: 26 November 1998 (26.11.98)

(21) International Application Number: PCT/US98/10535

(22) International Filing Date: 22 May 1998 (22.05.98)

(30) Priority Data:
60/048,505 22 May 1997 (22.05.97) US

(63) Related by Continuation (CON) or Continuation-in-Part (CIP) to Earlier Application
US 60/048,505 (CIP)
Filed on 22 May 1997 (22.05.97)

(71) Applicant *(for all designated States except US)*: THE SCRIPPS RESEARCH INSTITUTE [US/US]; 10550 North Torrey Pines Road, La Jolla, CA 92037 (US).

(72) Inventor; and
(75) Inventor/Applicant *(for US only)*: BOGER, Dale, L. [US/US]; 2819 Via Posada, La Jolla, CA 92037 (US).

(74) Agents: NORTHRUP, Thomas, E. et al.; The Scripps Research Institute, 10550 North Torrey Pines Road, TPC-8, La Jolla, CA 92037 (US).

(81) Designated States: AL, AM, AT, AU, AZ, BA, BB, BG, BR, BY, CA, CH, CN, CU, CZ, DE, DK, EE, ES, FI, GB, GE, GH, GM, GW, HU, ID, IL, IS, JP, KE, KG, KP, KR, KZ, LC, LK, LR, LS, LT, LU, LV, MD, MG, MK, MN, MW, MX, NO, NZ, PL, PT, RO, RU, SD, SE, SG, SI, SK, SL, TJ, TM, TR, TT, UA, UG, US, UZ, VN, YU, ZW, ARIPO patent (GH, GM, KE, LS, MW, SD, SZ, UG, ZW), Eurasian patent (AM, AZ, BY, KG, KZ, MD, RU, TJ, TM), European patent (AT, BE, CH, CY, DE, DK, ES, FI, FR, GB, GR, IE, IT, LU, MC, NL, PT, SE), OAPI patent (BF, BJ, CF, CG, CI, CM, GA, GN, ML, MR, NE, SN, TD, TG).

Published
With international search report.

(54) Title: ANALOGS OF DUOCARMYCIN AND CC-1065

(57) Abstract

Analogs and derivatives of duocarmycin and CC-1065 are provided. The compounds have use as antitumor antibiotics and as cell toxicity agents. The compounds have sequences specific DNA alkylating activity.

ANALOGS OF DUOCARMYCIN AND CC-1065

United States Government Rights in the Invention

Funds used to support some of the studies reported herein were provided by the United States Government (National Institutes of Health Grant, CA 55276.) The United States Government, therefore, may have certain rights in the invention disclosed herein.

Technical Field of the Invention

The field of this invention is antitumor antibiotics. More particularly, the present invention relates to analogs of duocarmycin and CC-1065, which analogs have antitumor antibiotics activity.

Background of the Invention

Duocarmycin SA (**1**) and duocarmycin A (**2**) constitute the parent members of a class of potent antitumor antibiotics related to CC-1065 (**3**) that derive their properties through a sequence selective alkylation of duplex DNA (FIG. 1). Since their disclosure, substantial efforts have been devoted to defining the characteristics of their DNA alkylation reactions, to determining the origin of their DNA alkylation selectivity, and to defining fundamental relationships between structure, functional reactivity, and biological properties.

Three models have been advanced to account for the DNA alkylation sequence selectivity. One model proposes a sequence-dependent phosphate protonation of the C4 carbonyl which activates the agent for DNA alkylation. (Warpehoski, M. A.; Hurley, L. H. *Chem. Res. Toxicol.* **1988**, *1*, 315; Hurley, L. H.; Reynolds, V. L.; Swenson, D. H.; Petzold, G. L.; Scahill, T. A. *Science* **1984**, *226*, 843. Reynolds, V. L.; Molineux, I. J.; Kaplan, D. J.; Swedson, D. H.; Hurley, L. H. *Biochemistry* **1985**, *24*, 6228. Hurley, L. H.; Lee, C.-S.; McGovren, J. P.; Warpehoski, M. A.; Mitchell, M. A.; Kelly, R. C.; Aristoff, P. A. *Biochemistry* **1988**, *27*, 3886. Scahill, T. A.; Jensen, R. M.; Swenson, D. H.; Hatzenbuhler, N. T.; Petzold, G.; Wierenga, W.; Brahme, N. D. *Biochemistry* **1990**, *29*, 2852; Hurley, L. H.; Warpehoski, M. A.; Lee, C.-S.; McGovren, J. P.; Scahill, T. A.; Kelly, R. C.; Mitchell, M. A.; Wicnienski, N. A.; Gebhard, I.; Johnson, P. D.; Bradford, V. S. *J. Am. Chem. Soc.* **1990**, *112*, 4633; Lin, C. H.; Beale, J. M.; Hurley, L. H. *Biochemistry* **1991**, *30*, 3597.) Another invokes alkylation at junctions of bent DNA without addressing the source of catalysis. (Lin, C. H.; Sun, D.; Hurley, L. H. *Chem. Res. Toxicol.* **1991**, *4*, 21. Lee, C.-S.; Sun, D.; Kizu, R.; Hurley, L. H. *Chem. Res. Toxicol.* **1991**, *4*, 203. Lin, C. H.; Hill, G. C.; Hurley, L. H. *Chem. Res. Toxicol.* **1992**, *5*, 167. Ding, Z.-M.; Harshey, R. M.; Hurley, L. H. *Nucl. Acids. Res.* **1993**, *21*,

4281. Sun, D.; Lin, C. H.; Hurley, L. H. *Biochemistry* **1993**, *32*, 4487. Thompson, A. S.; Sun, D.; Hurley, L. H. *J. Am. Chem. Soc.* **1995**, *117*, 2371.) A third model is based on the premise that distinct alkylation selectivities are controlled by the AT-rich noncovalent binding selectivity of the agents and their steric accessibility to the adenine N3 alkylation site. (Boger, D. L.; Johnson, D. S. *Angew Chem., Int. Ed. Engl.* **1996**, *35*, 1439. Boger, D. L.; Johnson, D. S. *Proc. Natl. Acad. Sci., U.S.A.* **1995**, *92*, 3642. Boger, D. L. *Acc. Chem. Res.* **1995**, *28*, 20. Boger, D. L. In *Advances in Heterocyclic Natural Product Synthesis*; Pearson, W. H., Ed.; JAI: Greenwich, 1992; Vol. 2, 1. Boger, D. L. *Chemtracts: Org. Chem.* **1991**, *4*, 329. Boger, D. L. In *Proc. R. A. Welch Found. Conf. Chem. Res., XXXV., Chem. Frontiers Med.* **1991**, *35*, 137. Boger, D. L. In *Heterocycles in Bioorganic Chemistry*; Bergman, J.; van der Plas, H. C.; Simonyl, M., Eds.; Royal Soc. of Chem.: Cambridge, 1991; 103. Coleman, R. S.; Boger, D. L. In *Studies in Natural Product Chemistry*; Rahman, A.-u.-, Ed.; Elsevier: Amsterdam, 1989; Vol. 3, 301; Boger, D. L.; Johnson, D. S.; Yun, W.; Tarby, C. M. *Bioorg. Med. Chem.* **1994**, *2*, 115. Boger, D. L.; Munk, S. A.; Zarrinmayeh, H.; Ishizaki, T.; Haught, J.; Bina, M. *Tetrahedron* **1991**, *47*, 2661. Boger, D. L.; Coleman, R. S.; Invergo, B. J .; Sakya, S. M.; Ishizaki, T.; Munk, S. A.; Zarrinmayeh, H.; Kitos, P. A.; Thompson, S. C. *J. Am. Chem. Soc.* **1990**, *112*, 4623.) This latter proposal accommodates and explains the reverse and offset 5 or 3.5 base-pair AT-rich adenine N3 alkylation selectivities of natural and unnatural enantiomers of duocarmycin and CC-1065 and offers a beautiful explanation for the identical alkylation selectivities of both enantiomers or simple derivatives thereof. Further support for this model includes the demonstrated AT-rich noncovalent binding of the agents, their preferential noncovalent binding coincidental with DNA alkylation, the demonstration that the characteristic DNA alkylation is also observed with isomeric alkylation subunits (*e.g.*, *iso*-CI and *iso*-CBI), and that it does not require the presence of the C4 carbonyl or even the activated cyclopropane.

In previous studies, the issue of catalysis with the noncovalent binding model has not been addressed. The chemical stability of duocarmycin and CC-1065 and the acid-catalysis requirement for addition of typical nucleophiles has led to the assumption that the DNA alkylation must also be an acid-catalyzed reaction. Although efforts have gone into supporting the extent and role of this acid catalysis, it remains largely undocumented for the DNA alkylation reaction. At pH 7.4, the DNA phosphate backbone is fully ionized (0.0001–0.00004% protonated). Consequently, it is unlikely that catalysis is derived from a

phosphate backbone delivery of a proton to the C4 carbonyl as advanced in the alkylation site model. Consistent with this, the rate of the DNA alkylation reaction for duocarmycin SA exhibits only a very modest pH dependence below pH 7 and essentially no dependence in the more relevant pH 7–8 range.

Brief Summary of the Invention

In one aspect, the present invention provides analog compounds of duocarmycin SA, duocarmycin A and CC-1065. An analog compound of the invention is represented by the following structure:

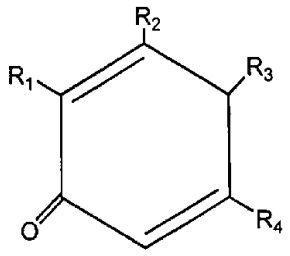

where said compound is fused to a first ring having a first vinylene group V_1 between R_1 and R_2, said first ring being one of the following structures, **A**, **B**, or **C**:

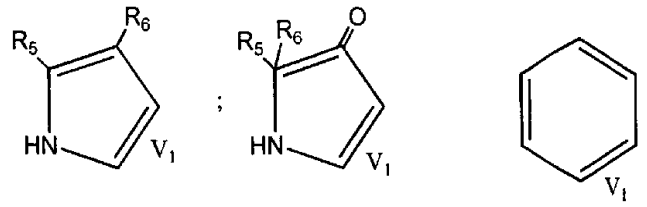

A **B** **C**

where said compound is also fused to a second ring having a second vinylene group V_2 between R_3 and R_4, said second ring being one of the following structures, **D**, **E**, or **F**:

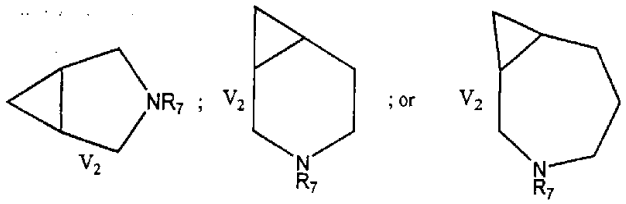

D E F

wherein R_5 is a hydrogen, $-CO_2(C_1-C_6(alkyl))$ or a radical represented by the following structure, G:

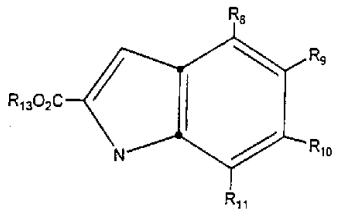

G

where R_6 is hydrogen or C_1-C_6(alkyl); R_7 is –H, $-CO_2(C_1-C_6(alkyl))$, $-CO(C_1-C_6(alkyl))$, $-CO_2$-*tert*-butyl, or $-COR_{14}$; R_8 is hydrogen or a first N-substituted pyrrolidine ring being fused at a third vinylene group V_3 between R_8 and R_9 represented by the following structure, H:

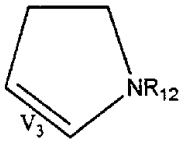

H

where R_9 is: -NH-C(O)-; R_{10} and R_{11} are each independently hydrogen, $-O-C_1-C_6$(alkyl) or $-C_1-C_6$(alkyl), wherein the –NH group is directly attached to G at the R_9 position and the C(O)- group is directly attached to the first ring at the R_5 position, if R_8, R_{10} and R_{11} are each hydrogen; said first N-substituted pyrrolidine ring radical, H, being fused at the third vinylene group V_3 between R_8 and R_9; and a radical represented by the structure, I:

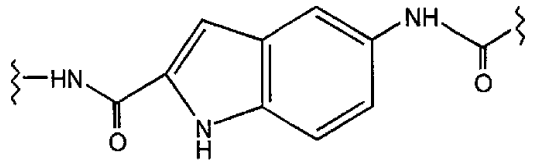

I

wherein the -NH group is directly attached to **G** at the R_9 position and the C(O)- group is directly attached to the first ring at the R_5 position, if $\mathbf{R_8}$, $\mathbf{R_{10}}$ and $\mathbf{R_{11}}$ are each hydrogen; with the following provisos:

if $\mathbf{R_8}$ participates in the first N-substituted pyrrolidine ring, then $\mathbf{R_9}$ also participates in the first N-substituted pyrrolidine ring;

if $\mathbf{R_9}$ participates in the first N-substituted pyrrolidine ring, then $\mathbf{R_8}$ also participates in the first N-substituted pyrrolidine ring;

if $\mathbf{R_8}$ and $\mathbf{R_9}$ participate in the first N-substituted pyrrolidine ring, then $\mathbf{R_{10}}$ and $\mathbf{R_{11}}$ are hydrogen; $\mathbf{R_{12}}$ is -C(O)- and a diradical represented by the following structure, **J**:

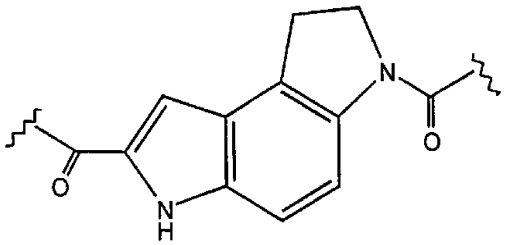

J

wherein the -C(O) group is directly attached to **H** at the R_{12} position and the N-C(O)- group is directly attached to the first ring at the R_5 position; $\mathbf{R_{13}}$ is hydrogen or C_1-C_6(alkyl); $\mathbf{R_{14}}$ is hydrogen, C_1-C_6(alkyl), -O-(C_1-C_6(alkyl)), or a radical represented by the structure, **K**:

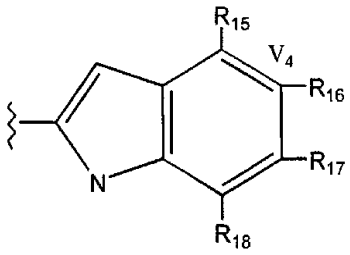

K

where $\mathbf{R_{15}}$ is hydrogen or a second N-substituted pyrolidine ring being fused at a fourth vinylene group $\mathbf{V_4}$ between $\mathbf{R_{15}}$ and $\mathbf{R_{16}}$ represented by the following structure, **L**:

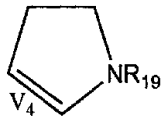

L

where $\mathbf{R_{16}}$ is:

-O-(C_1-C_6(alkyl)), C_1-C_6(alkyl), NH_2 or

said second N-substituted pyrolidine ring radical, **L**, being fused at a fourth vinylene group $\mathbf{V_4}$ between $\mathbf{R_{15}}$ and $\mathbf{R_{16}}$; or a radical represented by the following structure, **M**:

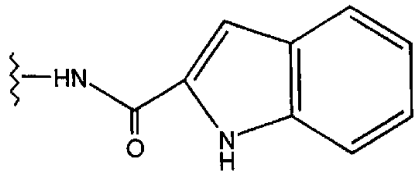

M

wherein the -NH group is directly attached to **K** at the R_{16} position if $\mathbf{R_{15}}$, $\mathbf{R_{17}}$ and $\mathbf{R_{18}}$ are each hydrogen; with the following provisos:

if $\mathbf{R_{15}}$ participates in the first N-substituted pyrrolidine ring, then $\mathbf{R_{16}}$ also participates in the first N-substituted pyrrolidine ring;

if $\mathbf{R_{16}}$ participates in the first N-substituted pyrrolidine ring, then $\mathbf{R_{15}}$ also participates in the first N-substituted pyrrolidine ring;

if $\mathbf{R_{15}}$ and $\mathbf{R_{16}}$ participate in the first N-substituted pyrrolidine ring, then $\mathbf{R_{17}}$ and $\mathbf{R_{18}}$ are hydrogen;

where $\mathbf{R_{17}}$ and $\mathbf{R_{18}}$ are independently hydrogen, -0-C_1-C_6(alkyl) or -C_1-C_6(alkyl);

$\mathbf{R_{19}}$ is -C(O)-$\mathbf{R_{20}}$ or a radical represented by the following structure, **N**:

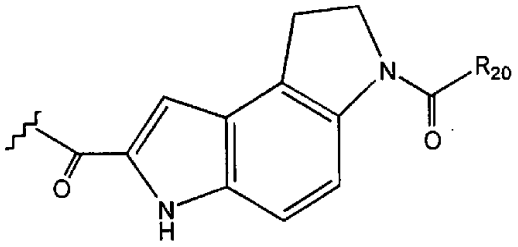

N

wherein the -C(O) group is directly attached to the second N-substituted pyrrolidine ring, **L**, at the R_{19} position; and $\mathbf{R_{20}}$ is NH_2 or -O-*tert*-butyl; the compound not being (+)-CC-1065, (+)-duocarmycin SA, or (+)-duocarmycin A. Compounds are shown herein with a particular enantiomer configuration. One of skill in the art will readily appreciate that all enantiomers of the compounds are contemplated as being a part of this invention.

In a preferred embodiment, a compound has **A** as the first ring. A preferred second ring is **D**. Exemplary and preferred compounds have the structures set forth hereinafter as reversed, sandwiched, shortened, simplified, and extended analogs. Further preferred compounds have a six- or seven member heterocyclic ring as part of the alkylation subunit.

In another aspect, the present invention provides a pharmaceutical composition containing a compound of formula I together with a physiologically acceptable diluent.

Still further, the present invention provides a process of alkylating DNA, the process including the step of exposing DNA to a compound or composition of this invention.

Brief Description of the Drawings

In the Drawings, which form a portion of the specification:

FIG. 1 shows the structures of duocarmycin SA, duocarmycin A and CC-1065.

FIG. 2 shows the structure and method of making analog compounds **17-20**.

FIG. 3 shows the structure and synthetic scheme for making analog compounds **23** and **24**.

FIG. 4 shows the structure and synthetic scheme for making analog compounds **30** and **31**.

FIG. 5 shows the synthetic scheme for making analog compound **37** and the structure of that compound.

FIG. 6 shows the structure and synthetic scheme for making analog compounds **40** and **41**.

FIG. 7 shows the structure and synthetic scheme for making analog compounds **53-56**.

FIG. 8 shows the structure and synthetic scheme for making analog compounds **60-62**.

FIG. 9 shows the synthetic scheme for making analog compounds **78** and **79**.

FIG. 10 shows the structure and synthetic scheme for preparing analog compounds **97** and **98**.

FIG. 11, shown in two panels as FIGS. 11a and 11b, shows the summary results of consensus DNA alkylation sequences alkylated by compounds of the present invention.

FIG. 12 shows summary data of the consensus alkylation sequence alkylated by further compounds of this invention.

FIG. 13 shows sequence preferences for analog compounds of the invention.

FIG. 14 shows *in vitro* cytotoxic activity of analog compounds of the invention containing indole derivatives.

FIG. 15 shows summary data of DNA alkylating efficiency of analog compounds of the invention.

FIG. 16 shows consensus sequences for DNA alkylation by key components in analog compounds of the present invention.

FIG. 17 shows the structure and synthetic scheme for making analog compounds **99-102**.

FIG. 18 shows the structure of analog compounds **72-79**.

FIG. 19 shows the *in vitro* cytotoxic activity of BOC derivatives analogs of the invention.

FIG. 20 shows the *in vitro* cytotoxic activity of trimethyloxyindole derivatives analogs of the invention.

Detailed Description of the Invention

I. The Invention

The present invention provides compounds that are analogs or derivatives of duocarmycin A, duocarmycin SA and CC-1065, compositions containing those compounds and the use of those compounds and compositions for alkylating DNA.

II. Compounds

A. Reversed and Sandwiched Analogs

Duocarmycin SA **(1)** contains a C6 methyl ester that complements the right-hand side linking amide. This provides the opportunity to introduce DNA binding subunits on either side of the alkylation subunit. Thus, coupling of a DNA binding subunit through the C6 carboxylate provides a novel class of agents referred to herein as reversed analogs. The reversed compounds (**17-20, 23, 24** FIG 2-3) exhibit an AT-rich alkylation selectivity that extends in the atypical reverse direction from an alkylation site. The predicted alkylation sites for the natural enantiomers coincide with those of the unnatural enantiomers of the typical extended agents. The predicted alkylation sites for the unnatural enantiomers of the reversed agents coincide with those of the natural enantiomers of the extended agents. Thus, a complete switch in the enantiomeric alkylation selectivity would be observed with the reversed analogs if it is controlled by the AT-rich binding selectivity. In contrast, the alkylation site model would require that natural enantiomers of both the extended and reversed agents alkylate the same sites rather than exhibit this switch.

Synthesis of the Reversed Analogs of Duocarmycin SA. The preparation of **17–20** was accomplished through coupling of the free amine of **9–12** (0.9 equiv, 2–4 h, 25 °C) with the C6 carboxylic acid of **8** (FIG. 2). While this was conducted as outlined in FIG. 2, the manner in which this could be accomplished was not straightforward. Hydrolysis (1–1.3 equiv LiOH) of *N*-BOC-DSA (**4**) cleanly provided **7** (93%) without competitive hydrolysis of the carbamate or addition to the cyclopropane. Prolonged reaction times (72 h) at 25 °C under typical conditions (LiOH, THF–CH_3OH–H_2O) provided predominately recovered starting material and the conversion to **7** was observed only upon warming (60 °C). Even under these conditions, only methyl ester hydrolysis was observed. Both the direct coupling of **7** (DCC, EDCI, DEPC) in the presence or absence of added $NaHCO_3$ or the use of preformed active esters (*e.g.*, imidazolide) provided only low yields (10–30%) of the desired agent with the more soluble coupling partners and failed altogether with the insoluble $CDPI_2$. Consequently, the preparation of **17–20** was more effectively accomplished in an indirect manner. Treatment of **7** with dilute HCl (0.05 N HCl–EtOAc, 25 °C, 30 min) provided **8** without *N*-BOC deprotection and no trace of the ring expansion HCl addition product was detected. Subsequent coupling of **8** with the **9–12** (0.9 equiv, 2 equiv EDCI, DMF, 2–4 h, 25 °C) proceeded in high yields (57–96%) and spirocyclization was effected by NaH (DMF, 0 °C, 30 min, 64–95%).

Modifications in the Terminal N^2 Acyl Substituent of the Reversed Analogs. To insure that the behavior of **17–20** was not substantially influenced by the nature of the N^2 substituent, both enantiomers of **23** and **24** terminating with a N^2-acetyl group or the free amine were prepared (FIG. 3). Thus, *N*-BOC deprotection of **14** (3.4 N HCl–EtOAc, 25 °C, 30 min) followed by spirocyclization or N^2 acetylation and spirocyclization afforded **24** and **23**, respectively.

Synthesis of the Sandwiched Analogs of Duocarmycin SA. An important complement to the extended and reversed analogs are the agents **30** (CDPI–DSA–CDPI) and **31** (CDPI–DSA–TMI) (FIG. X) referred to herein as sandwiched analogs (FIG. 4). Their examination was more informative than their initial consideration might suggest. The noncovalent binding model led us to predict that both enantiomers of **30** and **31** would alkylate the same sites independent of their absolute configuration and that their sites of DNA alkylation would be distinct from either enantiomer of both the

extended and reversed analogs. Such a demonstration would further distinguish the noncovalent binding model from the alkylation site model which would require that the natural enantiomers of the sandwiched analogs alkylate the same sites as (+)-**1**–**6**. Compounds 30 and 31 were prepared using *N*-BOC deprotection of **15** (4 N HCl–EtOAc, 25 °C, 30 min) followed by coupling of **25** with $CDPI_1$ (**26**, 68%) or **27** (0.95 equiv, 2 equiv EDCI, DMF, 25 °C, 6–15 h, 70%) and spirocyclization (NaH, DMF, 0 °C, 30 min) cleanly provided **30** (70%) and **31** (67%) (FIG. 4).

B. Shortened Simplified and Extended Analogs

Resolution of *N*-BOC-DSA. Optically active agents were prepared through chromatographic resolution of the *bis*-(*R*)-*O*-acetylmandelate ester of **37** or, more conveniently, through a new protocol of direct chromatographic resolution of *N*-BOC-DSA (**39**). Although the immediate precursors to **39** including **35** and **36** were not resolved by direct chromatographic means, the enantiomers of *N*-BOC-DSA were effectively separated on a semipreparative ChiralCel OD HPLC column (10 μm 2 × 25 cm, 30% 2-propanol/hexane, 7 mL/min, α = 1.24, ≥99.9% ee). Acid-catalyzed deprotection of **39** (4 N HCl–EtOAc, 25 °C, 30 min, 95–100%) was accompanied by clean addition of HCl to the cyclopropane and provided **33** (FIG. 5). Notably, no trace of the ring expansion product derived from addition of chloride to the more substituted C8a cyclopropane carbon was detected.

Simple Derivatives of the Alkylation Subunit. In studies that culminated in the total synthesis of (+)- and *ent*-(–)-**1**, we detailed the synthesis and examination of both enantiomers of *N*-BOC-DSA (**39**) and **44**. To generalize the properties of such simple derivatives, both enantiomers of **40** and **38** were prepared (FIG. 6). Treatment of **39** with 4 N HCl–EtOAc (25 °C, 30 min) followed by acylation with acetyl chloride or methyl chloroformate (2.0 equiv, 3.0 equiv $NaHCO_3$, THF, 25 °C, 1 h) provided **42** (97%) and **43** (46%). Spirocyclization to provide **40** (73%) and **41** (92%) was effected by treatment with NaH.

Modifications in the Right-hand Subunit: Role of the Methoxy Substituents. Modifications in the trimethoxyindole subunit of duocarmycin SA were made with the intention of defining the role of each of the three methoxy substituents. Treatment of **39** with 4 N HCl–EtOAc (25 °C, 30 min) followed by coupling (3 equiv EDCI, DMF, 25 °C, 4–15 h) of **38** with **45**–**48** (1.1 equiv) in the absence of added base

provided the precursors **49–52** (70–82%, FIG. 7). Spirocyclization was effected by treatment with NaH (3 equiv, THF–DMF 4–2:1, 0 °C, 30 min) to provide of **53–56** (87–96%). Coupling of **38** in the presence of base including $NaHCO_3$ led to competitive spirocyclization and the presence of adventitious moisture in the spirocyclization reaction mixture led to subsequent hydrolysis of the linking N^2 amide.

Substitutions for the DNA Binding Subunit: Extended Analogs. Three additional DNA binding subunits have proven representative and important to examine. These include $CDPI_1$, $CDPI_2$, and $indole_2$. The former typically provides agents analogous to **1–2** while the latter two derivatives are representative of the larger agents which exhibit a more extended 5 base-pair AT-rich DNA alkylation selectivity analogous to CC-1065 (**3**). In addition, the $indole_2$ derivatives maintain the cytotoxic potency of **1–3**, but typically exhibit more efficacious *in vitro* antitumor activity. The agents were prepared by acid-catalyzed deprotection of **39** (4 N HCl–EtOAc, 25 °C, 15–20 min) followed by immediate coupling (3 equiv EDCI, DMF, 12–24 h, 25 °C) of **37** with $CDPI_1$ (67%), $CDPI_2$ (67%), and $indole_2$ (81%) conducted in the absence of added base (FIG. 8). Spirocyclization to provide **60–62** was effected by treatment with NaH.

C. Analogs Incorporating an Alkylation Subunit Containing a b or 7 Member Heterocycle

Synthesis of *N*-BOC-CNA (78) and CNA (79). Attempts to extend the radical cyclization methodology employed for the five- and six-membered C-ring analogs in this class were unsuccessful. Reaction of the appropriately functionalized naphthalene with Bu_3SnH–AIBN (R = H, + TEMPO) resulted in simple reduction. The metal hydride reduction of the resulting aryl radical proved faster than the required 7-*exo-trig* radical cyclization even with substrates bearing an activated acceptor alkene.

The successful approach to the preparation of the CNA nucleus rested on the implementation of an alternative intramolecular Heck reaction. The starting material for both the Heck reaction and the radical cyclization attempts was prepared by *N*-alkylation of *N*-(*tert*-butyloxy-carbonyl)-4-(benzyloxy)-1-iodo-2-naphthylamine (**80**), readily available in three steps (60% overall) from 1,3-dihydroxynaphthalene, with the mesylate of 4-penten-1-ol to provide **81** (FIG. 9). A full two molar equivalents of benzyltributylammonium chloride was required to provide high yields of the alkylated

product using phase transfer conditions. An intramolecular Heck reaction conducted with 3 mole % of $Pd[P(Ph_3)]_4$ as catalyst furnished the desired cyclization product **82** in 89%. Careful removal of O_2 from the reaction mixture provided reproducible high yields and no palladium hydride induced isomerization of **83** to give the endocyclic olefin was detectable by ^1H NMR of the crude reaction mixture.

Similar observations were made with the substrate ($R = CO_2CH_3$) bearing an activated electron-deficient acceptor alkene, but the reaction proved unsuccessful with the substrate (R = OTHP) bearing an electron-rich acceptor alkene. In principle, both successful cyclization products can be converted into appropriately C-1 substituted and functionalized tetrahydronaphtho[2,1-*b*]azepines for use in the preparation of **78–79**.

Hydroboration followed by oxidative workup converted the exocyclic olefin into the desired alcohol **83.** Efforts to convert this alcohol to the corresponding chloride upon treatment with Ph_3P–CCl_4 proceeded in modest yields (*ca.* 50%). Much higher conversions were realized by treatment of **83** with mesyl chloride in the presence of Et_3N to provide **84** in 89%. Removal of the benzyl group through transfer hydrogenolysis (4 wt. equiv of 10% Pd–C, aqueous HCO_2NH_4–THF, 25 °C, 2 h, 89%) afforded **85** and set the stage for the final spirocyclization.

Winstein Ar-3' spirocyclization was effected by treatment of **85** with DBU (3 equiv, CH_3CN) and smoothly provided **78** (87%). Due to its unusual reactivity, careful chromatographic conditions were required and pretreatment of the chromatographic support (SiO_2) with Et_3N resulted in much higher yields (*i.e.*, 87% versus 40–50%). Treatment of **85** with 3.9 M HCl–EtOAc removed the BOC group to afford the unstable amine hydrochloride which was taken directly into the subsequent cyclization step. Addition of 10 equiv of DBU as a dilute solution in CH_3CN resulted in good conversion to **79** (77%). Conventional chromatography provided the relatively stable CNA which gave crystals suitable for X-ray analysis (CH_3CN–CH_3OH).

Synthesis of *N*-CO_2Me-CNA (97) and CNA–TMI (98). Efforts to acylate the amine hydrochloride resulting from BOC deprotection of **85** at this late stage in the synthesis were unsuccessful. The only azepine amenable to *N*-acylation was the free amine derived from **83** which bore the exocyclic olefin. Incorporation of the sp^2 hybridized carbon presumably alters the conformation of the fused seven-membered ring in a manner that allows *N*-acylation. Synthesis of the amine hydrochloride **88**

through treatment with 3.9 N HCl–EtOAc (25 °C, 40 min) provided a relatively well-behaved solid amine salt that served as a short term storage intermediate for further acylations (FIG. X). Liberation of the free amine with $NaHCO_3$ followed by treatment with methyl chloroformate provided **89** in 94% yield. High yields (80%) were also realized for EDCI coupling of **88** and 5,6,7-trimethoxyindole-2-carboxylic acid to form the advanced analog **90**. Exposure of the acylated products to the same sequence of synthetic transformations detailed for **78–79** gave good to excellent yields of the desired products **91–96**. Unlike *N*-BOC-CNA (**78**), *N*-CO_2Me-CNA (**97**) proved to be a crystalline solid and recrystallization from 10% EtOAc–hexanes gave X-ray quality crystals. Spirocyclization of TMI derivative **96** gave a lower yield of ring closed product **96** (48%) due to its high reactivity and more challenging chromatography requirements for purification (FIG. 10).

Resolution. In order to obtain the separate enantiomers of both **78** and **96**, various synthetic intermediates were subjected to direct chromatographic resolution on a semipreparative chiracel OD column. The intermediates **84**, **87** and **92** proved to have the greatest separation and were resolved (>99.9% ee) in sufficient quantities to be carried on to the respective final products. The assignment of the absolute configuration for (+)-**78** was based initially on the relative cytotoxic potencies of (+)- and *ent*-(–)-*N*-BOC-CNA, with the former exhibiting more potent activity which is consistent with observations made for **1–3** and **76-77**. Ultimately, the absolute configuration for (+)-**78** was confirmed and unambiguously established by X-ray structure analysis[24] of the resolved *seco*-derivative (–)-(1*R*)-**87** bearing a heavy atom and subsequent conversion to (+)-**78**.

A detailed description of the synthesis of compounds of this invention is set forth hereinafter in the Examples. The present invention further contemplates intermediates formed during synthesis of those compounds. This invention still further contemplates compositions containing a compound of the invention as set forth above. Preferably, the composition is an aqueous composition.

III. Uses

Compounds of this invention alkylate selective sequences in DNA target molecules. The compounds thus have cytotoxic activity and can be used as antitumor antibiotics. Details of the activity of particular compounds are set forth below.

A. Reversed and Sandwiched Analogs

DNA Alkylation Studies. The DNA alkylation properties of the reversed and sandwiched agents were examined within five segments of duplex DNA. With both enantiomers of the reversed analogs $CDPI_2$–DSA (**20**) in hand, their comparison with the enantiomers of DSA–$CDPI_2$ was addressed. The key question was whether the enantiomeric alkylation selectivity of **20** would switch with the simple reversal of the orientation of the DNA binding subunits (noncovalent binding model) or whether the two natural enantiomers would behave in an identical or comparable manner (alkylation site model).

The natural enantiomer of the reversed agent, (+)-$CDPI_2$-DSA (**20**), was found to alkylate the same sites and to exhibit the same sequence selectivity as the unnatural enantiomer of CC-1065 and the extended agent, *ent*-(–)-DSA-$CDPI_2$. Thus, a complete reversal of the enantiomeric alkylation selectivity was observed with (+)-**20** and these results are only consistent with the noncovalent binding model. The natural enantiomer of the reversed analog (+)-$CDPI_2$-DSA (**20**) alkylated the same, single high affinity site in w794 (5′-AATTT) as the unnatural enantiomers (–)-CC-1065 and (–)-DSA-$CDPI_2$ without detectable alkylation at the single, high affinity site observed with the natural enantiomers (+)-CC-1065 and (+)-DSA-$CDPI_2$ (5′-AATTA).

Within the six-base A-rich sequence of w836 DNA (+)-duocarmycin SA alkylated each of the four 3′ adenines (5′-AAAAAA) corresponding nicely to 3′→5′ binding across a 3.5 base-pair AT-rich site. The natural enantiomer of the extended analog (+)-DSA-$CDPI_2$ also alkylates only the 3′ adenines (5′-AAAAAA) in this sequence corresponding to the same 3′→5′ binding but across a more extended 5 base-pair AT-rich sequence restricting alkylation to the first three versus four 3′ adenines. In this same sequence, the unnatural enantiomer of the extended agent, *ent*-(–)-DSA-$CDPI_2$, alkylates the 5′ terminal adenines in accordance with 5′→3′ binding across a 5 base-pair AT-rich binding site (5′-AAAAAA). Consistent with the offset AT-rich binding site of the unnatural enantiomers due to the diastereomeric nature of the adducts, *ent*-(–)-DSA-$CDPI_2$ does not alkylate the terminal 5′ adenine, but does alkylate the following four 5′ adenines. Indicative of the complete switch in the enantiomeric alkylation selectivity of the reversed agents, the natural enantiomer of **20** alkylated the same sites as *ent*-(–)-DSA-$CDPI_2$ while the unnatural enantiomer of **20** alkylated the

same sites as the natural enantiomer (+)-DSA-CDPI$_2$. In addition to establishing that the noncovalent binding selectivity of the agents is controlling the DNA alkylation selectivity, the comparisons also establish that the two enantiomers are subject to the same polynucleotide recognition features. In related studies, it is maintained that the two enantiomers are subject to different polynucleotide recognition elements.

The consensus alkylation sequence of (+)-CDPI$_2$-DSA (**20**) is summarized in FIGs 11a and 11b. All alkylation sites were found to be adenine and essentially each adenine N3 alkylation site was flanked by a 5′ and 3′ A or T base. The preference for this three-base sequence followed the order: 5′-A<u>A</u>A > 5′-A<u>A</u>T ≥ 5′-T<u>A</u>A > 5′-T<u>A</u>T). There was also a strong preference for the second and third 3′ base to be A or T and the preferences distinguished the high affinity versus lower affinity alkylation sites. Thus, (+)-CDPI$_2$-DSA exhibits a 5 base-pair AT-rich alkylation selectivity that corresponds to 5′→3′ binding in the minor groove starting at the 5′ base preceding the alkylation site and extending over the alkylated adenine in the 3′ direction covering the three adjacent 3′ bases, *e.g.* 5′-A<u>A</u>AAA.

The consensus alkylation selectivity of (–)-CDPI$_2$-DSA is also summarized in FIGs 11a and 11b. All alkylation sites were found to be adenine and essentially each adenine N3 alkylation site was flanked by two 5′ A or T bases. The preference for this three-base sequence followed the order: 5′-AA<u>A</u> > 5′-TA<u>A</u> > 5′-TT<u>A</u> > 5′-AT<u>A</u>. There was also a preference for the third and fourth 5′ bases to be A or T and this distinguished the high affinity versus low affinity sites. Thus, (–)-CDPI$_2$-DSA exhibits a 5 base-pair AT-rich alkylation selectivity starting at the alkylated adenine and extending in the 3′→5′ direction across the four adjacent 5′ bases, *e.g.* 5′-AAAA<u>A</u>.

Examination of **17–19** revealed the same characteristics except that they exhibited either a 5 (**18**) or 3.5 (**17** and **19**) base-pair AT-rich selectivity corresponding to their sizes and lengths. CDPI$_1$-DSA (**19**) was found to behave analogous to duocarmycin SA albeit with the reversed enantiomeric alkylation selectivity. With w794 DNA, the natural enantiomers of **17–20** preferentially alkylate the single high affinity site of the unnatural enantiomers of **1–3** and do not alkylate the typical natural enantiomer site. The smaller and shorter reversed analogs also proved less efficient at alkylating DNA. This efficiency followed the predictable trends of **20** > **18** > **19** > **17** and was more sensitive to the size of the agents than the typical extended agents.

Moreover, the full set of reversed analogs **17–20** alkylated DNA at substantially slower rates and ultimately with lower efficiencies. Typically, the reactions for the reversed analogs were conducted at 37 °C for 5 days (versus 25 °C, < 12 h) and even then were 10–1000× less efficient than **1–3** and related agents. In fact, their behavior proved more similar to the simple derivatives **4–6** than **1–3**.

DNA Alkylation Properties of Agents Containing Modifications in the Terminal N^2 Substituent of the Reversed Analogs. The agents **23** and **24** were examined in efforts to determine whether the terminal N^2-BOC group of the reversed analogs was contributing to their reduced rate and efficiency of DNA alkylation. The three agents exhibited no differences in their DNA alkylation selectivity and only small differences in both the rate and efficiency of DNA alkylation. Moreover, the magnitude of these differences was much smaller than might be anticipated. The acetyl derivative **23** was found to be 2–5× more efficient than the BOC derivative **18**, and the terminal NH agent **24** was about an order of magnitude less efficient than **18**. While these trends nicely follow the expected relative reactivities of the agents (**23** > **18** >> **24**), all three were still substantially slower (*ca.* 1000×) and much less efficient (*ca.* 100×) at alkylating DNA than the typical extended analog DSA-indole$_2$. The unnatural enantiomers of **23** and **24**, like that of **18**, were approximately 10× less effective than the natural enantiomers.

DNA Alkylation Properties of the Sandwiched Analogs of Duocarmycin SA. Consistent with the noncovalent binding model, both enantiomers of CDPI-DSA-CDPI (**30**) alkylated the same sites and their selectivity proved distinct from either enantiomer of the extended or reversed agents DSA-CDPI$_2$ or CDPI$_2$-DSA (**20**). The consensus alkylation sequence for (+)- and *ent*-(–)-**30** is summarized in FIG. 12. All alkylation sites were found to be adenine and essentially all adenine N3 alkylation sites were flanked by a 5′ and 3′ A or T base. The preference for this three-base sequence follows the order: 5′-A<u>A</u>A > 5′-A<u>A</u>T ≥ 5′T<u>A</u>A > 5′T<u>A</u>T. In addition, there was a very strong preference for both of the second 5′ and 3′ bases to be A or T. Exceptions typically involved one but not both of these locations and the preference was strongest on the 5′ side of the alkylation site, *e.g.* 5′-AA<u>A</u>AG > 5′-CA<u>A</u>AA. Thus, alkylation was observed at adenines central to a 5 base-pair AT-rich sequence, e.g. 5′-AA<u>A</u>AA. With w836 DNA, (+)- and *ent*-(–)-**30** exhibited identical alkylation profiles within the stretch

of six adenines and alkylated those central to the sequence rather than the 3′ or 5′ terminal adenines characteristic of (+)- or *ent*-(–)-DSA-CDPI$_2$. Very few of the alkylation sites overlap with those of either enantiomer of the extended or reversed analogs and those that do are typically found in a long stretch of A's containing multiple alkylation sites for all agents.

Models of the DNA Alkylation Reactions. Both enantiomers of *N*-BOC-DSA exhibit an identical 2 base-pair alkylation selectivity (5′-A<u>A</u> > 5′-T<u>A</u>) with a requirement for a single 5′ A or T base adjacent to the adenine N3 alkylation site. For the natural enantiomer, this involves 3′ adenine N3 alkylation with agent binding in the 3′→5′ direction relative to the alkylated strand across the adjacent 5′ base. For the unnatural enantiomer, this similarly involves adenine N3 alkylation but with a reversed 5′→3′ binding orientation. As a consequence of the diastereomeric relationship of the adducts and in spite of the reversed 5′→3′ binding orientation, *ent*-(–)-*N*-BOC-DSA covers the same adjacent 5′ base as (+)-*N*-BOC-DSA. Thus, both enantiomers occupy the same binding site surrounding the alkylated adenine.

Models of alkylation at the high affinity w794 DNA site by the natural enantiomer of the extended agent (+)-DSA-CDPI$_2$ and the unnatural enantiomer of the reversed agent *ent*-(–)-CDPI$_2$-DSA highlight the origin of the switch in the inherent enantiomeric alkylation selectivity with the reversed analogs. The natural enantiomer, (+)-DSA-CDPI$_2$, alkylates the 3′ adenine and extends in the typical 3′→5′ direction over the adjacent four 5′ bases (5′-AATT<u>A</u>). The unnatural enantiomer of the reversed analog, *ent*-(–)-CDPI$_2$-DSA, also alkylates the 3′ adenine albeit with the reversed orientation of the alkylation subunit but with the DNA binding subunits extending in the atypical 3′→5′ direction over the same adjacent four 5′ bases (5′-AATT<u>A</u>). Thus, the natural enantiomer of DSA-CDPI$_2$ and the unnatural enantiomer of the reversed analog CDPI$_2$-DSA bind and cover the exact same AT-rich 5 base-pair region surrounding the adenine N3 alkylation site.

The unnatural enantiomer of the typical agent alkylates adenine N3 and binds across a 5 base region in the 5′→3′ direction in the minor groove which is opposite that of the typical natural enantiomers. Because of the diastereomeric nature of the adducts and analogous to *ent*-(–)-*N*-BOC-DSA, the binding site starts at the 5′ site adjacent to the alkylation site and extends in the 5′→3′ direction covering the adenine N3 alkylation

site and the following three 3′ bases (5′-AATTT). Consequently, the 5 base-pair AT-rich binding site surrounding the alkylation site for *ent*-(–)-DSA-CDPI$_2$ is analogous to that of the natural enantiomer except that it extends in the reverse direction in the minor groove relative to the alkylated adenine and is offset by one base-pair. The natural enantiomer of the reversed analog, (+)-CDPI$_2$-DSA, covers the same 5 base-pair AT-rich region surrounding the alkylated adenine but with the reversed orientation of the alkylation subunit and with the DNA binding subunits extending in the atypical 5′→3′ direction.

The natural enantiomer CDPI-DSA-CDPI (**30**) binds in the minor groove with the alkylation subunit extending in the 3′→5′ direction with the binding subunits covering 2 base-pairs on both the 5′ and 3′ side of the alkylation site. The binding extends slightly farther to the 5′ side (2.5 base-pairs) than the 3′ side (2 base-pairs) and this accounts nicely for the stronger and slightly extended AT preference on the 5′ side of the alkylation site. The unnatural enantiomer of 30 exhibits identical characteristics except that the alkylation subunit binds in the minor groove with the alkylation subunit extending in the reverse 5′→3′ direction relative to the alkylation strand covering the same 5 base AT-rich site surrounding the central alkylated adenine. This unusual feature of the two enantiomers binding and alkylating the same 5 base-pair AT-rich sites is analogous to (+)- and *ent*-(–)-*N*-BOC-DSA except that the latter smaller agents only cover 2 base-pairs.

Sequence Preferences. Each of the classes of agents have been shown to exhibit an adenine N3 alkylation selectivity that contains a three-base AT sequence including and surrounding the alkylated adenine (FIG. 13). Although it is tempting to assign a special significance to the sequence preferences, the results are most consistent with a purely statistical preference. The most frequently alkylated sequence for each class is 5′-AAA and the extent of alkylation diminishes as the A content gets smaller. In contrast to 5′-AAA, the mixed sequences contain competitive alkylation sites on the complementary unlabeled strand which diminish the apparent alkylation efficiency on the labeled strand. It is likely that a majority of the apparent selectivity is simply a statistical preference exaggerated by competitive unlabeled strand alkylation rather than unique characteristics embodied in the individual sequences. The exception to this generalization is the unusually effective alkylation of 5′-TTA by (+)-DSA-CDPI$_2$

representative of the typical natural enantiomers including (+)-CC-1065 and (+)-duocarmycin SA and the under represented alkylation of 5′-ATA by the unnatural enantiomers of the reversed analogs including *ent*-(–)-$CDPI_2$-DSA. The significance of this is not yet known.

Rates and Efficiencies of DNA Alkylation. In the course of examining the reversed and sandwiched agents, substantial differences in the rates and efficiencies of DNA alkylation were observed. First and foremost, extraordinarily slow rates were observed for the reversed agents at sites that are alkylated rapidly by the typical agents and extraordinarily fast rates were observed by the sandwiched agents at new sites not previously observed. It is thus likely that the characteristics responsible for the effective alkylation are not uniquely imbedded in the DNA sites or associated with the alkylated adenine but with structural features of the agents and intimately related to the source of catalysis for the reaction.

Consequently, these differences were quantitated by establishing the relative rate constants (k_{rel}, 5×10^{-6} M agent, 25 °C) for alkylation of the w836 high affinity alkylation sites within the six base A sequence (5′-AAAAAA) that both enantiomers of all three agent classes effectively alkylate. After just 1–5 min, the natural enantiomer of the typical extended agent, (+)-DSA-$CDPI_2$ (+E), and both enantiomers of the sandwiched analog **30**, CDPI-DSA-CDPI (+ and –S), exhibit extensive alkylation. In contrast, the unnatural enantiomer of the typical extended agent, *ent*-(–)-DSA-$CDPI_2$ (–E), requires 6 h to approach the same level of DNA alkylation and both enantiomers of the reversed analog, $CDPI_2$-DSA (+ and –R), require 72 h to reach a detectable and diminished level of DNA alkylation. Although the reversed natural enantiomer was faster than the unnatural enantiomer, neither comes even close to the rates exhibited by (+)-DSA-$CDPI_2$ or (+)- and *ent*-(–)-CDPI-DSA-CDPI (**30**) and more closely approximate the rates of DNA alkylation observed with *N*-BOC-DSA (**4**) which lacks the DNA binding subunits altogether.

An Additional Structural Requirement for Catalysis of the DNA Alkylation Reaction and Source of Catalysis. The DNA alkylation rate of the extended as well as the sandwiched agents is exceptionally fast and typical of this class of agents while that of all reversed agents is exceptionally slow proceeding at rates similar to those of *N*-BOC-DSA (**4**). Although there are many potential explanations for this, it is not due to

differences in the noncovalent binding affinity of the agent. In addition, the DNA alkylation selectivity of the reversed versus extended analogs simply reversed with these agents and no new sites were detected. Thus, it was the rates but not the sites that were altered.

Complementing these observations, the rapid rate of DNA alkylation by the sandwiched analogs was observed at a new set of alkylation sites independent of the absolute configuration of the agent indicating that the source of catalysis was not uniquely imbedded in the original DNA alkylation sites. Rather, the distinguishing feature between the extended or sandwiched analogs and the reversed analogs is the presence of the right-hand heteroaryl N^2 amide. Thus, a rigid extended N^2 amide substituent is required for rapid and effective alkylation of duplex DNA. With the sandwiched analogs, this effect is independent of the sites of DNA alkylation and the enantiomeric configuration of the alkylation subunit. We suggest that upon binding to DNA with the adoption of a helical bound conformation, the inherent twist of the alkylation subunit N^2 amide in the reversed analogs is not altered and, thus, not activated for nucleophilic addition. Consequently, they undergo DNA alkylation at rates comparable to those of the simple derivatives such as **4**. The simple derivatives including **4** and the reversed agents **17–20** both require extended reaction times (2--7 days, 25–37 °C) for substantial or complete alkylation with **17–20** being only marginally faster and ultimately 10–100× more efficient. These small differences can be attributed to the more effective noncovalent minor groove binding properties of **17–20**. The larger 10^3–10^4 rate differences between **1–3** and **17–20** may be attributed to the DNA binding-induced conformational change uniquely imposed on **1–3** and related agents. In the absence of the extended right-hand subunit, DNA minor groove binding no longer requires an induced twist in the N^2 amide linkage depriving the agent of this additional activation toward DNA alkylation.

Cytotoxic Activity. The *in vitro* cytotoxic activity of the agents is summarized in FIG. 14. Several important trends were observed which parallel the observations made in the DNA alkylation studies. Foremost, the natural enantiomers of the reversed analogs were 100–1000× less potent than the corresponding extended analogs while the two sandwiched analogs **30** and **31** were essentially equipotent with the typical agents. The reversed analogs proved essentially indistinguishable (**17, 18, 23**) or less than 10×

more potent (**19, 20**) than the simple derivatives, *N*-BOC-DSA (**4**) and *N*-Ac-DSA, that lack DNA binding subunits altogether. This is analogous to the observations made in the DNA alkylation studies where **17–20** and **23–24** were found to alkylate DNA with a rate and efficiency similar to those of **4** rather than **1–3**. Consistent with the trends observed in the DNA alkylation studies, the unnatural enantiomers of the agents generally were approximately 10× less potent than the natural enantiomers. The exceptions to this generalization are DSA-$CDPI_2$, $CDPI_2$-DSA, and the sandwiched analogs where the two enantiomers proved nearly equipotent.

Like the natural enantiomers, the unnatural enantiomers of the reversed agents were also much less potent than the corresponding unnatural enantiomers of the extended analogs although the magnitude of the differences was somewhat smaller (20–100× versus 100–1000×). However, they proved to be even more comparable in potency to the unnatural enantiomers of *N*-BOC-DSA (**4**) and *N*-Ac-DSA lacking the attached DNA binding subunits. The nature of the terminal N^2 acyl substituent did not alter these observations in a substantial manner. The corresponding natural and unnatural enantiomers of **18** and **23** proved essentially indistinguishable while **24** was noticeably less potent. This latter effect could be anticipated given the remarkable stability of the alkylation subunits lacking a N^2 acyl substituent and the resulting less effective DNA alkylation. Thus, consistent with the trends observed in the rates and efficiencies of DNA alkylation and independent of the nature of the simple N^2 substituent, the reversed analogs proved comparable in cytotoxic potency to the simple derivatives **4** and *N*-Ac-DSA lacking the DNA binding subunits rather than **1–3** and the related extended analogs.

The potent cytotoxic activity of the sandwiched analogs is observed with a class of agents that exhibit a significantly different selectivity of DNA alkylation than preceding agents and one which is the same for both the natural and unnatural enantiomers. Since both enantiomers are essentially equipotent and exhibit the same DNA alkylation selectivity, this could permit the use of the more readily available racemic agents in the development of potential clinical candidates with confidence that both enantiomers contribute productively and equivalently to the expression of the resulting properties.

The cytotoxic activities of the more potent, extended derivatives plateau at 3–4

pM and closely follow established trends relating chemical stability and cytotoxic potency. Since the duocarmycin SA alkylation subunit is among the most stable examined to date, the cytotoxic activity of such analogs is among the most potent yet described.

The seco precursor agents, *e.g.* **13–16**, **22**, **28** and **29**, exhibited cytotoxic activity that was not distinguishable from the corresponding cyclopropane containing agents **17–20**, **23**, **30** and **31**, respectively, indicating that their spirocyclization to the biologically potent agents under the conditions of assay is not limiting.

Conclusions. A number of key features contribute to the sequence selective DNA alkylation by members of this class of agents. The reaction constitutes nucleophilic addition of the most sterically accessible of the two most nucleophilic sites in the minor groove (adenine N3 versus guanine N3). The clean regioselectivity for exclusive addition to the least substituted cyclopropane carbon represents the stereoelectronically-preferred site of attack which is further reinforced by the destabilizing torsional and steric interactions that would accompany addition to the more substituted carbon with ring expansion and is characteristic of S_N2 addition of a hindered nucleophile. Consistent with the noncovalent binding model, the length-dependent AT-rich alkylation selectivity is derived from the preferential noncovalent binding selectivity of the agents in the deeper, narrower AT-rich minor groove. The reverse and offset AT-rich alkylation selectivity of the enantiomers and the switch in the inherent enantiomeric alkylation selectivity of the reversed analogs establish that both enantiomers are subject to the same polynucleotide recognition features. Finally, a DNA binding-induced conformational change in the agent induces a twist in the linking N^2 amide resulting in loss of the alkylation subunit vinylogous amide stabilization catalyzing the DNA alkylation reaction. Since the binding-induced conformational change is greatest within the narrower, deeper AT-rich minor groove, this leads to selective catalysis within the preferred binding sites. An important ramification of the binding-induced substrate ground state destabilization is that it further serves to stabilize the inherently reversible DNA alkylation reaction.

This alternative source of catalysis for the DNA alkylation reaction explains a number of observations. It is consistent with the lack of a substantial pH dependence on the rate of reaction and explains the growing number of instances where the rates of

DNA alkylation were not found to follow the relative rates of acid-catalyzed reactivity. It explains the extraordinarily slow DNA alkylation rates of the reversed analogs and suggests that the small differences between the reversed analogs and simple derivatives such as **4** constitute those attributable to the enhanced minor groove binding. The remaining larger differences between the reversed analogs and the typical agents, and thus the bulk of the distinctions between **1–3** and **4–6**, constitute the catalysis derived from the DNA binding-induced conformational change in the agent. It is consistent with the well established view that the unusual stability of the agents is derived from the vinylogous amide conjugation and that its disruption should lead to significant increases in reactivity. Moreover, it offers new insights into the reversibility of the DNA alkylation reaction and suggests that both the rate of retroalkylation and the reaction equilibrium is shifted to favor adduct formation through a binding-induced destabilization of the substrate ground state. It explains the important effects of selected substituents that are located in the minor groove of the bound agents, *e.g.* duocarmycin SA C6-CO_2Me and C5′-OMe, and even offers a new insight into the origin of the distinctions between the enantiomers of the typical agents such as **1–3**. This shape selective catalysis coincides within the preferred noncovalent binding sites. That the sequence selectivity is controlled by the noncovalent binding selectivity is defined by the fact that the identical selectivities are observed with agents not subject to this source of catalysis including the reversed analogs albeit with alkylation at much slower rates.

B. Shortened and Extended Analogs

DNA Alkylation Efficiency and Selectivity. The DNA alkylation properties of the agents were examined within five 145–155 base-pair segments of DNA. The five clones of phage M13mp10 contain SV40 nucleosomal DNA inserts: w794 (nucleotide no. 5238–138) and its complement w836 (nucleotide no. 5189–91), c988 (nucleotide no. 4359–4210) and its complement c820 (nucleotide no. 4196–4345), and c1346 (nucleotide no. 1632–1782). The alkylation site identification and the assessment of the relative selectivity among the available sites were obtained by thermally-induced strand cleavage of the singly 5′ end-labeled duplex DNA after exposure to the agents. A statistical treatment of the alkylation sites proved more revealing than a conventional analysis that considers only the observed alkylation sites. This evaluation that includes the consideration of sites *not* alkylated helped define the composite consensus sequence

and highlighted subtle features not apparent from a simple consideration only of the alkylated sites.

Simple Derivatives of the Alkylation Subunit. The consensus alkylation selectivity of both enantiomers of **40** and **41** alongside *N*-BOC-DSA (**39**) and (+)-duocarmycin SA is summarized in Table 3. First and foremost, the simple derivatives are much less efficient (10^3–10^4×) and exhibit a different and less selective DNA alkylation selectivity than duocarmycin SA. Like **39**, both enantiomers of **40** and **41** alkylate the same sites exhibiting an identical two base-pair AT-rich alkylation selectivity (5′-A<u>A</u> > 5′-T<u>A</u>) although there are subtle differences in the relative efficiencies of alkylation at the individual sites. The apparent preference of 5′-A<u>A</u> > 5′-T<u>A</u> is purely statistical and the complementary unlabeled strand for the mixed sequence contains an identical 5′-TA site whose competitive alkylation diminishes the apparent alkylation efficiency of the labeled strand. Importantly, significant distinctions in the alkylation selectivities of such simple derivatives (BOC = $COCH_3$ = CO_2CH_3) were not seen: they are all much less selective than **1–3**. The identical alkylation selectivity of both enantiomers of such simple derivatives is a natural consequence of the reversed binding orientations and the diastereomeric relationship of the adducts that result in the two enantiomers covering the exact same binding site surrounding the alkylated adenine. The factors controlling the alkylation selectivity are simply reaction at the sterically most accessible of the two most nucleophilic minor groove sites (adenine N3 versus guanine N3) and the depth of minor groove penetration available to the agent at the binding region surrounding the alkylation site. For simple derivatives including **39–41**, this is possible only when the adjacent 5′ base is A or T.

The distinctions between the agents lie in the efficiencies of DNA alkylation. The natural enantiomers of **40** and **41** alkylate DNA at 10^{-3} M and were approximately 10× more efficient than (+)-*N*-BOC-DSA. The similarities in **40** and **41** and the less effective DNA alkylation by *N*-BOC-DSA suggest that the differences simply may be due to the size of the substituent. The unnatural enantiomers of **40** and **41** were approximately 10× less effective at alkylating DNA while the relative distinctions between (+)- and *ent*-(–)-*N*-BOC-DSA were smaller. In addition to the much higher concentrations (10^3–10^4×) required to detect alkylation with **39–41**, it also requires much more vigorous reaction conditions (37 °C, 24 h versus 4 °C, 2–10 h). These data

suggest that in the absence of the extended right-hand subunit, DNA minor groove binding does not induce a twist in the N^2 amide and deprives the agent of this activation toward DNA alkylation.

Modifications in the Trimethoxyindole Subunit: Role of the Methoxy Substituents. DNA alkylation by the natural enantiomers of **53–56** were compared with that of **1** in w794 DNA. All five agents exhibited identical DNA alkylation selectivities and the distinctions observed were in the rates and efficiencies. When the incubation was conducted at 25 °C for 24 h, **54** was found to be essentially indistinguishable from **1** itself, **55** and **56** (**55**> **56**) were 5–10× less efficient than **1**, and **53** was 20× less efficient than **1** (Table 5). These trends in the efficiency of DNA alkylation were found to parallel the relative trends in cytotoxic potency. The relative rates of DNA alkylation for **1**, **54**, and **53** (10^{-5} M, 25 °C, 1–72 h) were also examined within w794 DNA at the single high affinity site of 5′-d(AATTA). (+)-Duocarmycin SA (**1**) and **54** were nearly indistinguishable with **1** exhibiting a slightly faster rate (k_{rel} = 1.3–2.3) and both were substantially faster than **53** (k_{rel} = 18–33).

Similar observations were made with the unnatural enantiomers (FIG. 15). Consistent with past observations, they all were found to alkylate DNA with a slower rate (*ca.* 50×)[7] and lower efficiency (*ca.* 10×) than the corresponding natural enantiomer. Detection of alkylation required both higher agent concentrations (10–50×) and longer reaction times (72 versus 24 h). The distinctions between enantiomeric pairs of agents diminished as the number of methoxy groups were reduced and were greatest when the C5 methoxy group was present.

Thus, the C7 and C6 methoxy groups, which lie on the outer face of the DNA-agent complex, individually contribute little (C6 > C7) to the properties of duocarmycin SA. In contrast, the C5 methoxy group that is deeply imbedded in the minor groove contributes prominently to its properties. The agent containing a single C5 methoxy substituent proved essentially indistinguishable from duocarmycin SA indicating that it alone is sufficient for observation of the full potency of the natural product. This is consistent with a role in which the C5 methoxy group provides further noncovalent binding stabilization for the inherently reversible DNA alkylation reaction by virtue of its placement deep in the minor groove. More importantly, the C5 methoxy group of duocarmycin SA extends the rigid length of the DNA binding subunit. Its presence

results in an increase in the inherent twist in the helical conformation of the DNA bound agent with the helical rise of the agent adjusted at the site of linking amide. This alters the vinylogous amide conjugation in the alkylation subunit and increases the inherent reactivity of the agent contributing to the catalysis of the DNA alkylation reaction. Removing the C5 methoxy substituent shortens the length of the right-hand subunit, decreases the inherent twist in the linking amide in the DNA bound conformation, and results in less effective activation of the agent for DNA alkylation.

Additional subtle features that were revealed include the unusual DNA alkylation efficiency of (+)-DSA-indole$_1$ (**53**). Although it proved to be 6–10× less effective than duocarmycin SA, it is comparatively more effective than the indole derivative of CPI[20] or CBI.[7] Moreover, the relative DNA alkylation rates of the DSA-based agents substantially exceed those of the corresponding CPI-based agents despite their reduced reactivities. This is likely due to the presence of the C6 methyl ester which similarly extends the rigid length of the alkylation subunit. Consequently, even with a short suboptimal right-hand subunit, the presence of the C6 methyl ester insures more effective activation for DNA alkylation.

Extended Analogs: DSA-CDPI$_1$, DSA-CDPI$_2$, and DSA-indole$_2$. The examination of the agents **60-62** proved more important in our studies than anticipated. Their side-by-side comparison with the reversed analogs detailed in the accompanying paper not only provided a definitive demonstration of the origin of the DNA alkylation selectivity, but also provided insights into the the source of catalysis. Under the conditions of the assay, **60-62** alkylated DNA at concentrations as low as 10^{-6}–10^{-7} M and did so with essentially the same efficiency. The consensus alkylation sequences for (+)- and *ent*-(–)-DSA-CDPI$_2$ are summarized in FIG. 16. Without exception, all alkylation sites proved to be adenine under the conditions of the assay. Each adenine alkylation site was flanked by at least two 5′ A or T bases with a preference that follows the order of 5′-AA<u>A</u> > 5′-TT<u>A</u> > 5′-TA<u>A</u> ≥ 5′-AT<u>A</u>. There was also a strong preference for the fourth and fifth 5′ bases to be A or T, and this preference distinguished the high affinity versus low affinity alkylation sites. Consistent with expectations, (+)- and *ent*-(–)-DSA-CDPI$_2$ exhibited a 5 base-pair AT-rich DNA alkylation selectivity identical to those of (+)- and *ent*-(–)-CC-1065 and distinguishable from the shorter 3.5 base-pair AT-rich selectivity of duocarmycin SA. Similar

observations were made with (+)-DSA-indole$_2$. The relative selectivity of alkylation among the available sites proved to be greater with (+)-DSA-CDPI$_2$ than (+)-DSA-CDPI$_1$. Characteristic of this enhanced selectivity, (+)-DSA-CDPI$_2$ failed to alkylate the minor w794 site (5′-CAAAG) while (+)-DSA-CDPI$_1$ prominently alkylates this minor site, requiring concentrations only 10× that for alkylation at the major 5′-AATTA site.

The alkylation profiles of the unnatural enantiomers **60-62** are very distinct from those of the natural enantiomers. Without exception, all alkylation sites proved to be adenine under the conditions of the assay and nearly all of the 3′ and 5′ bases flanking the adenine N3 alkylation site proved to be A or T (FIG. 16). There proved to be a preference for the following three base-pair sequences: 5′-AAA > 5′-AAT ≥ 5′-TAA > 5′-TAT. The high affinity alkylation sites, *e.g.* 5′-AATTT, each proved consistent with 5′ adenine alkylation, agent binding in the minor groove in the 5′→3′ direction from the alkylation site covering 3.5 or 5 base-pairs across an AT-rich region. The unnatural enantiomer AT-rich alkylation selectivity relative to the adenine N3 alkylation site is reversed and offset from that observed with the natural enantiomers. Consistent with expectations, *ent*-(–)-DSA-CDPI$_2$ exhibited a 5 base-pair AT-rich alkylation selectivity identical to *ent*-(–)-CC-1065 readily distinguishable from the shorter 3.5 base-pair selectivity of *ent*-(–)-duocarmycin SA and related smaller agents (FIG. 16). The unnatural enantiomers also exhibited a slower rate and lower efficiency (10–100×) of DNA alkylation than the corresponding natural enantiomer.

Thus, the results show that the depth of minor groove penetration by the agent and steric accessibility to the alkylation site are likely important features contributing to the observed selectivity of DNA alkylation. For simple derivatives of the alkylation subunit, sufficient minor groove access to the reacting center is possible with a single 5′ A or T base adjacent to the alkylation site. For the extended agents including **60-62**, sufficient minor groove penetration may be possible only when two or more adjacent bases are A or T and this AT-rich selectivity nicely corresponds to the size of the agent (FIG. 16). Further contributing to this AT-rich alkylation selectivity of the longer agents is their preferential noncovalent binding within the narrower, deeper AT-rich groove.

Rate of DNA Alkylation: pH Dependence. The effects of pH on the DNA

alkylation rate were studied by establishing the (+)-duocarmycin SA relative and first order rate constants (k_{obs}) for alkylation of the single w794 high affinity alkylation site (5′-AATTA,) at the pH of 6.0, 6.6, 7.1, 7.6, and 8.1 (10^{-6} M, 25 °C, 10 mM phosphate buffer, 0–3 h). Because this was conducted using w794 DNA additionally containing >7000 base-pairs and multiple binding sites within the unlabeled portion of the DNA, the comparisons were conducted at concentrations that provide saturated binding and restrict the kinetic analysis to the pseudo-first order rate constant for alkylation. Although the rate of DNA alkylation was found to increase with decreasing pH, the rate change was small (< 2× over 2 pH units) and inconsistent with a first order dependence on acid concentration. Moreover, between pH 7 and 8 which may be considered the most relevant range, the rate dependence on pH essentially disappeared. Just as significant, comparison of the psuedo-first order rate constant for DNA alkylation at this site, $k = 1.69 \times 10^{-4}$ s^{-1} (pH 7.1), with the calculated pseudo-first order rate constant for acid-catalyzed solvolysis ($k = 1.08 \times 10^{-10}$ s^{-1}) at pH 7 revealed that the bulk of catalysis for the DNA alkylation reaction cannot be accounted for by this source. Perhaps the magnitude of this difference is best recognized by simply stating that at pH 7, the $t_{½}$ for solvolysis is 202 years (7.4×10^4 days) while that of DNA alkylation is 1.1 h. The relative lack of dependence on the acid concentration (pH) especially in the most relevant pH range of 7–8 in conjunction with the observations made in the accompanying paper has led us to propose an alternative source of reaction catalysis.

Catalysis: DNA Binding Induced Conformational Change in the Agent Results in Activation. Studies of the extent and structural origin of the rate acceleration for the DNA alkylation reaction have led to the proposal that catalysis for the DNA alkylation reaction is derived from a DNA binding-induced conformational change in the agent that disrupts the vinylogous amide stabilization of the alkylation subunit and activates the agent for nucleophilic addition. This conformational change results from adoption of a helical bound conformation that follows the curvature and pitch of the DNA minor groove. The helical rise in the bound conformation of the rigid agents is adjusted by twisting the linking N^2 amide which is the only available flexible site. The twisting of the χ_1 dihedral angle of the linking amide (χ_2 ~0°) diminishes the N^2 lone pair conjugation with the cyclohexadienone, disrupts the vinylogous amide stabilization of the alkylation subunit, and increases its inherent reactivity. An

alternative possibility involves a twisting of the χ_2 dihedral angle diminishing the amide conjugation and increasing the N^2 vinylogous amide conjugation. This would increase the basicity of the C4 carbonyl leading to more effective protonation. There is evidence to suggest this can result in both increased or decreased reactivity depending on the extent of the vinylogous amide conjugation and all studies concur that even subtle perturbations can result in large changes in reactivity.

N-Acylation of the nitrogen (*e.g.* *N*-CO_2Me-CNA versus CNA) reduces the vinylogous amide conjugation, lengthens bond c, and results in a substantial increase in inherent reactivity. Typically accompanying this reduction in the vinylogous amide conjugation is an increase in the length of the reacting cyclopropane bond. One interpretation of this is that both the cyclopropane conjugation and its inherent reactivity increase as the cross-conjugated vinylogous amide π-overlap is diminished. Additional features including the alignment of the cyclopropane may further contribute to the cyclopropane conjugation (CBQ aligned but CBI offset by 20°) and the cyclopropane bond lengths and reactivity of CBQ versus CBI also reflect this effect on the relative degree of conjugation. More importantly, within the series of *N*-acyl derivatives, both the length of bond c diagnostic of the extent of vinylogous amide conjugation and the reactivity smoothly increase as the χ_1 dihedral angle increases. The reactivity of *N*-CO_2Me-CNA (or *N*-BOC-CNA) is extraordinary exhibiting a $t_{1/2}$ of only 2.1 h at pH 7 in the absence of deliberate added acid catalysis. It is 10^3–10^4× more reactive than *N*-BOC-DSA and represents an agent that benefits from little, if any, vinylogous amide stabilization. This level of reactivity is greater than that required. In fact, it is the reactivity and χ_1 dihedral angle of *N*-BOC-CBQ that may more closely approximate that required for the DNA alkylation catalysis provided by the DNA binding induced conformational change in **1–3**. Its inherent reactivity at pH 7 coupled with the rate enhancements afforded a bound species that might provide a further 10^2× rate acceleration approximates the rates observed with the DNA alkylation reaction.

This has important ramifications on the source of the DNA alkylation selectivity. The inherent twist and helical rise of the bound conformation of the agent is greatest within the narrower, deeper AT-rich minor groove. This leads to preferential activation of the agent for DNA alkylation within extended AT-rich minor groove sites and complements their preferential AT-rich noncovalent binding selectivity. Thus, both

shape-selective recognition (preferential AT-rich noncovalent binding) and shape-dependent catalysis (extended AT-rich > GC-rich activation by twist in N^2 amide) combine to restrict S_N2 alkylation to accessible adenine N3 nucleophilic sites within the preferred binding sites. Importantly, this ground state destabilization of the substrate only activates the agent (*e.g.*, arms the warhead) for a rate determining S_N2 nucleophilic addition and requires the subsequent proper positioning and accessibility to an adenine N3 site. Although a subtle point, this accounts nicely for the identical alkylation selectivities of CC-1065 (**3**) and **63–67** which lack both the C4 carbonyl and the activated cyclopropane but which alkylate DNA at substantially slower rates. Thus, the alkylation selectivity is controlled by the identical AT-rich noncovalent binding selectivity of the agents, but **63–67** react much slower in part because they lack the capabilities for activation by the DNA binding-induced conformation change.

This source of catalysis requires an extended and rigid N^2 amide substituent and the absence of such a substituent with **39–41** accounts nicely for their relatively slow and ineffective DNA alkylation. The noncovalent binding derived from the attached right-hand subunits accounts for a much smaller part of the difference in the rates of DNA alkylation between **39–41** and **1**. More importantly, this source of catalysis would lead to distinctions, not similarities, in the DNA alkylation selectivities of **39-41** versus **1.**

Reaction Regioselectivity and Stereochemistry: Subtle Features Contributing to the DNA Alkylation Regioselectivity. Studies of the inherent solvolysis regioselectivity and stereochemistry in conjunction with the structural studies have also provided important insights into the mechanism of nucleophilic addition and subtle features contributing to the regioselectivity of the DNA alkylation reaction. A study of the acid-catalyzed nucleophilic additions to *N*-BOC-DSA (**39**) established that solvolysis preferentially occurs with cleavage of the C7b–C8 bond with addition of a nucleophile to the least substituted C8 cyclopropane carbon versus cleavage of the C7b–C8a bond with ring expansion and addition to C8a. The latter cleavage would place a developing partial positive charge on a preferred secondary versus primary center and this preference was overridden by the inherent stereoelectronic control of the reaction regioselectivity. Preparative acid-catalyzed addition of CH_3OH to *N*-BOC-DSA (0.12 equiv CF_3SO_3H, 0.01 M in CH_3OH, 0 or 25 °C, 1–3 h, 88–93%) cleanly

provided two products **66** and **67** in a 6.5–4:1 ratio with the greater selectivity observed at 0 versus 25 °C (Scheme 5). Similarly, solvolysis of **39** (0.24 equiv CF_3SO_3H, 0.01 M in 20% H_2O–THF, 25 °C, 48 h, 95–96%) provided a 6:1 ratio of **35** to **68**. The mechanistic course of the reaction was established by subjecting both racemic and natural (+)-**39** to the acid-catalyzed methanolysis or solvolysis. Resolution on a Diacel ChiralCel AD HPLC column separated both enantiomers of the two reaction products and those derived from optically active (+)-**39** were found to consist of a single enantiomer. Although the generation of a single enantiomer of **66** would be consistent with either a S_N1 or S_N2 ring opening reaction, the generation of a single enantiomer of **67** establishes that the ring expansion proceeds with clean inversion of the reaction center stereochemistry in a S_N2 reaction. This is consistent with kinetic studies of the acid-catalyzed nucleophilic addition where the rate of reaction exhibits a first order dependence on both the acid concentration (pH) as well as the nucleophile indicative of a mechanism involving rapid and reversible C4 carbonyl protonation followed by a slow, rate determining S_N2 nucleophilic attack on the activated cyclopropane.

Important insights into the solvolysis regioselectivity may be derived from the structural studies. The distinguishing feature controlling the regioselectivity appears to be the relative stereoelectronic alignment of the two cyclopropane bonds available for cleavage. Within a class of agents whose cyclopropane alignment with the π-system would be expected to be similar due to structural constraints, the regioselectivity nicely follows the reactivity with the more stable agents providing the more selective reaction: *e.g.* *N*-BOC-DSA (6–4:1) > CPI (4:1) > *N*-BOC-DA (3:2). However, this fails to hold true when comparing between classes of agents: *e.g.* *N*-BOC-CBI (≥20:1) versus *N*-BOC-DSA (6–4:1) versus *N*-BOC-CNA (≤1:20). Thus, additional important factors contribute to this reaction regioselectivity. In the comparisons that can be made from the available X-ray structures, the selectivity more accurately reflects the relative degree of stereoelectronic alignment of the two available cyclopropane bonds and this alone accounts for the reaction regioselectivity. This is illustrated beautifully with the observation of the clean, smooth, and complete reversal of the reaction regioselectively as one progress through the series *N*-BOC-CBI (≥20:1), *N*-BOC-CBQ (3:2), and *N*-BOC-CNA (≤1:20).

The observation of exclusive adenine N3 addition to the C8 cyclopropane

carbon in the DNA alkylation studies of **1** and related agents is not consistent with expectations that the inherent acid-catalyzed nucleophilic addition regioselectivity controls the DNA alkylation regioselectivity. This exclusive DNA alkylation regioselectivity was not only observed in our studies with **1** or **2** and their enantiomers but is general with all agents examined to date that undergo solvolysis with a mixed regioselectivity including the CPI-based agents and CC-1065 (4:1 regioselectivity) and the CBQ-based agents (3:2 regioselectivity). Examination of each of these agents has led only to detection of adducts derived from adenine N3 addition to the least substituted cyclopropane carbon. Moreover, each of these studies quantitated the adduct formation and, in the case of duocarmycin A (86–92%), duocarmycin SA (95–100%) CC-1065 (> 85%), and the CBQ-based agents (>75%), established that the regioselectivity of the DNA alkylation reaction is greater than that of solvolysis. Although several explanations may be advanced for these observations, the three most prominent are preferential adoption of binding orientations that favor normal adenine N3 addition (proximity effects), the adoption of DNA bound conformations that impose full stereoelectronic control on the reaction, and the significant destabilizing torsional strain and steric interactions that accompany the abnormal addition. The data reported herein show that the latter subtle effect of preferential S_N2 addition of a large nucleophile to the least substituted carbon is likely most substantial. Consequently, the clean regioselectivity of the characteristic adenine N3 alkylation reaction benefits not only from stereoelectronic control but additional important subtle effects characteristic of the S_N2 addition of a large nucleophile that further enhance the normally observed regioselectivity.

Reversibility. The cyclopropane ring of the duocarmycins is very easily introduced through Ar-3′ spirocyclization. This occurs so readily that the precursor agents will often close upon formation or upon exposure to chromatography supports (*e.g.*, SiO_2). Although the reactions are usually conducted with strong base (NaH, DBU, Et_3N), the most stable of the agents including **35** may be prepared by simple exposure to even aqueous 2–5% $NaHCO_3$. The present studies show that the adoption of the DNA bound and alkylated conformation no longer facilitates Ar-3′ spirocyclization with reversal of the DNA alkylation reaction and that this further contributes to the unusual stability of the DNA adducts. Not only does this ground state

destabilization of the substrate account for the rate acceleration for formation of adduct by lowering the apparent activation energy but it contributes to a shift in the equilibrium to favor adduct formation since the product does not contain the vinylogous amide and is not similarly destabilized by adopting a helical conformation. This subtle feature is likely more important to the expression of the biological properties than even the role in catalysis.

DNA Alkylation Studies: Selectivity and Efficiency. Eppendorf tubes containing singly ^{32}P 5′-end-labeled double-stranded DNA (9μL) in TE buffer (10 mM Tris, 1 mM EDTA, pH 7.5) were treated with the agents in DMSO (1 μL, at the specified concentrations). The solutions were mixed by vortexing and brief centrifugation and subsequently incubated at 4 °C, 25 °C or 37 °C for 24–72 h. The covalently modified DNA was separated from unbound agent by EtOH precipitation of the DNA. The EtOH precipitations were carried out by adding *t*-RNA as a carrier (1 μL, 10 μg/μL), 3 M NaOAc (0.1 volume) and –20 °C EtOH (2.5 volumes). The solutions were mixed and chilled at –78 °C in a REVCO freezer for 1 h or longer. The DNA was reduced to a pellet by centrifugation at 4 °C for 15 min and washed with –20 °C 70% EtOH (in TE containing 0.2 M NaCl). The pellets were dried in a Savant Speed Vac concentrator and resuspended in TE buffer (10 μL). The solutions of alkylated DNA were warmed at 100 °C for 30 min to induce cleavage at the adenine N3 alkylation sites. After brief centrifugation, formamide dye solution (5 μL) was added. Prior to electrophoresis, the samples were denatured by warming at 100 °C for 5 min, placed in an ice bath, centrifuged briefly, and the supernatant (2.8 μL) was loaded onto a gel. Sanger dideoxynucleotide sequencing reactions were run as standards adjacent to the agent treated DNA reaction samples. Polyacrylamide gel electrophoresis (PAGE) was run on an 8% sequencing gel under denaturing conditions (19:1 acrylamide: *N,N*-methylenebisacrylamide, 8 M urea) in TBE buffer (100 mM Tris, 100 mM boric acid, 0.2 mM Na_2EDTA). PAGE was pre-run for 30 min with formamide dye solution prior to loading the samples. Autoradiography of dried gels was carried out at –78 °C using Kodak X-Omat AR film and a Picker Spectra™ intensifying screen.

Relative Rates of DNA Alkylation for (+)-1, 53, and 54. Following the procedure detailed above, Eppendorf tubes containing 5′ end-labeled w794 DNA (9 μL) in TE buffer (pH 7.5) were treated with (+)-duocarmycin SA, **53**, or **54** (1 μL, 10^{-5} M in

DMSO). At these concentrations (10^{-4}–10^{-6} M), the rate of DNA alkylation was independent of agent concentration indicating saturated binding. The solutions were mixed and incubated at 25 °C for 1, 3, 6, 12, 24, 48, and 72 h, respectively. Subsequent isolation of the alkylated DNA by EtOH precipitation, resuspension in TE buffer (10 μL, pH 7.5), thermolysis (30 min, 100 °C), concurrent PAGE, and autoradiography were conducted as detailed above. The relative rate for the alkylation at the 5′-AATTA site was derived from the slopes of the plots of percent integrated optical density (IOD) of the high affinity alkylation site cleavage bands versus time.

Relative Rates of DNA Alkylation for (+)-1 at pH 6–8. Eppendorf tubes containing 5′ end-labeled w794 DNA (9μL) in phosphate buffer (10 mM) at pH 6.0, 6.6, 7.1, 7.6, and 8.1 were prepared. The solutions at each pH were treated with (+)-duocarmycin SA (1 μL, 10^{-6} M in DMSO), mixed and incubated at 25 °C for 0.5, 1.0, 1.5, 2.0 and 3.0 h. At this concentration (10^{-4}–10^{-6} M), the rate of DNA alkylation was independent of agent concentration indicating saturated binding. The reactions were stopped at each time interval by EtOH precipitation of the DNA. The alkylated DNA was resuspended in TE buffer (10 μL, pH 7.5) and heated at 100 °C for 30 min follwed by PAGE and autoradiography as detailed above.

Conclusions. Of the naturally occurring agents, duocarmycin SA is chemically the most stable and biologically the most potent. It exhibits the greatest inherent reaction regioselectivity and participates most effectively in the characteristic DNA alkylation reaction. The comparison of six X-rays structures suggest that the relative degree of stereoelectronic alignment of the two available cyclopropane bonds alone may account for the solvolysis regioselectivity. The exclusive DNA alkylation regioselectivity of the adenine N3 addition reaction exceeds that of the typical acid-catalyzed reactions for all agents examined to date. Several explanations may account for the observations including the adoption of binding orientations that favor the normal addition, the adoption of DNA bound conformations that impose complete stereoelectronic control on the reaction, and the destabilizing torsional strain and steric interactions that accompany the abnormal addition. The latter effects are most significant and simply represent the expected preferential S_N2 addition of a large, hindered nucleophile to the least substituted 2° versus 3° carbon of the activated cyclopropane.

The DNA alkylation selectivity of both enantiomers of a series of analogs of **1** were examined and proved consistent with prior studies. Both enantiomers of simple derivatives of the alkylation subunit (**39–41**) behave comparably and alkylate the same sites in DNA (5′-A<u>A</u> > 5′-T<u>A</u>). This unusual behavior of the enantiomeric agents is a natural consequence of the reversed binding orientations and the diastereomeric relationship of the adducts that result in the two enantiomers covering the exact same binding site surrounding the alkylated adenine. The advanced analogs of **1–3** exhibited a different and larger 3.5 or 5 base-pair AT-rich adenine N3 alkylation selectivity that corresponds nicely to the length or size of the agent. For the natural enantiomers, the alkylation sites correspond to 3′ adenine N3 alkylation with agent binding in the 3′→5′ direction across a 3.5 or 5 base-pair AT-rich sequence, *e.g.* 5′-AAAA<u>A</u>. For the unnatural enantiomers, the alkylation sites correspond to 5′ adenine N3 alkylation with agent binding in the reverse 5′→3′ direction across a 3.5 or 5 base-pair AT-rich sequence that starts with the 5′ base that precedes the alkylated adenine and extends over the alkylation site to the adjacent 3′ side, *e.g.* 5′-A<u>A</u>AAA.

A study of the pH dependence of the rate of DNA alkylation revealed little effect in the pH range of 7–8 and only a modest effect below pH 7. This proved consistent with recent observations that the rate of DNA alkylation does not necessarily follow the relative rates of acid-catalyzed nucleophilic addition. As a consequence of this and consistent with the emerging model of the origin of the DNA alkylation selectivity, an alternative mechanism of activating the agent for DNA alkylation was introduced based on a DNA binding-induced conformational change in the agent which twists the linking N^2 amide and disrupts the vinylogous amide stabilization of the alkylation subunit. Further support of this mechanism of activation is provided in the accompanying article. An important consequence of this source of activation is that it is expected to be greatest within the narrower, deeper AT-rich minor groove further complementing the noncovalent minor groove binding selectivity of the agents. Thus, the shape-selective binding selectivity and shape-dependent catalysis combine to restrict S_N2 alkylation to accessible adenine N3 nucleophilic sites within the preferred 3.5–5 base-pair AT-rich binding sites.

The study of analogs containing modifications in the trimethoxyindole subunit revealed that the C5 methoxy substituent is necessary and sufficient for observation of

the full effectiveness of the natural product while the C6 and C7 (C6 > C7) methoxy substituents contribute little to its properties. In addition to its contribution to the noncovalent binding stabilization derived from its imbedded minor groove location, its simple presence increases the rigid length of the right-hand subunit increasing the inherent twist in the DNA bound helical conformation. This more effectively disrupts the vinylogous amide stabilization in the alkylation subunit and further increases the inherent reactivity of the DNA bound agent. A similar role is proposed for the C6 methyl ester which extends the rigid length of the left-hand alkylation subunit.

The agents exhibited cytotoxic potencies consistent with the trends observed in the relative DNA alkylation efficiencies and each of the analog classes was found to follow a well-established relationship between chemical stability and cytotoxic potency. Since the duocarmycin SA alkylation subunit is the most stable of the naturally occurring alkylation subunits, its derivative analogs are the most potent disclosed to date. These studies are summarized in the accompanying article.

C. AnalogsContaining a Modified Heterocycle

Chemical Solvolysis: Reactivity. Both the study of the rate of acid-catalyzed solvolysis and the regioselectivity of cyclopropyl ring opening have proven to be key to understanding of the structural features that dictate the properties of the duocarmycin and CC-1065 alkylation subunits. Comparison of the rate of solvolysis allows for the identification of the functional features that contribute to the stabilization or activation of the cyclopropane while studies regarding the regioselectivity of the acid-catalyzed ring opening have proven key to understanding the mechanism of the DNA alkylation reaction. To date, the preferred nucleophilic addition sites appear to be dictated by the relative stereoelectronic alignment of the scissile cyclopropyl bonds with the cyclohexadienone π-system but may be influenced by the relative reactivity. Moreover, both S_N2 and S_N1 mechanisms have been advanced to account for the generation of the abnormal ring expansion solvolysis products. In instances of mixed reaction regioselectivity, the clean generation of single DNA alkylation products derived from adenine N3 addition exclusively to the least substituted cyclopropane carbon indicates that additional subtle features inherent in the reaction contribute to its regioselectivity.

The solvolysis reactivities of *N*-BOC-CNA (**78**) and CNA (**79**) were followed spectrophotometrically by UV at both pH 3 (50% CH_3OH–buffer, buffer = 4:1:20 v/v/v

0.1 M citric acid, 0.2 M Na_2HPO_4, H_2O) and pH 7 (50% CH_3OH–H_2O). The reactivity of both **78** ($t_{1/2}$ = 1.7 min at pH 3) and **79** ($t_{1/2}$ = 37 min at pH 3) proved remarkable. CNA (**79**) was considerably more stable than *N*-BOC-CNA (**78**). Both were sufficiently reactive to undergo rapid solvolysis even at pH 7. Comparison of the solvolytic reactivity of *N*-BOC-CNA with representative prior analogs reveal a reactivity that is between that of *N*-BOC-CBQ and the exceptionally reactive *N*-BOC-CI. Particularly informative are comparisons of the benzo series of agents that differ only in the C-ring size (*i.e.*, **76–79**). Solvolysis reactivity smoothly increases through the series CBI < CBQ < CNA with both the *N*-BOC derivatives and the free NH derivatives. The reactivity of both *N*-BOC-CNA and CNA proved to be 4750 and 1500× more reactive than the corresponding CBI derivatives. Moreover, *N*-BOC-CNA exhibited a first-order rate constant for the solvolysis at pH 7 which is of the same order of magnitude as the characteristically rapid DNA alkylation reactions of **1–3** without deliberate added catalysis. The agents containing the free NH, and thus the greatest degree of vinylogous amide conjugation, were 10–40× more stable to solvolysis than the corresponding *N*-BOC derivatives.

Chemical Solvolysis: Regioselectivity and Mechanism. Treatment of *N*-BOC-CNA (**78**) with 0.12 equiv of CF_3SO_3H in a mixture of H_2O and THF resulted in clean solvolysis (>96%) to provide a single product (FIG. 17). No *N*-BOC deprotection or olefin formation was observed. Comparison of this single product to **101** that would result from H_2O attack at the less substituted cyclopropyl carbon indicated that ring expansion had occurred exclusively to afford **99**. None of the typical seven-membered ring solvolysis product **101** could be detected in the crude reaction mixture by ^1H NMR or HPLC. Treatment of **78** with CH_3OH under similar conditions gave an analogous result, providing excellent conversion exclusively to the abnormal ring expansion product **100**. Although minor amounts of the ring expansion solvolysis products have been observed with related systems, the solvolysis of *N*-BOC-CNA represents the first observation of either predominant or exclusive ring expansion derived from cleavage of the internal cyclopropane bond. Similarly, treatment of **78** with 1.5 equiv of HCl in THF (–78 °C, 15 min) cleanly provided **102** (> 20:1, 99%) and not **87**. This observation is especially significant. In some, but not all, of the prior instances of mixed solvolysis regioselectivity, the addition of HCl still cleanly provided the typical

addition product derived from attack at the least substituted carbon rather than the ring expansion addition observed with the generation of **102**. The clean addition of HCl to **78** to provide the ring expansion product **102** illustrates that the stereoelectronic control of the addition directs even the larger nucleophiles to the more hindered cyclopropyl carbon.

In an effort that established the mechanistic course of the reaction, both racemic and optically active (+)-**78** were subjected to acid-catalyzed solvolysis (0.12 equiv of CF_3SO_3H, H_2O–THF, 25 °C, 5 min) to provide **99**. Resolution on a Diacel Chiracel OG analytical HPLC column separated both enantiomers of the reaction product. The product derived from optically active (+)-**78** provided one enantiomer of the ring expanded product. The generation of a single enantiomer of **99** establishes that the cleavage of the internal cyclopropane bond does not proceed with generation of a free carbocation (S_N1) but instead occurs with clean inversion of the reaction center stereochemistry in an S_N2 ring opening reaction. These results are in agreement with the similarly unambiguous results of solvolysis studies of *N*-BOC-CBQ, *N*-BOC-DSA, and *N*-BOC-DA which also afford a single enantiomer of the minor ring expansion products but contrasts the studies with a CPI-derivative where racemization is reported to occur. This growing set of observations and especially that of the exceptionally reactive *N*-BOC-CNA detailed herein suggest the latter CPI studies should be reexamined employing a more definitive basis for establishing the optical purity of the ring expansion solvolysis product.

X-ray Structural Correlations with Solvolysis Regioselectivity. The single-crystal X-ray structure determination of *N*-CO_2Me-CNA (**97**) and CNA (**79**) was conducted in expectations of providing structural insights into its reversed solvolysis regioselectivity and extraordinary reactivity. To insure the comparisons were accurately made between the appropriately acylated and nonacylated derivatives, we have also extended the efforts to secure a total of eight X-ray crystal structures including both a simple *N*-acyl and the free NH derivative of CNA, CBQ, and CBI, as well as two seco precursors.

Comparison of the X-ray structures allows for a confirmation of the conclusions that have been drawn between the relative stereoelectronic alignment of the reacting cyclopropane bonds and solvolysis regioselectivity. The newly obtained X-ray

structure for *N*-CO_2Me-CBI containing the five-membered C-ring, like that of CBI itself, reveals that the bent orbital of the cyclopropane bond extending to the least substituted carbon is nearly perpendicular to the plane of the cyclohexadienone and consequently overlaps well with developing π-system of the phenol solvolysis product. In contrast, the cyclopropane bond extending to the more substituted carbon is less effectively aligned and nearly orthogonal to the π-system. Reflecting this relative alignment, the cleaved C8b-C9 bond is the longest (1.544 versus 1.521 Å) and weakest of these two bonds. Thus, the cyclopropane cleavage occurs under stereoelectronic control with preferential addition of the nucleophile at the least substituted carbon (>20:1). This stereoelectronic control overrides any intrinsic electronic preference for ring expansion ring opening with partial positive charge development on the more substituted cyclopropane carbon but may also benefit from the characteristic preference for S_N2 nucleophilic attack to occur at the least substituted carbon.

In contrast, the previously obtained X-ray structure for *N*-BOC-CBQ (77) containing the 6-membered C-ring revealed that the cyclopropane is ideally conjugated and aligned with the π-system and the two potential cyclopropane cleavage bonds are perfectly bisected by the cyclohexadienone π-system. Such a bond orientation is consistent with the loss of solvolytic regioselectivity for *N*-BOC-CBQ which shows only a slight preference for nucleophilic addition at the less substituted cyclopropane carbon (3:2). Given an inherent preference for partial positive charge delocalization onto a secondary versus primary center, one might have anticipated preferential cleavage of the C9b-C10a bond. However, the bond extending to the less substituted cyclopropyl carbon is weaker as judged by its longer bond length (1.543 Å versus 1.528 Å) suggesting that any inherent preference for cleavage of the C9b-C10a bond is offset by this lower bond strength of the C9b-C10 bond. In addition, S_N2 nucleophilic attack at the more substituted tertiary center is sterically disfavored. Given that the ring expansion solvolysis occurs with clean inversion of stereochemistry, the developing torsional strain that accompanies nucleophilic addition with ring expansion may be especially significant and also contributing to the small regioselectivity preference.

Inspection of the X-ray crystal structure of *N*-CO_2Me-CNA reveals that the cyclopropane possesses alignment features of both *N*-CO_2Me-CBI and *N*-BOC-CBQ. Like *N*-CO_2Me-CBI, the cyclopropane is nonideally conjugated with the π-system but

rises above rather than dips below the plane of the cyclohexadienone such that now the bond to the more substituted cyclopropane carbon enjoys the better stereoelectronic alignment. Thus, the smooth reversal of solvolysis regioselectivity with *N*-BOC-CNA may be attributed to the relative stereoelectronic alignment of the breaking C10b-C11a bond combined with any intrinsic electronic stabilization inherent in its greater substitution. Notably, this combination of stereoelectronic and electronic features is sufficient to overcome the destabilizing steric interactions that must accompany S_N2 addition at the more substituted center. Diagnostic of the regioselectivity of nucleophilic addition, the cleaved C10b-C11a bond is longer (1.565 Å versus 1.525 Å) and weaker than the C10b-C11 bond extending to the less substituted cyclopropane carbon. Like the geometric alignment of *N*-BOC-CBQ but unlike *N*-BOC-CBI, *N*-CO_2Me-CNA possesses a near perfect geometric orientation with respect to the plane bisecting the cyclohexadienone, deviating little from a perfect backside alignment.

Thus, consistent with comparisons that can be made from all such structural studies to date, the solvolysis reaction regioselectivity accurately reflects the relative stereoelectronic alignment of the two available cyclopropane bonds. This is beautifully illustrated with the clean, smooth, and complete reversal of the reaction regioselectivity as one progresses through the series *N*-BOC-CBI (>20:1), *N*-BOC-CBQ (3:2), and *N*-BOC-CNA (<1:20).

X-ray Structural Correlations with Solvolysis Reactivity. The solvolysis reactivity increases that occur in the series CNA > CBQ > CBI are the consequence of a previously unappreciated structural feature of the CC-1065 and duocarmycin alkylation subunits. Although the alkylation subunit vinylogous amide has been recognized as a structural feature contributing to its unusual stability, the extent of this stabilization has not been established nor has the structural, chemical, and biological consequences of its presence or disruption been defined. We recently highlighted that one of the most prominent structural features of the alkylation subunits that is directly observable in their X-ray structures is the alternating shortened and lengthened bonds within the vinylogous amide with the most diagnostic feature being the shortened C-N bond length. This provides the opportunity to establish by X-ray the relative extent of the vinylogous amide conjugation that accompanies structural modifications within the alkylation subunit and, ultimately, the ability to correlate this with the properties and

chemical reactivity of the agents. Such comparisons within the CBI, CBQ, and CNA series proved especially revealing.

The direct comparisons of the full set of X-ray structures in the series provide a superb assessment of the extent of vinylogous amide conjugation and ultimately, the relative reactivity of the agents. First, *N*-acylation (*e.g.*, *N*-CO_2Me-CBI versus CBI) reduces the vinylogous amide conjugation, lengthens bond c, and results in a substantial increase in reactivity. This is observed with each of the three sets of agents. Typical C-N bond lengths for a fully conjugated vinylogous amide are 1.312–1.337 Å. Thus, that of CBI (bond c, 1.337 Å) is diagnostic of a fully engaged vinylogous amide while that of *N*-CO_2Me-CBI (1.390 Å) is substantially diminished. Accompanying this reduction in the vinylogous amide conjugation that results from *N*-acylation is an increase in length of the reacting cyclopropane bonds and a readjustment of the cyclopropane alignment to a more idealized conjugation with the cyclohexadienone π-system. This illustrates that both the cyclopropane conjugation and its inherent reactivity increase as the cross-conjugated vinylogous amide π-overlap is diminished. One of the more important conclusions that can be drawn from these correlations is that the pronounced solvolysis stability of the free NH derivatives is due to this cross-conjugated and fully engaged vinylogous amide. Despite their increased basicity which would facilitate C-4 carbonyl protonation, they are much less reactive than the corresponding *N*-acyl derivatives toward acid-catalyzed nucleophilic addition reactions.

More importantly, these same trends are observed within the *N*-acyl series. As one moves across the series of *N*-CO_2Me-CBI, *N*-BOC-CBQ, and *N*-CO_2Me-CNA, the length of bond c increases (1.390, 1.415, and 1.428 Å) diagnostic of the loss of the cross-conjugated vinylogous amide. Correspondingly, the length, conjugation, and reactivity of the scissile cyclopropane bonds increase tracking with the relative reactivity of the agents. Accompanying these changes and responsible for this loss of vinylogous amide conjugation is an increase in the χ_1 dihedral angle. Notably, the χ_1 dihedral angle of *N*-CO_2Me-CNA is so large that the acyl group is nearly perpendicular to the plane of the cyclohexadienone π-system and the agent benefits from little, if any, vinylogous amide conjugation. This is reflected in its bond c length of 1.428 Å. Throughout this series, the χ_2 dihedral angle is maintained at *ca.* 0° illustrating the preferential maintenance of the N carbamate conjugation versus that of the vinylogous

amide. However, *N*-BOC-CBQ exhibits a slightly larger χ_2 dihedral angle suggesting some carbamate distortion in efforts to maintain the vinylogous amide conjugation. These observations have important implications on the source of catalysis for the DNA alkylation reaction which is discussed in the following section.

An additional and more subtle structural feature that contributes to reactivity is seen in the structural comparisons of the NH derivatives. This series does not exhibit a completely smooth correlation between the χ_1 torsion angle, the length of bond c, and reactivity. CBI boasts a torsion angle of 15.7° but is significantly less reactive than CBQ which has a smaller torsion angle of 6.9°. In the case of the NH derivatives, the X-ray χ_1 torsional angles reveal nothing about the pyramidalization of the nitrogen and the resulting orientation of its lone pair. Therefore, it is difficult to assess the relative extent of π-overlap simply by measuring the χ_1 angle. However, the identical C-N bond lengths for CBI and CBQ suggest that both benefit from comparable vinylogous amide conjugation. The structural difference that accounts for their 10-fold different reactivities lies in the lengths of the scissile cyclopropyl bonds (Figure 9). CBI has bond lengths of 1.508 Å and 1.532 Å for the C8b-C9a and C8b-C9 bonds, respectively, while those of CBQ are 1.525 Å and 1.539 Å. In turn, this may be attributed to the perfect geometrical (backside) alignment of the CBQ cyclopropane not accessible to CBI. Presumably, this increases the CBQ cyclopropane conjugation, lengthens the scissile cyclopropane bonds and results in an increased reactivity. In contrast to CBI and CBQ which have similar c bond lengths but different cyclopropyl alignments, CBQ and CNA have similar cyclopropyl alignments but substantially different χ_1 dihedral angles and different c bond lengths of 1.336 versus 1.376 Å, respectively. This difference, diagnostic of the extent of vinylogous amide conjugation, is accompanied by a large increase in the CNA scissile cyclopropane bond lengths indicative of a much greater degree of conjugation and accounts for over a hundred-fold difference in reactivity. Thus, the degree of cyclopropane conjugation and its resulting reactivity is not only related to its geometrical alignment but also to the extent of the cross-conjugated vinylogous amide stabilization.

Thus, the geometrical constraints imposed by the fused five-membered C-ring found in the natural products dictate the regioselectivity of cleavage of the cyclopropane ring. More importantly, the agents display a beautiful interplay between the cross-

conjugated stability provided by the vinylogous amide and the extent of cyclopropane conjugation that is central to their functional reactivity. Structural perturbations that diminish the vinylogous amide conjugation, increase the cyclopropyl conjugation and its inherent reactivity. One particularly important structural perturbation is the χ_1 dihedral angle of the linking amide of the *N*-acyl derivatives of the alkylation subunits. As the χ_1 dihedral angle is increased, the nitrogen lone pair remains conjugated with the acyl group carbonyl disrupting the vinylogous amide conjugation resulting in very substantial increases in the cyclopropane reactivity. One fundamental insight gained from these comparisons is the extent of the vinylogous amide conjugation and the contribution it makes to the unusual stability of the CBI and DSA alkylation subunits.

Catalysis of the DNA Alkylation Reaction. The remarkable chemical stability of **1–3** and the acid-catalysis requirement for addition of typical nucleophiles have led to the assumption that the DNA alkylation must also be an acid-catalyzed reaction. Although efforts have gone into supporting the extent and role of this acid catalysis, it remains largely undocumented for the DNA alkylation reaction. At pH 7.4, the DNA phosphate backbone is fully ionized (0.0001–0.00004% protonated). Consequently, it is unlikely that the catalysis is derived from a phosphate backbone delivery of a proton to the C4 carbonyl as advanced in related efforts. Although increases in the local hydronium ion concentrations surrounding "acidic domains" of DNA have been invoked to explain DNA mediated acid-catalysis, nucleotide reactivity, and extrapolated in studies with **1** to alkylation site catalysis, the remarkable stability of **1–3** even at pH 5 suggests that it is unlikely to be the source of catalysis. Consistent with this, the rate of the DNA alkylation reaction exhibits only a very modest pH dependence below pH 7 and essentially no dependence in the more relevant pH 7–8 range.

In conjunction with the results of these studies which document the lack of pH dependence on the rate of DNA alkylation and related studies that demonstrated that a rigid N^2 amide substituent is required for catalysis, an alternative source of catalysis became apparent. The studies detailed herein along with a number of additional unrelated observations have led us to propose that catalysis for the DNA alkylation reaction is derived from a DNA binding-induced conformational change in the agent that disrupts the vinylogous amide stabilization of the alkylation subunit and activates the agent for nucleophilic addition. This conformational change results from adoption

of a helical bound conformation that follows the curvature and pitch of the DNA minor groove. The helical rise in the bound conformation of the rigid agents is adjusted by twisting the linking N^2 amide which is the only available flexible site. The twisting of the χ_1 dihedral angle of the linking amide (χ_2 ~0°) diminishes the N^2 lone pair conjugation with the cyclohexadienone, disrupts the vinylogous amide stabilization of the alkylation subunit, and increases its inherent reactivity. An alternative possibility involves a twisting of the χ_2 dihedral angle diminishing the amide conjugation and increasing the N^2 vinylogous amide conjugation. This would increase the basicity of the C4 carbonyl leading to more effective protonation. Notably, both are consistent with the studies that demonstrate even subtle perturbations in the vinylogous amide have a remarkably large impact on reactivity ($\rho = -3.0$). Although our present studies do not directly distinguish between these two possibilities, the latter reflects changes that occur upon *N*-deacylation (*e.g.*, *N*-BOC-CBI to CBI, decreased reactivity) while the former reflects the changes observed in going to the product of the reaction (fully engaged amide, $\chi_2 = 0°$; no vinylogous amide, χ_1 ~20–35° and lengthened bond c). It is consistent with a DNA bound conformation of duocarmycin SA established by ^{1}H NMR which exhibited at 44 ± 2° twist between the planes of the two subunits with the bulk of the twist being accommodated in χ_1. The remarkably large and appropriate reactivity changes observed herein that accompany such a decoupling of the vinylogous amide including that resulting from a twist in the χ_1 dihedral angle is consistent with this as a source of catalysis. The reactivity of *N*-CO_2Me-CNA is extraordinary exhibiting a $t_{1/2}$ of only 2.1 h at pH 7 in the absence of deliberate added acid catalysis. It is 10^3–10^4× more reactive than *N*-BOC-DSA and represents an agent that benefits from little, if any, vinylogous amide stabilization. This level of reactivity is greater than that required. In fact, it is the reactivity and χ_1 dihedral angle of *N*-BOC-CBQ that may more closely approximate that required for the DNA alkylation catalysis provided by the DNA binding induced conformational change in **1–3**. Its inherent reactivity at pH 7 coupled with the rate enhancements afforded a bound species that might provide a further 10^2× rate acceleration approximates the rates observed with the DNA alkylation reaction.

This has important ramifications on the source of the DNA alkylation selectivity. The inherent twist and helical rise of the bound conformation of the agent is greatest within the narrower, deeper AT-rich minor groove. This leads to preferential

activation of the agent for DNA alkylation within extended AT-rich minor groove sites and complements their preferential AT-rich noncovalent binding selectivity. Thus, both shape-selective recognition (preferential AT-rich noncovalent binding) and shape-dependent catalysis (extended AT-rich > GC-rich activation by twist in N^2 amide) combine to restrict S_N2 alkylation to accessible adenine N3 nucleophilic sites within the preferred binding sites. Importantly, this ground state destabilization of the substrate only activates the agent for a rate determining S_N2 nucleophilic addition and requires the subsequent proper positioning and accessibility to an adenine N3 site.

This source of catalysis requires an extended and rigid N^2 amide substituent and the absence of such a substituent with **72–74** (FIG. 18) accounts nicely for their slow and ineffective DNA alkylation. The noncovalent binding derived from the attached right-hand subunits accounts for a much smaller part of the difference in the rates of DNA alkylation between **72–74** and **1–3**. More importantly, this source of catalysis would lead to distinctions, not similarities, in the DNA alkylation selectivities of **72–74** versus **1** contrary to the consequences of alternative proposals that have been advanced.

***In Vitro* Cytotoxic Activity.** The *in vitro* cytotoxic activity of the agents proved to be consistent with past observations that have illustrated a direct correlation between solvolysis stability and cytotoxic potency. The CNA-based agents exhibited cytotoxic activity that was less potent than the corresponding duocarmycin based agents but more potent than the corresponding CI-based agents (FIGs. 19 and 20). The natural enantiomers of the CNA-based agents were found to be more potent than the unnatural enantiomers. Interestingly, the natural enantiomer of the full analog of duocarmycin SA, CNA–TMI (**87**), was only 5–10× more potent than *N*-BOC-CNA (**78**) and the difference in potency of the unnatural enantiomers was even smaller (1–2×). While this may simply be due to the extraordinary reactivity of the agents which preclude effective DNA alkylation, this also suggests that the twisted conformation of the full analogs may be sufficient to disfavor minor groove binding providing agents that are comparable to analogs lacking the attached DNA binding subunits altogether.

Aqueous Solvolysis of *N*-BOC-CNA (78) and CNA (79). Samples of **78** (150 μg) and **79** (150 μg) were dissolved in CH_3OH (1.5 mL) and the resulting solutions were mixed with aqueous buffer (pH 3, 1.5 mL, 4:1:20 (v:v:v) 0.1 M citric acid, 0.2 M Na_2HPO_4, and deionized H_2O respectively). Similarly, a solution of **78** (150 μg) in

CH_3OH (1.5 mL) was mixed with deionized H_2O (pH 7, 1.5 mL). The UV spectra of the solutions were measured immediately after mixing with the appropriate aqueous solution. The blank and the solvolysis reaction solutions were stoppered, protected from light, and allowed to stand at 25 °C. The total reaction times reflect those required to observe no further change in absorbance. For the solvolysis of **78** at pH 3, the UV spectrum was taken every 30 s for 10 min and then every 3 min for the next 40 min. The decrease of the absorbance at 319 nm was monitored. The solvolysis rate was calculated from the least squares treatment ($r = 0.998$) of the slope of a plot of time versus $\ln[A_o-A_f)/(A-A_f)]$; $k = 6.90 \times 10^{-3}$ s^{-1}, $t_{½} = 1.7$ min, 0.028 h. For the solvolysis of **78** at pH 7, the UV spectrum was monitored every 5 min for 19 h. The rate was calculated from the least squares treatment of the same type of plot as above ($r = 0.999$); $k = 9.16 \times 10^{-5}$ s^{-1}, $t_{½} = 126$ min, 2.1 h. For the solvolysis of **79** at pH 3, the UV spectrum was monitored every 2 min for the first 110 min and then every 10 min for the next 4 h. The decrease in the absorbance at 345 nm was recorded. The solvolysis rate constant was calculated from the least squares treatment of the same type of plot as above ($r = 0.999$); $k = 3.10 \times 10^{-4}$ s^{-1}, $t_{½} = 37$ min, 0.62 h.

Since these observations sharply contrast the proposed important role of acid catalysis for activation of the agents toward DNA alkylation which has served as the basis for one prominent proposal for the origin of the DNA alkylation selectivity, we have examined in detail the pH dependence of the rate of DNA alkylation for duocarmycin SA (**1**) and CCBI-TMI over a physiologically relevant range. The study was conducted by quantitating the relative (k_{rel}) and pseudo first-order rate constants (k_{obs}) for alkylation of the single, w794 high affinity alkylation site (5' -AATTA) at a pH of 6.0, 6.6, 7.1, 7.6, and 8.1 for (+)-duocarmycin SA (**1**) and at a pH of 6.1, 6.8, 7.6, and 8.0 for (+)-CCBI-TMI (**3**, 10^{-6} M, 25 °C, 10 mM phosphate buffer, 0–4 h). Although the rate of DNA alkylation was found to increase with decreasing pH in both cases, the rate change was remarkably small (<3× over 2 pH units) and inconsistent with a first-order dependence of acid concentration. Between pH 6–7, the slope of the plot of pH versus log k_{obs} was 0.2–0.3, far lower than that of 1.0 required of a first-order dependence on acid concentration. Moreover, between pH 7 and 8, which may be considered the physiologically relevant range, the rate dependence on pH essentially disappeared. A qualitative comparison of the pseudo first-order rate constant for DNA

alkylation at this site, $k = 1.58 \times 10^{-4}$ s^{-1} (pH 7.6) for **1** and $k = 3.36 \times 10^{-4}$ (pH 7.6) for **3** with the calculated first-order rate constants for acid-catalyzed solvolysis ($k = 2.7 \times 10^{-11}$ s^{-1} and $k = 2.5 \times 10^{-11}$ s^{-1}, respectively) at pH 7.6 suggest that the bulk of catalysis for the DNA alkylation reaction cannot be accounted for by this source. Perhaps the magnitude of this difference is best recognized by simply noting that at pH 7.6, the calculated $t_{1/2}$ for solvolysis of **1** is 820 years (3×10^5 d) while that of the DNA alkylation is 1.2 h.

Moreover, this rate of DNA alkylation was relatively independent of the buffer exhibiting only small differences in k_{obs} and the buffer had little impact on the pH dependence. The presence or absence of EDTA had or no effect on the rate of DNA alkylation for CCBI-TMI in either Tris or phosphate buffer and the alkylation was somewhat slower in phosphate versus Tris buffer (1.7-1.5×).

Throughout the pH range, (+)-CCBI-TMI was shown to alkylate the w794 high affinity alkylation site 1.9–2.5× faster than (+)-**1**, corresponding nicely with earlier studies[9] in which CCBI-TMI proved to exhibit the fastest relative rate at this same site: CCBI-TMI (2.5×) > MCBI-TMI (1.9×) > CBI-TMI (1.0×) > DSA (0.9×) (pH 7.5, Table X). In these studies, the rate of DNA alkylation did not correlate with the relative reactivity of the agents toward acid-catalyzed solvolysis (MCBI > CBI > CCBI) suggesting that other factors are responsible for the catalysis of the DNA alkylation reaction.

The relative lack of dependence on acid-concentration (pH) especially in the relevant pH range of 7–8, in conjunction with other studies have suggested an alternative source of catalysis responsible for the rapid rate of DNA alkylation by **1–3**. We have proposed that catalysis for the DNA alkylation reaction is derived from a DNA binding induced conformational change in the agent that disrupts the N^2 vinylogous amide stabilization of the alkylation subunit and activates the agent for nucleophilic addition. This conformational change results from adoption of a helical bound conformation that follows the curvature and pitch of the DNA minor groove. The helical rise in the bound conformation of the rigid agents is adjusted by twisting the linking N^2 amide which is the only available flexible site. The twisting of the linking amide diminishes the N^2 lone pair conjugation with the cyclohexadienone, disrupts the vinylogous amide stabilization of the alkylation subunit, and increases its inherent

reactivity. For the substituted CBI series of agents, the impact of the C7 substituent (R = CN≥ OCH_3 > H) is unrelated to its effect on the rate of acid-catalyzed nucleophilic addition (R = OCH_3 > H > CN) and seems to be related simply to its presence rather than electronic nature. We suggest this is due to the resulting extended length of the alkylation subunit with substituent placement in the minor groove and the corresponding increase in the inherent twist of the linking N^2 amide that accompanies minor groove binding. The documentation of remarkably large and appropriate reactivity increases that accompany the decoupling of the vinylogous amide stabilization within the alkylation subunits support this as the source of catalysis.

EXAMPLES

A Experimental

2-((*tert*-Butyloxy)carbonyl)-1,2,8,8a-tetrahydrocyclopropa[*c*]pyrrolo[3,2-*e*]indol-4-one-6-carboxylic Acid (7). A solution of **4** (56 mg, 163 μmol) in THF–CH_3OH–H_2O (3:2:1, 1.6 mL) was treated with 0.17 mL of aqueous 1 N LiOH (1.05 equiv) and the reaction mixture was warmed at 60 °C under Ar for 1 h. An additional 0.041 mL of aqueous 1 N LiOH (0.25 equiv) was added and the solution was warmed at 60 °C for an additional 30 min. The reaction mixture was allowed to cool to 25 °C and the solvent was removed under a stream of N_2. H_2O (2 mL) was added and the aqueous layer was extracted with EtOAc (2 × 2 mL). EtOAc (2 mL) was added to the aqueous layer, followed by aqueous 1 N $KHSO_4$ (0.21 mL, 1 equiv). The mixture was diluted with H_2O (35 mL) and extracted with EtOAc (3 × 35 mL). The combined organic extract was washed with H_2O (35 mL) and dried (Na_2SO_4). Concentration under reduced pressure provided **7** (50.0 mg, 93%) as a yellow film: ^1H NMR (acetone-d_6, 400 MHz) δ 11.15 (s, 1H, NH), 6.77 (s, 1H, C3-H), 6.75 (d, 1H, J = 2.0 Hz, C7-H), 4.03–4.01 (m, 2H, C1-H_2), 2.90–2.86 (m, 1H, C8a-H), 1.70 (dd, 1H, J = 7.7, 4.4 Hz, C8-H), 1.52 (s, 9H, $C(CH_3)_3$), 1.40 (t, 1H, J = 4.4 Hz, C8-H); IR (film) ν_{max} 3204, 2963, 1721, 1667, 1597, 1393, 1277, 1258, 1155, 1137, 798 cm^{-1}; FABHRMS (NBA–CsI) *m/z* 331.1290 (M^+ + H, $C_{17}H_{18}N_2O_5$ requires 331.1294).

(+)-**7**: $[\alpha]_D^{23}$ +190 (*c* 0.2, CH_3OH).

ent-(–)-**7**: $[\alpha]_D^{23}$ –193 (*c* 0.2, CH_3OH).

General Procedure for the Preparation of 13–16: 7-[(Methyl 1,2-Dihydro-3*H*-pyrrolo[3,2-*e*]indole-3-yl)carbonyl-7-carboxylate]-3-((*tert*-butyloxy)carbonyl)-

1-(chloromethyl)-5-hydroxy-1,2-dihydro-3*H*-pyrrolo[3,2-*e*]indole (15). A solution of **7** (3.1 mg, 9.4 μmol) in EtOAc (0.70 mL) under Ar was treated with 4 N HCl–EtOAc (12 μL, 47 μmol, 5 equiv) over 10 s. The yellow reaction mixture was stirred at 25 °C for 30 min and was concentrated under a stream of N_2. The resultant yellow residue containing **8** was dissolved in DMF (0.17 mL) and treated sequentially with **11** (1.7 mg, 7.9 μmol, 0.9 equiv) and EDCI (3.4 mg, 17.6 μmol, 2.0 equiv). The reaction mixture was stirred for 2 h at 25 °C before the solvent was removed under reduced pressure and the residual solid was slurried in 0.5 mL H_2O. The solid was collected by centrifugation and washed with 1% aqueous HCl (1 × 0.5 mL) and H_2O (1 × 0.5 mL). Drying the solid *in vacuo* afforded **15** (4.3 mg, 96%) as a tan solid: mp 188–190 °C (d); ^{1}H NMR (acetone-d_6, 400 MHz) δ 10.99 (s, 1H, NH), 10.40 (s, 1H, NH), 8.81 (br s, 1H, OH), 8.41 (m, 1H, C4′-H), 7.59 (br s, 1H, C4-H), 7.41 (d, 1H, J = 8.9 Hz, C5′-H), 7.22 (d, 1H, J = 1.5 Hz), 7.12 (s, 1H), 4.80–4.62 (m, 2H), 4.20–4.10 (m, 2H), 4.04 (dd, 1H, J = 11.8, 4.0 Hz), 4.04–3.92 (m, 1H, C1-H), 3.89 (s, 3H, OCH_3), 3.73 (t, 1H, J = 9.3 Hz, C2′-H), 3.49 (t, 2H, J = 8.3 Hz, C1′-H_2), 1.55 (s, 9H, $C(CH_3)_3$); IR (neat) ν_{max} 3327, 2975, 2933, 1690, 1669, 1607, 1524, 1436, 1389, 1369, 1327, 1255, 1213, 1141 cm^{-1}; FABHRMS (NBA–CsI) *m/z* 697.0809 (M^+ + Cs, $C_{29}H_{29}N_4O_6Cl$ requires 697.0830).

(1*S*)-**15**: $[\alpha]_D^{22}$ –23 (*c* 0.2, THF).

ent-(1*R*)-**15**: $[\alpha]_D^{23}$ +27 (*c* 0.2, THF).

General Procedure for the Preparation of 17–20, Method A: 6-[7-[Methyl 1,2-Dihydro-(3*H*-pyrrolo[3,2-*e*]indole-3-yl)carbonyl-7-carboxylate]-1,2-dihydro-(3*H*-pyrrolo[3,2-*e*]indole-3-yl)carbonyl]-2-((*tert*-butyloxy)carbonyl)-1,2,8,8a-tetrahydrocyclopropa[*c*]pyrrolo[3,2-*e*]indol-4-one (20, CDPI$_2$-DSA). A portion of NaH (1.1 mg, 60%, 26.7 μmol, 10 equiv) in DMF at 0 °C under Ar was treated with a solution of **16** (2.0 mg, 2.67 μmol, 1.0 equiv) in DMF (0.25 mL), and the reaction mixture was stirred for 45 min at 0 °C. The reaction mixture was directly subjected to flash chromatography (0.5 × 5 cm SiO_2, 15% DMF–toluene) to afford **20** (1.8 mg, 95%) as a pale yellow solid: mp 213–215 °C (d); ^{1}H NMR (DMF-d_7, 400 MHz) δ 11.99 (s, 1H, NH), 11.79 (s, 1H, NH), 11.73 (d, 1H, J = 1.6 Hz, NH), 8.42–8.20 (m, 2H), 7.46 (app t, 2H, J = 9.2 Hz), 7.20 (d, 1H, J = 1.6 Hz), 7.17 (d, 1H, J = 1.4 Hz), 6.81 (s, 1H), 6.68 (s, 1H), 4.75 (t, 2H, J = 8.4 Hz), 4.55 (app q, 2H, J = 7.9 Hz), 4.07 (dd, 1H, J = 11.2, 4.9 Hz), 4.04–3.99 (m, 1H), 3.93 (s, 3H), 3.57–3.45 (m, 4H, partially obscured by

H_2O), 3.00 (dt, 1H, J = 7.8, 4.3 Hz, C8a-H), 1.82 (dd, 1H, J = 7.7, 3.7 Hz, C8-H), 1.53 (s, 9H, $C(CH_3)_3$), 1.49 (t, 1H, J = 4.4 Hz, C8-H); IR (neat) ν_{max} 3324, 2958, 2931, 2871, 1709, 1703, 1620, 1582, 1530, 1511, 1503, 1434, 1378, 1348, 1256, 1211, 1163, 1143, 1022 cm^{-1}; FABHRMS (NBA) *m/z* 713.2757 (M^+ + H, $C_{40}H_{36}N_6O_7$ requires 713.2724).

(+)-$CDPI_2$-DSA (**20**): $[\alpha]_D^{23}$ +56 (*c* 0.1, DMF).

ent-(–)-$CDPI_2$-DSA (**20**): $[\alpha]_D^{23}$ –60 (*c* 0.1, DMF).

***N*-(Methyl 1*H*-Indol-5-yl-2-carboxylate)-3-((*tert*-butyloxy)carbonyl)-1-(chloromethyl)-5-hydroxy-1,2-dihydro-3*H*-pyrrolo[3,2-*e*]indole-7-carboxamide (13):** (4.3 mg, 96%) as a tan solid: mp 215–218 °C (d); ^{1}H NMR (acetone-d_6, 400 MHz) δ 10.92 (s, 1H, NH), 10.62 (s, 1H, NH), 9.56 (s, 1H, OH), 8.77 (br s, 1H, NHCO), 8.29 (d, 1H, J = 1.5 Hz, C4′-H), 7.64 (dd, 1H, J = 8.9, 2.0 Hz, C6′-H), 7.58 (br s, 1H, C4-H), 7.51 (d, 1H, J = 8.9 Hz, C7′-H), 7.31 (d, 1H, J = 1.5 Hz), 7.18 (d, 1H, J = 1.2 Hz), 4.17 (t, 1H, J = 10.5 Hz, C2-H), 4.08 (dd, 1H, J = 10.8, 3.4 Hz), 4.01 (dd, 1H, J = 11.6, 4.5 Hz), 3.91 (s, 3H, OCH_3), 3.73 (dd, 1H, J = 10.6, 9.2 Hz), 2.95 (m, 1H), 1.55 (s, 9H, $C(CH_3)_3$); IR (neat) ν_{max} 3329, 2976, 1693, 1669, 1592, 1535, 1479, 1438, 1393, 1366, 1348, 1253, 1154 cm^{-1}; FABHRMS (NBA–NaI) *m/z* 538.1602 (M^+ + H, $C_{27}H_{27}N_4O_6Cl$ requires 538.1619).

(1*S*)-**13**: $[\alpha]_D^{22}$ +3 (*c* 0.2, THF).

ent-(1*R*)-**13**: $[\alpha]_D^{23}$ –4 (*c* 0.2, THF).

***N*-{2-[*N*-(2-Methoxycarbonyl-1*H*-indol-5-yl)carbamoyl-1*H*-indol-5-yl}-3-(*tert*-butyloxycarbonyl)-1-(chloromethyl)-5-hydroxy-1,2-dihydro-3*H*-pyrrolo[3,2-*e*]indole-7-carboxamide (14):** The coupling reaction mixture was stirred for 4 h at 25 °C and chromatography (0.5 × 6.0 cm SiO_2, 7–10% CH_3OH–CH_2Cl_2 gradient elution) afforded pure **14** (80%) as a tan solid: ^{1}H NMR (acetone-d_6, 400 MHz) δ 10.95 (s, 1H, NH), 10.92 (s, 1H, NH), 9.62 (s, 1H, NH), 9.55 (s, 1H, NH), 8.31–8.28 (m, 2H), 7.68 (dd, 1H, J = 8.9, 1.9 Hz), 7.60 (d, 1H, J = 8.8 Hz), 7.55 (d, 1H, J = 8.8 Hz), 7.52 (d, 1H, J = 8.9 Hz), 7.34 (s, 1H), 7.29 (s, 1H), 7.18 (d, 1H, J = 2.0 Hz), 4.17 (t, 1H, J = 10.7 Hz, C2-H), 4.09 (dd, 1H, J = 11.0, 3.0 Hz, C2-H), 4.03 (dd, 1H, J = 10.5, 4.5 Hz, C*H*HCl), 3.98–3.88 (m, 1H, C1-H), 3.89 (s, 3H, OCH_3), 3.73 (dd, 1H, J = 12.6, 11.0 Hz, CH*H*Cl), 1.55 (s, 9H, $C(CH_3)_3$); IR (neat) ν_{max} 3277, 2921, 1694, 1650, 1541, 1254, 1141 cm^{-1}; FABMS (NBA–CsI) *m/z* 829 (M^+ + Cs, $C_{36}H_{33}N_6O_7Cl$ requires 829).

7-[7-[(Methyl 1,2-Dihydro-3*H*-pyrrolo[3,2-*e*]indole-3-yl)carbonyl-7-carboxylate]-1,2-dihydro-(3*H*-pyrrolo[3,2-*e*]indole-3-yl)carbonyl]-3-((*tert*-butyloxy)carbonyl)-1-(chloromethyl)-5-hydroxy-1,2-dihydro-3*H*-pyrrolo[3,2-*e*]indole (16): The coupling reaction mixture was stirred for 4 h at 25 °C followed by chromatography (0.5 × 5 cm SiO_2, 15% DMF–toluene) to afford pure **16** (57%) as a tan solid: mp 210–211 °C (d); ^{1}H NMR (DMF-d_7, 400 MHz) δ 11.99 (s, 1H, NH), 11.74 (d, 1H, J = 1.6 Hz), 11.09 (s, 1H, NH), 9.97 (br s, 1H, OH), 8.42 (br s, 1H), 8.41 (m, 2H), 7.50 (d, 1H, J = 8.9 Hz), 7.46 (d, 1H, J = 8.8 Hz), 7.39 (d, 1H, J = 2.0 Hz), 7.23 (d, 1H, J = 1.6 Hz), 7.18 (d, 1H, J = 0.9 Hz), 4.79 (m, 2H), 4.76 (t, 2H, J = 8.4 Hz), 4.27 (dd, 1H, J = 10.7, 3.0 Hz), 4.21 (t, 1H, J = 12.5 Hz), 4.10-4.00 (m, 2H), 3.92 (s, 3H), 3.95 (t, 1H, J = 4.4 Hz), 3.56 (t, 4H, J = 7.9 Hz), 1.57 (s, 9H); IR (neat) ν_{max} 3321, 2956, 2925, 1701, 1609, 1508, 1431, 1370, 1335, 1253, 1208, 1142, 1020 cm^{-1}; FABHRMS (NBA) *m/z* 749.2480 (M^+ + H, $C_{40}H_{37}N_6O_7Cl$ requires 749.2491).

(1*S*)-**16**: $[\alpha]_D^{22}$ –24 (*c* 0.1, DMF).

ent-(1*R*)-**16**: $[\alpha]_D^{23}$ +27 (*c* 0.2, DMF).

Method B: 6-[(Methyl 1,2-Dihydro-3*H*-pyrrolo[3,2-*e*]indole-3-yl)carbonyl-7-carboxylate]-2-((*tert*-butyloxy)carbonyl)-1,2,8,8a-tetrahydrocyclopropa[*c*]-pyrrolo[3,2-*e*]indol-4-one (19, CDPI$_1$-DSA). A solution of **11** (2.0 mg, 9.1 μmol), EDCI (2.6 mg, 13.6 μmol, 1.5 equiv), and $NaHCO_3$ (3.8 mg, 45.5 μmol, 5 equiv) in DMF (0.18 mL) at 25 °C under Ar was treated with **7** (3.0 mg, 9.1 μmol) and the reaction mixture was stirred for 16 h at 25 °C. The reaction mixture was directly subjected to flash chromatography (0.5 × 5 cm SiO_2, EtOAc) to afford **19** (2.3 mg, 51%) as a pale yellow film: ^{1}H NMR (DMSO-d_6, 400 MHz) δ 12.00 (d, 1H, J = 1.6 Hz, NH), 11.96 (s, 1H, NH), 8.13 (br s, 1H, C4′-H), 7.29 (d, 1H, J = 9.2 Hz, C5′-H), 7.12 (d, 1H, J = 1.2 Hz, C8′-H), 6.63 (s, 1H), 6.50 (s, 1H), 4.37 (m, 2H, C2′-H_2), 3.96 (dd, 1H, J = 11.1, 4.8 Hz, C1-H), 3.90 (d, 1H, J = 10.9 Hz, C1-H), 3.87 (s, 3H, OCH_3), 3.30 (m, 2H, C1-H_2, obscured by H_2O), 2.89 (dt, 1H, J = 7.7, 4.8 Hz, C8a-H), 1.69 (dd, 1H, J = 7.7, 4.0 Hz, C8-H), 1.43 (t, 1H, J = 4.2 Hz, C8-H); IR (film) ν_{max} 3302, 2958, 2930, 2849, 1710, 1692, 1613, 1434, 1390, 1366, 1311, 1256, 1212, 1140 cm^{-1}; FABHRMS (NBA–CsI) *m/z* 529.2080 (M^+ + H, $C_{29}H_{28}N_4O_6$ requires 529.2087).

(+)-CDPI$_1$-DSA (**19**): $[\alpha]_D^{22}$ +89 (*c* 0.1, THF).

ent-(–)-CDPI$_1$-DSA (**19**): $[\alpha]_D^{23}$ –87 (*c* 0.1, THF).

***N*-(Methyl 1*H*-Indol-5-yl-2-carboxylate)-2-((*tert*-butyloxy)carbonyl)-1,2,8,8a-tetrahydrocyclopropa[*c*]pyrrolo[3,2-*e*]indol-4-one-7-carboxamide (17, Indole$_1$-DSA):** 30 min at 0 °C followed by chromatography (0.5 × 5 cm SiO_2, 15% DMF-toluene) afforded **17** (2.0 mg, 71%) as a pale yellow solid: mp 204–205 °C (d); ^{1}H NMR (acetone-d_6, 400 MHz) δ 11.43 (s, 1H, NH), 10.91 (s, 1H, NH), 9.66 (s, 1H, NH), 8.25 (d, 1H, J = 1.6 Hz, C4′-H), 7.64 (dd, 1H, J = 8.9, 1.6 Hz, C6′-H), 7.51 (d, 1H, J = 8.9 Hz, C7′-H), 7.19 (s, 1H), 6.80 (s, 1H), 6.77 (br s, 1H), 4.03 (m, 2H, C1-H_2), 3.88 (s, 3H, OCH_3), 2.82 (m, 1H, C8a-H, partially obscured by H_2O), 1.70 (dd, 1H, J = 7.6, 4.0 Hz, C8-H), 1.51 (s, 9H, $C(CH_3)_3$), 1.45 (t, 1H, J = 4.2 Hz, C8-H); IR (neat) ν_{max} 3189, 2958, 2922, 1711, 1651, 1593, 1533, 1443, 1393, 1370, 1280, 1257, 1145, 1090 cm^{-1}; FABMS (NBA) *m/z* 503 (M^+ + H, $C_{27}H_{26}N_4O_6$ requires 503).

(+)-Indole$_1$-DSA (**17**): $[\alpha]_D^{23}$ +60 (*c* 0.1, DMF).

ent-(–)-Indole$_1$-DSA (**17**): $[\alpha]_D^{23}$ –67 (*c* 0.1, DMF).

***N*-{2-[*N*-(2-Methoxycarbonyl-1*H*-indol-5-yl)]carbamoyl-1*H*-indol-5-yl}-2-(*tert*-butyloxycarbonyl)-1,2,8,8a-tetrahydrocyclopropa[*c*]pyrrolo[3,2-*e*]indol-4-one-6-carboxamide (18, Indole$_2$-DSA):** Chromatography (0.5 × 6.0 cm SiO_2, 5–10% CH_3OH–CH_2Cl_2 gradient elution) afforded **18** (64%) as a tan solid: ^{1}H NMR (DMSO-d_6, 400 MHz) δ 11.92 (s, 1H, NH), 11.76 (br s, 1H, NH), 11.70 (s, 1H, NH), 10.16 (s, 1H, NH), 9.99 (s, 1H, NH), 8.14 (d, 2H, J = 6.8 Hz), 7.59 (d, 1H, J = 8.9 Hz), 7.44–7.42 (m, 3H), 7.37 (s, 1H), 7.17 (s, 1H), 6.78 (s, 1H), 6.54 (s, 1H), 3.98–3.89 (m, 2H, C1-H_2), 3.87 (s, 3H, OCH_3), 2.93 (m, 1H, C8a-H), 1.69 (m, 1H, C8-H), 1.49 (s, 9H, $C(CH_3)_3$), 1.34 (t, 1H, J = 7.4 Hz, C8-H); IR (neat) ν_{max} 3284, 2930, 1709, 1594, 1541, 1255, 1140 cm^{-1}; FABHRMS (NBA–CsI) *m/z* 793.1357 (M^+ + Cs, $C_{36}H_{32}N_6O_7$ requires 793.1387).

(+)-**18**: $[\alpha]_D^{25}$ +58 (*c* 0.07, THF).

ent-(–)-**18**: $[\alpha]_D^{25}$ –50 (*c* 0.02, THF).

***N*-{2-[*N*-(2-Methoxycarbonyl-1*H*-indol-5-yl)]carbamoyl-1*H*-indol-5-yl}-3-acetyl-1-(chloromethyl)-5-hydroxy-1,2-dihydro-3*H*-pyrrolo[3,2-*e*]indole-7-carboxamide (22).** A suspension of **14** (1.6 mg, 2.3 μmol, 1.0 equiv) in 3.4 N HCl–EtOAc (0.6 mL) was stirred for 30 min at 25 °C. The reaction mixture was concentrated and the residue of **21** was taken up in DMF (0.1 mL) and treated sequentially with CH_3COOH (16 μL, 0.175 M in DMF, 1.2 equiv) and EDCI (1.3 mg,

6.9 μmol, 3.0 equiv). The reaction mixture was stirred for 15 h at 25 °C. The solvent was removed under reduced pressure and the residual solid was slurried in 0.4 mL H_2O. The solid was collected by centrifugation and washed with 1% aqueous HCl (0.4 mL) and H_2O (0.4 mL) to afford crude **22**. Flash chromatography (0.5 × 4.5 cm SiO_2, 25% DMF–toluene) afforded pure **22** (0.6 mg, 40%) as a tan solid: ^{1}H NMR (DMSO-d_6, 400 MHz) δ 11.91 (s, 1H, NH), 11.70 (s, 1H, NH), 11.34 (s, 1H, NH), 10.15 (s, 1H, NH), 10.07 (s, 1H, NH), 9.76 (s, 1H, OH), 8.16 (s, 2H), 7.73 (s, 1H), 7.59 (dd, 1H, J = 9.3, 1.9 Hz), 7.53 (d, 1H, J = 8.9 Hz), 7.45 (t, 2H, J = 9.1 Hz), 7.40 (s, 1H), 7.38 (s, 1H), 7.17 (d, 1H, J = 0.9 Hz), 4.35 (m, 1H, C2-H), 4.14–4.11 (m, 1H, C2-H), 4.05–4.01 (m, 2H, C*H*HCl, C1-H), 3.90–3.87 (m, 1H, CH*H*Cl), 3.87 (s, 3H, OCH_3), 2.16 (s, 3H, CH_3); IR (neat) ν_{max} 3279, 2922, 1678, 1645, 1556, 1532, 1434, 1410, 1214, 1017 cm^{-1}; ESIMS *m/z* 639 (M^+ + H, $C_{33}H_{27}N_6O_7Cl$ requires 639).

***N*-{2-[*N*-(2-Methoxycarbonyl-1*H*-indol-5-yl)]carbamoyl-1*H*-indol-5-yl}-2-acetyl-1,2,8,8a-tetrahydrocyclopropa[*c*]pyrrolo[3,2-*e*]indole-4-one-6-carboxamide (23, Indole$_2$-DSA-COCH$_3$).** A suspension of NaH (0.5 mg, 60%, 12.5 μmol, 5.0 equiv) in THF (0.12 mL) at 0 °C under Ar was treated with a solution of **22** (2.5 mg, 2.5 μmol, 1.0 equiv) in 50% THF–DMF (0.24 mL). The reaction mixture was stirred for 30 min at 0 °C. The crude reaction mixture was purified by preparative TLC (12 × 20 cm SiO_2, 20% DMF–toluene) to afford **24** (1.1 mg, 70%) as a pale yellow solid: ^{1}H NMR (DMSO-d_6, 400 MHz) δ 12.10 (br s, 1H, NH), 11.91 (s, 1H, NH), 11.72 (s, 1H, NH), 10.17 (s, 1H, NH), 10.01 (s, 1H, NH), 8.15 (d, 2H, J = 6.8 Hz), 7.59 (dd, 1H, J = 8.9, 2.0 Hz), 7.45 (s, 2H), 7.44 (d, 1H, J = 8.7 Hz), 7.37 (s, 1H), 7.17 (s, 1H), 6.79 (s, 1H), 4.14–4.10 (m, 2H, C1-H_2), 3.87 (s, 3H, OCH_3), 2.95 (m, 1H, C8a-H), 2.19 (s, 3H, CH_3), 1.71 (m, 1H, C8-H), 1.46 (m, 1H, C8-H); IR (neat) ν_{max} 3282, 2923, 1646, 1590, 1539, 1390, 1256 cm^{-1}; ESIMS (negative ion) *m/z* 601 (M^- – H, $C_{33}H_{26}N_6O_6$ requires 601).

(+)-**23**: $[\alpha]_D^{25}$ +24 (*c* 0.07, DMF).

ent-(–)-**24**: $[\alpha]_D^{25}$ –20 (*c* 0.02, DMF).

***N*-{2-[*N*-(2-Methoxycarbonyl-1*H*-indol-5-yl)]carbamoyl-1*H*-indol-5-yl}-1,2,8,8a-tetrahydrocyclopropa[*c*]pyrrolo[3,2-*e*]indol-4-one-6-carboxamide (24, Indole$_2$-DSA-NH).** A suspension of crude **14** (4.0 mg, 7.0 μmol, 1.0 equiv) in 3.6 N HCl–EtOAc (1.3 mL) was stirred for 30 min at 25 °C. The reaction mixture was concentrated and dried. The residue was taken up in DMF (0.45 mL) and added to a

suspension of NaH (0.8 mg, 60%, 2.1 μmol, 3.0 equiv) at 0 °C. The mixture was stirred for 30 min at 0 °C and filtered (4 × 0.5 cm SiO_2). The filtrate was concentrated and purified by PTLC (12 × 20 cm SiO_2, 30% DMF–toluene) to afford **24** (2.3 mg, 75%) as a pale yellow solid: ^{1}H NMR (DMSO-d_6, 400 MHz) δ 11.95 (s, 1H, NH), 11.91 (s, 1H, NH), 11.67 (s, 1H, NH), 10.14 (s, 1H, NH), 9.90 (s, 1H, NH), 8.15 (s, 1H), 8.14 (s, 1H), 7.59 (dd, 1H, J = 9.0, 2.0 Hz), 7.46 (s, 1H), 7.45–7.43 (m, 3H), 7.36 (d, 1H, J = 1.8 Hz), 7.17 (d, 1H, J = 1.3 Hz), 6.68 (d, 1H, J = 2.0 Hz), 5.29 (s, 1H, C3-H), 3.87 (s, 3H, OCH_3), 3.68 (dd, 1H, J = 10.4, 4.9 Hz, C1-H), 3.50 (d, 1H, J = 10.8 Hz, C1-H), 2.93–2.91 (m, 1H, C8a-H), 1.55 (dd, 1H, J = 7.8, 2.2 Hz, C8-H), 1.23 (m, 1H, C8-H); IR (neat) ν_{max} 3251, 2913, 1703, 1635, 1590, 1528, 1308, 1231, 1015 cm^{-1}; FABHRMS (NBA) *m/z* 561.1872 (M^+ + H, $C_{31}H_{24}N_6O_5$ requires 561.1886).

(+)-**24**: $[\alpha]_D^{25}$ +27 (*c* 0.05, DMF).

ent-(−)-**24**: $[\alpha]_D^{25}$ −28 (*c* 0.05, DMF).

7-[(Methyl 1,2-Dihydro-(3*H*-pyrrolo[3,2-*e*]indole-3-yl)carbonyl-7-carboxy-late)-3-(3-carbamoyl-1,2-dihydro-3*H*-pyrrolo[3,2-*e*]indol-7-yl)carbonyl]-1-(chloromethyl)-5-hydroxy-1,2-dihydro-3*H*-pyrrolo[3,2-*e*]indole (28). A solution of **15** (5.0 mg, 8.8 μmol) in 4.0 N HCl–EtOAc (0.3 mL) was stirred for 40 min at 25 °C. The reaction mixture was concentrated to afford crude **25**. The crude hydrochloride salt **25** was taken up in DMF (0.17 mL) and treated sequentially with $CDPI_1$[30] (**26**, 2.0 mg, 8.34 μmol, 0.95 equiv) and EDCI (3.4 mg, 17.6 μmol, 2 equiv). The reaction mixture was stirred for 15 h at 25 °C. The solvent was removed under reduced pressure and the residual solid was slurried in 0.5 mL H_2O and collected by centrifugation. The solid was washed with 1% aqueous HCl (1 × 0.5 mL) and H_2O (1 × 0.5 mL) and dried under reduced pressure. Chromatography (0.5 × 5 cm SiO_2, 30% DMF–toluene) afforded **28** (4.1 mg, 68%) as a yellow solid: ^{1}H NMR (DMF-d_7, 400 MHz) δ 11.98 (s, 1H, NH), 11.51 (s, 1H, NH), 11.27 (s, 1H, NH), 10.11 (br s, 1H, OH), 8.44–8.32 (m, 2H), 7.92 (s, 1H), 7.46 (d, 1H, J = 9.0 Hz), 7.41 (s, 1H), 7.37 (d, 1H, J = 8.9 Hz), 7.18 (s, 1H), 7.09 (s, 1H), 6.10 (s, 2H, NH_2), 4.89 (t, 1H, J = 8.7 Hz), 4.81–4.74 (m, 2H), 4.64 (dd, 1H, J = 11.1, 3.9 Hz), 4.30 (dd, 1H, J = 10.6, 3.4 Hz), 4.27–4.20 (m, 1H), 4.16 (t, 2H, J = 8.9 Hz), 4.05 (dd, 1H, J = 10.6, 8.0 Hz), 3.93 (s, 3H, OCH_3), 3.53 (t, 2H, J = 8.3 Hz, partially obscured by H_2O), 3.40 (t, 2H, J = 8.3 Hz, partially obscured by H_2O); IR (neat) ν_{max} 3329, 2958, 1701, 1670, 1610, 1560, 1429, 1366, 1330, 1257, 1212 cm^{-1};

ESIMS *m/z* 692 ($M^+ + H$, $C_{36}H_{30}N_7O_6Cl$ requires 692).

(1*S*)-**28**: $[\alpha]_D^{23}$ +11 (*c* 0.1, DMF).

ent-(1*R*)-**28**: $[\alpha]_D^{23}$ –10 (*c* 0.1, DMF).

7-[(Methyl 1,2-Dihydro-3*H*-pyrrolo[3,2-*e*]indole-3-yl)carbonyl-7-carboxylate]-3-[(5,6,7-trimethoxyindol-2-yl)carbonyl]-1-(chloromethyl)-5-hydroxy-1,2-dihydro-3*H*-pyrrolo[3,2-*e*]indole (29). A solution of **15** (3.6 mg, 5.7 μmol) in 4.0 N HCl–EtOAc (0.25 mL) was stirred for 30 min at 25 °C. The reaction mixture was concentrated to afford crude **25** as a dark green solid. The crude hydrochloride salt **25** was taken up in DMF (0.11 mL) and treated sequentially with **27**[12] (1.3 mg, 5.38 μmol, 0.95 equiv) and EDCI (2.2 mg, 11.32 μmol, 2 equiv). The reaction mixture was stirred for 6 h at 25 °C. The solvent was removed under reduced pressure and the residual solid was slurried in 0.5 mL H_2O and collected by centrifugation. The solid was washed with 1% aqueous HCl (1 × 0.5 mL) and H_2O (1 × 0.5 mL) and dried under reduced pressure. Chromatography (0.5 × 5 cm SiO_2, 15% DMF–toluene) afforded **29** (2.5 mg, 70%) as a yellow solid: ^{1}H NMR (DMSO-d_6, 400 MHz) δ 12.02 (s, 1H, NH), 11.37 (s, 1H, NH), 11.27 (s, 1H, NH), 9.71 (br s, 1H, OH), 8.29 (m, 1H), 7.70 (br s, 1H), 7.34 (d, 1H, *J* = 8.9 Hz, C7′-H), 7.23 (s, 1H), 7.15 (d, 1H, *J* = 1.2 Hz), 6.98 (s, 1H), 6.81 (br s, 1H), 4.68–4.59 (m, 3H), 4.37 (dd, 1H, *J* = 11.6, 3.0 Hz), 4.20 (dd, 1H, *J* = 10.8, 3.0 Hz), 4.08–4.04 (m, 1H, C1-H), 3.92 (s, 3H, OCH_3), 3.88 (s, 3H, OCH_3), 3.88 (m, obscured by OCH_3, 1H, C2′-H), 3.81 (s, 3H, OCH_3), 3.78 (s, 3H, OCH_3), 3.43 (m, 2H, C1′-H_2); IR (neat) ν_{max} 3346, 2956, 2928, 2864, 1697, 1647, 1633, 1612, 1556, 1530, 1504, 1456, 1436, 1370, 1329, 1307, 1254, 1230, 1212, 1111, 1047, 1021 cm^{-1}; FABMS (NBA) *m/z* 699 ($M^+ + H$, $C_{36}H_{32}N_5O_8Cl$ requires 699).

(1*S*)-**29**: $[\alpha]_D^{23}$ –10 (*c* 0.08, DMF).

ent-(1*R*)-**29**: $[\alpha]_D^{23}$ +11 (*c* 0.1, DMF).

2-[(3-Carbamoyl-1,2-dihydro-3*H*-pyrrolo[3,2-*e*]indol-7-yl)carbonyl]-6-[7-methoxycarbonyl-1,2-dihydro-3*H*-pyrrolo[3,2-*e*]indol-3-yl)carbonyl]-1,2,8,8a-tetrahydrocyclopropa[*c*]pyrrolo[3,2-*e*]indole (30, CDPI-DSA-CDPI). A suspension of NaH (0.6 mg, 60%, 16.0 μmol, 5.0 equiv) in DMF (0.1 mL) at 0 °C under Ar was treated with a solution of **28** (2.2 mg, 3.2 μmol, 1.0 equiv) in DMF (0.22 mL), and the reaction mixture was stirred for 30 min at 0 °C. The reaction mixture was concentrated under reduced pressure and subjected to chromatography (0.5 × 6.0 cm SiO_2, 20–30%

DMF–toluene gradient elution) to afford **30** (1.5 mg, 70%) as a yellow solid: ^{1}H NMR (DMSO-d_6, 400 MHz) δ 12.05 (br s, 1H, NH), 12.00 (br s, 1H, NH), 11.69 (br s, 1H, NH), 8.17 (br s, 1H, C4′-H), 8.01 (d, 1H, J = 8.9 Hz, C4′′-H), 7.30 (d, 1H, J = 8.5 Hz, C5′-H), 7.21 (d, 1H, J = 8.6 Hz, C5′′-H), 7.11 (s, 1H), 7.01 (s, 1H), 6.75 (s, 1H), 6.71 (s, 1H), 6.12 (s, 2H, NH_2), 4.61–4.59 (m, 1H, C1-H), 4.48–4.45 (m, 3H, C2′-H_2, C1-H), 3.97 (t, 2H, J = 8.7 Hz, C2′′-H), 3.90 (s, 3H, OCH_3), 3.30–3.28 (m, 4H, C1′-H_2, C1′′H_2, obscured by H_2O), 3.03 (m, 1H, C8a-H), 1.79 (m, 1H, C8-H), 1.62 (m, 1H, C8-H); IR (neat) ν_{max} 3354, 2923, 1703, 1605, 1497, 1441, 1374, 1328, 1256, 1200 cm^{-1}; ESIMS *m/z* 656 (M^+ + H, $C_{36}H_{29}N_7O_6$ requires 656).

(+)-**30**: $[\alpha]_D^{25}$ +54 (*c* 0.07, DMF).

ent-(–)-**30**: $[\alpha]_D^{25}$ –57 (*c* 0.07, DMF).

6-[7-Methoxycarbonyl-1,2-dihydro-3*H*-pyrrolo[3,2-*e*]indol-3-yl)carbonyl]-2-[(5,6,7-trimethoxyindol-2-yl)carbonyl]-1,2,8,8a-tetrahydrocyclopropa[*c*]-pyrrolo[3,2-*e*]indol-4-one (31, CDPI-DSA-TMI). A suspension of NaH (0.4 mg, 60%, 9.5 μmol, 5.0 equiv) in DMF (50 μL) at 0 °C under Ar was treated with a solution of **29** (1.3 mg, 1.9 μmol, 1.0 equiv) in DMF (150 μL), and the reaction mixture was stirred for 30 min at 0 °C. The mixture was concentrated under reduced pressure and subjected to chromatography (0.5 × 6.0 cm SiO_2, 12% DMF–toluene) to afford **31** (0.8 mg, 67%) as a yellow solid: ^{1}H NMR (DMSO-d_6, 400 MHz) δ 12.01 (s, 1H, NH), 11.58 (s, 1H, NH), 8.10 (br s, 1H, C4′-H), 7.30 (d, 1H, J = 9.0 Hz, C5′-H), 7.11 (s, 1H), 7.04 (s, 1H), 6.91 (s, 1H), 6.70 (s, 1H), 6.45 (s, 1H), 4.48–4.42 (m, 3H, C2′-H_2, C1-H), 4.28 (d, 1H, J = 10.1 Hz, C1-H), 3.90 (s, 3H, OCH_3), 3.87 (s, 3H, OCH_3), 3.80 (s, 3H, OCH_3), 3.79 (s, 3H, OCH_3), 3.32 (m, 2H, C1′-H_2, obscured by H_2O), 3.00–2.98 (m, 1H, C8a-H), 1.83–1.82 (m, 1H, C8-H), 1.68–1.67 (m, 1H, C8-H); IR (neat) ν_{max} 3303, 2923, 1703, 1646, 1615, 1441, 1374, 1303, 1251, 1200 cm^{-1}; ESIMS m/*z* 662 (M^+ + H, $C_{36}H_{31}N_5O_8$ requires 662).

(+)-**31**: $[\alpha]_D^{25}$ +49 (*c* 0.03, DMF).

ent-(–)-**31**: $[\alpha]_D^{25}$ –46 (*c* 0.05, DMF).

Preparation of 10:

5-[(*tert*-Butyloxycarbonyl)amino]indole-2-carboxylic Acid. A solution of *N*-BOC-5-amino-2-(methoxycarbonyl)indole (57 mg, 0.2 mmol, 1.0 equiv) in THF–CH_3OH–H_2O (2.4 mL) was treated with aqueous 1 N LiOH (0.24 mL, 0.24 mmol,

1.2 equiv). The reaction mixture was warmed at 60 °C for 2 h. The solvent was concentrated under a N_2 stream and H_2O (3 mL) was added. This solution was treated with 10% aqueous HCl until the mixture was acidic. The insoluble solid was collected by centrifugation and washed with H_2O (2 × 3 mL). Drying the solid afforded the title compound (53 mg, 96%) as a white solid: mp 235–250 °C (decomp.); ^{1}H NMR (acetone-d_6, 400 MHz) δ 10.74 (br s, 1H, COOH), 8.26 (br s, 1H, NH), 7.95 (br s, 1H, NH), 7.43 (d, 1H, J = 8.9 Hz, C6-H), 7.42 (s, 1H, C3-H), 7.39 (dd, 1H, J = 8.9, 1.9 Hz, C7-H), 7.13 (dd, 1H, J = 2.1, 0.8 Hz, C4-H), 1.49 (s, 9H, $C(CH_3)_3$); IR (neat) ν_{max} 3351, 1698, 1536, 1236, 1177 cm^{-1}; FABHRMS (NBA–NaI) *m/z* 299.1003 (M^+ + Na, $C_{14}H_{16}N_2O_4$ requires 299.1008).

***N*-[(2-Methoxycarbonyl)indol-5-yl]-5-[(*tert*-butyloxycarbonyl)amino]indole-2-carboxamide.** A solution of the carboxylic acid above (44 mg, 0.16 mmol, 1.0 equiv) and 5-amino-2-(methoxycarbonyl)indole (30 mg, 0.16 mmol, 1 equiv) in 33% DMF–THF (3 mL) was treated with EDCI (61 mg, 0.32 mmol, 2.0 equiv). The resulting reaction mixture was stirred for 15 h at 25 °C. The mixture was concentrated under reduced pressure, and the residual solid was slurried in 3 mL of H_2O containing 3 drops of 10% aqueous HCl. The solid was collected by centrifugation and then washed with H_2O (3 × 3 mL). Chromatography (1 × 12 cm SiO_2, 50% EtOAc–hexane) afforded the title compound (61 mg, 85%) as a tan solid: mp 255–256 °C; ^{1}H NMR (acetone-d_6, 400 MHz) δ 10.95 (s, 1H, NH), 10.91 (s, 1H, NH), 9.67 (s, 1H, NH), 8.30 (s, 1H, NH), 8.24 (s, 1H), 7.94 (s, 1H), 7.69 (dd, 1H, J = 8.9, 2.0 Hz, C7′-H), 7.51 (d, 1H, J = 8.9 Hz), 7.47 (d, 1H, J = 8.8 Hz), 7.33 (dd, 1H, J = 8.8, 2.0 Hz, C7-H), 7.28 (d, 1H, J = 0.5 Hz), 7.17 (dd, 1H, J = 2.2, 0.8 Hz, C4-H), 3.88 (s, 3H, OCH_3), 1.49 (s, 9H, $C(CH_3)_3$); IR (neat) ν_{max} 3302, 1698, 1643, 1536, 1477, 1437, 1364, 1295, 1236, 1157 cm^{-1}; FABHRMS (NBA–NaI) *m/z* 449.1838 (M^+ + H, $C_{24}H_{24}N_4O_5$ requires 449.1825).

***N*-[2-(Methoxycarbonyl)indol-5-yl]-5-aminoindole-2-carboxamide (10).** A solution of the above compound (30 mg, 0.07 mmol) in trifluoroacetic acid (2.6 mL) was stirred for 45 min at 25 °C under Ar. The reaction mixture was concentrated, and the residual solid was slurried in 5% aqueous $NaHCO_3$ solution (3 mL). The insoluble solid was collected by centrifugation and washed with H_2O (3 × 3 mL). Drying the solid in vacuo afforded **10** (21 mg, 91%) as a tan solid: mp >350 °C; ^{1}H NMR (acetone-d_6, 400 MHz) δ 10.90 (br s, 1H, NH), 10.53 (br s, 1H, NH), 9.43 (br s, 1H, NH), 8.27 (d,

1H, J = 1.9 Hz), 7.65 (dd, 1H, J = 8.8, 2.0 Hz, C6′-H), 7.50 (d, 1H, J = 8.9 Hz, C7′-H), 7.31 (d, 1H, J = C7-H), 7.16 (s, 1H), 7.05 (s, 1H), 6.83 (s, 1H), 6.75 (dd, 1H, J = 8.6, 2.1 Hz, C6-H), 4.23 (br s, 2H, NH_2), 3.88 (s, 3H, OCH_3); IR (neat) ν_{max} 3262, 1697, 1533, 1441, 1236 cm^{-1}; FABHRMS (NBA–NaI) m/z 349.1313 ($M^+ + H$, $C_{19}H_{16}N_4O_3$ requires 349.1301).

Resolution of *N*-BOC-DSA (39). 2-Propanol and hexane (Fisher, HPLC grade) were filtered through a Millipore HV filter (pore size = 0.45 μm) and degassed by stirring under vacuum. A Waters Prep LC 4000 HPLC system equipped with a Diacel ChiralCel OD column (2 ×25 cm, 10 μm) was equilibrated with 30% 2-propanol-hexane at a flow rate of 7 mL/min. (±)-*N*-BOC-DSA (**39**)[17] was dissolved in CH_3OH (20 mg/mL) and 0.5–1.0 mL (10–20 mg) aliquots were injected at 20–25 min intervals. The effluent was monitored at 254 nm, and the fractions containing resolved **40** were collected: natural (+)-**39** (t_R = 19.5 min) and *ent*-(−)-**36** (t_R = 23.5 min), α = 1.24.

General Procedure for the Preparation of 49-51 and 57-59: Methyl 3-[[5-[((1*H*-Indol-2-yl)carbonyl)amino]-1*H*-indol-2-yl]carbonyl]-1-(chloromethyl)-5-hydroxy-1,2-dihydro-3*H*-pyrrolo[3,2-*e*]indole-7-carboxylate (59). A solution of **36** (2.0 mg, 5.25 μmol) in 4 N HCl–EtOAc (0.25 mL) was stirred for 20 min at 25 °C. The reaction mixture was concentrated to afford **38** as a gray powder. The hydrochloride salt was taken up in DMF (0.12 mL) and treated sequentially with EDCI (3.5 mg, 15.75 μmol, 3.3 equiv) and indole$_2$ (1.9 mg, 6.04 μmol, 1.1 equiv). The reaction mixture was stirred for 12 h at 25 °C before the solvent was removed under reduced pressure. The residual solid was slurried in 0.1 mL H_2O and the solid was collected by centrifugation. Chromatography (1 × 5 cm SiO_2, 20% DMF–toluene) afforded **59** (2.5 mg, 81%) as a gray solid: mp >230 °C; ^1H NMR (DMSO-d_6, 400 MHz) δ 11.73 (d, 1H, J = 1.2 Hz, NH), 11.68 (d, 1H, J = 1.6 Hz, NH), 11.65 (s, 1H, NH), 10.61 (s, 1H, NH), 9.83 (s, 1H, OH), 8.20 (d, 1H, J = 1.6 Hz), 7.82 (br s, 1H), 7.67 (d, 1H, J = 7.9 Hz), 7.55 (dd, 1H, J = 8.8, 1.8 Hz), 7.48 (s, 1H), 7.46 (s, 1H), 7.42 (s, 1H), 7.29 (1H, J = 2.0 Hz), 7.21 (dt, 1H, J = 8.2, 1.2 Hz), 7.15 (d, 1H, J = 1.4 Hz), 7.06 (dt, 1H, J = 8.0, 0.8 Hz), 4.77 (t, 1H, J = 10.6 Hz, C2-H), 4.45 (dd, 1H, J = 10.9, 3.9 Hz, C2-H), 4.15–4.05 (m, 2H), 3.98 (dd, 1H, J = 7.0, 3.9 Hz), 3.87 (s, 3H, OCH_3); IR (neat) ν_{max} 3393, 2966, 2916, 1711, 1693, 1662, 1646, 1631, 1612, 1553, 1537, 1517, 1485, 1234, 1134 cm^{-1}; FABHRMS (NBA–NaI) m/z 582.1540 ($M^+ + H$, $C_{31}H_{24}N_5O_5Cl$

requires 582.1544).

(1*S*)-**59**: $[\alpha]_D^{23}$ +27 (*c* 0.15, DMF).

ent-(1*R*)-**59**: $[\alpha]_D^{23}$ –29 (*c* 0.10, DMF).

General Procedure for the Preparation of 53-56 and 60-62: Methyl 2-[[5-[((1*H*-Indol-2-yl)carbonyl)amino]-1*H*-indol-2-yl]carbonyl]-1,2,8,8a-tetrahydrocyclopropa[*c*]-pyrrolo[3,2-*e*]indol-4-one-6-carboxylate (62, DSA-indole$_2$). A portion of NaH (0.4 mg, 60%, 10.3 μmol, 3 equiv) at 0 °C under Ar was treated with a solution of **59** (2.0 mg, 3.4 μmol, 1.0 equiv) in DMF (0.25 mL), and the reaction mixture was stirred for 90 min at 0 °C. The reaction mixture was directly subjected to flash chromatography (1 × 5 cm SiO_2, 15% DMF–toluene) to afford **62** (1.6 mg, 85%) as a pale yellow solid: mp > 230 °C; ^{1}H NMR (DMSO-d_6, 400 MHz) δ 12.64 (s, 1H, NH), 11.81 (d, 1H, *J* = 1.6 Hz, NH), 11.72 (d, 1H, *J* = 1.2 Hz, NH), 10.18 (s, 1H, OH), 8.20 (d, 1H, *J* = 1.5 Hz), 7.66 (d, 1H, *J* = 8.0 Hz), 7.59 (dd, 1H, *J* = 8.9, 2.0 Hz), 7.47 (s, 1H), 7.45 (s, 1H), 7.41 (d, 1H, *J* = 1.4 Hz), 7.22 (d, 1H, *J* = 2.2 Hz), 7.20 (dd, 1H, *J* = 8.2, 1.1 Hz), 7.06 (dt, 1H, *J* = 7.5, 0.7 Hz), 6.80 (s, 1H), 6.79 (d, 1H, *J* = 7.1 Hz), 4.58 (dd, 1H, *J* = 10.5, 5.1 Hz, C1-H), 4.44 (d, 1H, *J* = 10.5 Hz, C1-H), 3.79 (s, 3H, OCH_3), 3.05 (m, 1H, C8a-H), 1.78 (dd, 1H, *J* = 7.7, 3.8 Hz, C8-H), 1.60 (t, 1H, *J* = 4.5 Hz, C8-H); IR (neat) ν_{max} 3317, 2953, 2921, 2853, 1712, 1658, 1649, 1642, 1592, 1554, 1515, 1390, 1310, 1260 cm^{-1}; FABHRMS (NBA) *m/z* 546.1789 (M^+ + H, $C_{31}H_{23}N_5O_5$ requires 546.1777).

(+)-**62**: $[\alpha]_D^{23}$ +65 (*c* 0.16, DMF).

ent-(–)-**62**: $[\alpha]_D^{23}$ –69 (*c* 0.19, DMF).

Methyl 3-Acetyl-1-(chloromethyl)-5-hydroxy-1,2-dihydro-3*H*-pyrrolo[3,2-*e*]indole-7-carboxylate (42). A solution of *N*-BOC-DSA (**39**, 2.2 mg, 6.4 μmol, 1.0 equiv) in 4 N HCl–EtOAc (0.3 mL) was stirred for 30 min at 25 °C. The reaction mixture was concentrated to afford **38** as a gray solid. The hydrochloride salt was taken up in THF (80 μL) and treated sequentially with $NaHCO_3$ (1.6 mg, 19.2 μmol, 3.0 equiv) and $ClCOCH_3$ (50 μL, 0.26 M in THF, 2.0 equiv) at 0 °C under Ar. The reaction mixture was stirred for 1 h at 25 °C and directly subjected to flash chromatography (0.5 x 5.0 cm SiO_2, 50– 67% EtOAc–hexane gradient elution) to afford **42** (2.0 mg, 97%) as a white solid: ^{1}H NMR (acetone-d_6, 400 MHz) δ 10.69 (br s, 1H), 8.85 (br s, 1H), 7.93 (s, 1H), 7.21 (s, 1H), 4.35 (dd, 1H, *J* = 10.5, 9.8 Hz), 4.15– 4.04 (m, 3H), 3.88 (s, 3H),

3.80 (dd, 1H, J = 10.3, 8.1 Hz), 2.18 (s, 3H); IR (neat) ν_{max} 3333, 2964, 1697, 1615, 1415, 1256, 1164 cm^{-1}; FABHRMS (NBA) *m/z* 323.0807 ($M^+ + H$, $C_{15}H_{15}N_2O_4Cl$ requires 323.0799).

(1*S*)-**42**: $[\alpha]_D^{25}$ –48 (*c* 0.1, CH_3OH).

ent-(1*R*)-**42**: $[\alpha]_D^{25}$ +44 (*c* 0.08, CH_3OH).

Methyl 2-Acetyl-1,2,8,8a-tetrahydrocyclopropa[*c*]pyrrolo[3,2-*e*]indol-4-one-6-carboxylate (40, *N*-Ac-DSA). A suspension of NaH (0.7 mg, 60%, 18.6 μmol, 3.0 equiv) in THF (0.12 mL) at 0 °C under Ar was treated with a solution of **42** (2.0 mg, 6.2 μmol, 1.0 equiv) in 50% THF–DMF (0.3 mL), and the reaction mixture was stirred for 30 min at 0 °C. Hexane (0.2 mL) was added, and the mixture was subjected to flash chromatography (0.5 x 6.0 cm SiO_2, 83–100% EtOAc–hexane gradient elution) to afford **40** (1.3 mg, 73%) as a white solid: ^1H NMR (acetone-d_6, 400 MHz) δ 11.28 (br s, 1H, NH), 7.18 (br s, 1H, C3-H), 6.69 (s, 1H, C7-H), 4.18 (m, 2H, C1-H_2), 3.82 (s, 3H, OCH_3), 2.93–2.91 (m, 1H, C8a-H), 2.21 (s, 3H, CH_3), 1.72 (dd, 1H, J = 7.7, 3.9 Hz, C8-H), 1.44 (t, 1H, J = 4.5 Hz, C8-H); IR (neat) ν_{max} 3214, 2953, 1712, 1690, 1518, 1393, 1267, 1213 cm^{-1}; FABHRMS (NBA) *m/z* 287.1043 ($M^+ + H$, $C_{15}H_{15}N_2O_4$ requires 287.1032).

(+)-**40**: $[\alpha]_D^{25}$ +148 (*c* 0.05, CH_3OH).

ent-(–)-**40**: $[\alpha]_D^{25}$ –145 (*c* 0.04, CH_3OH).

Methyl 1-(Chloromethyl)-5-hydroxy-3-(methoxycarbonyl)-1,2-dihydro-3*H*-pyrrolo[3,2-*e*]indole-7-carboxylate (43). A solution of *N*-BOC-DSA (**39**, 2.2 mg, 6.4 μmol, 1.0 equiv) in 4 N HCl–EtOAc (0.3 mL) was stirred for 30 min at 25 °C. The reaction mixture was concentrated to afford **38** as a gray solid. The hydrochloride salt was taken up in THF (0.2 mL) and treated sequentially with $NaHCO_3$ (1.6 mg, 19.2 μmol, 3.0 equiv) and $ClCO_2CH_3$ (50 μL, 0.26 M in THF, 2.0 equiv) at 0 °C under Ar. The reaction mixture was stirred at 25 °C for 1 h, concentrated and subjected to flash chromatography (0.5 × 5.0 cm SiO_2, 50% EtOAc–hexane) to afford **43** (1.0 mg, 46%) as a white solid: ^1H NMR (acetone-d_6, 400 MHz) δ 10.63 (br s, 1H), 8.23 (br s, 1H), 7.59 (br s, 1H), 7.19 (s, 1H), 4.19 (dd, 1H, J = 11.4, 9.5 Hz), 4.09–3.98 (m, 3H), 3.87 (s, 3H), 3.78 (dd, 1H, J = 10.8, 8.2 Hz), 3.76 (s, 3H); IR (neat) ν_{max} 3313, 2954, 1687, 1456, 1344, 1251, 1154 cm^{-1}; FABHRMS (NBA) *m/z* 338.0735 (M^+, $C_{15}H_{15}N_2O_5Cl$ requires 338.0669).

(1*S*)-**43**: $[\alpha]_D^{25}$ –25 (*c* 0.03, CH_3OH).

ent-(1*R*)-**43**: $[\alpha]_D^{25}$ +27 (*c* 0.03, CH_3OH).

Methyl 2-(Methoxycarbonyl)-1,2,8,8a-tetrahydrocyclopropa[*c*] pyrrolo[3,2-*e*]indol-4-one-6-carboxylate (41, *N*-CO_2Me-DSA). A suspension of NaH (0.3 mg, 60%, 8.4 μmol, 3.0 equiv) in THF (80 μL) at 0 °C under Ar was treated with a solution of **43** (1.0 mg, 2.8 μmol, 1.0 equiv) in 50% THF–DMF (160 μL), and the reaction mixture was stirred for 30 min at 0 °C. Hexane (0.2 mL) was added, and the mixture was subjected to flash chromatography (0.5 × 6.5 cm SiO_2, 50–67% EtOAc–hexane gradient elution) to afford **41** (0.8 mg, 92%) as a white solid: ^{1}H NMR (acetone-d_6, 400 MHz) δ 6.69 (s, 2H, C3-H and C7-H), 4.08–4.05 (m, 2H, C1-H_2), 3.82 (s, 3H, OCH_3), 3.79 (s, 3H, OCH_3) 2.95–2.90 (m, 1H, C8a-H), 1.71 (dd, 1H, *J* = 7.7, 4.0 Hz, C8-H), 1.45 (t, 1H, *J* = 4.5 Hz, C8-H); IR (neat) ν_{max} 3405, 3262, 2923, 1718, 1595, 1441, 1390, 1267 cm^{-1}; FABHRMS (NBA) *m/z* 303.0987 (M^+ + H, $C_{15}H_{14}N_2O_5$ requires 303.0981).

(+)-**41**: $[\alpha]_D^{25}$ +130 (*c* 0.05, CH_3OH).

ent-(–)-**41**: $[\alpha]_D^{25}$ –130 (*c* 0.04, CH_3OH).

General Procedure for the Preparation of 49-52: Methyl 3-[(5-Methoxyindol-2-yl)carbonyl]-1-(chloromethyl)-5-hydroxy-1,2-dihydro-3*H*-pyrrolo[3,2-*e*]indole-7-carboxylate (50). A solution of *N*-BOC-DSA (**39**, 2.1 mg, 6.1 μmol, 1.0 equiv) in 4 N HCl–EtOAc (0.3 mL) was stirred for 30 min at 25 °C. The reaction mixture was concentrated to afford **38** as a gray solid. The hydrochloride salt was taken up in DMF (0.11 mL) and treated sequentially with 5-methoxyindole-2-carboxylic acid (1.3 mg, 6.7 μmol, 1.1 equiv) and EDCI (3.5 mg, 18.3 μmol, 3.0 equiv). The reaction mixture was stirred for 15 h at 25 °C before the solvent was concentrated under reduced pressure. Chromatography (0.5 × 6.0 cm SiO_2, 3% CH_3OH–CH_2Cl_2) afforded **50** (2.0 mg, 70%) as a pale yellow solid: ^{1}H NMR (acetone-d_6, 400 MHz) δ 10.73 (s, 1H, NH), 10.67 (s, 1H, NH), 8.87 (br s, 1H, OH), 7.99 (s, 1H, C4-H), 7.47 (d, 1H, *J* = 8.9 Hz, C7'-H), 7.29 (s, 1H, C8-H), 7.17 (d, 1H, *J* = 2.4 Hz, C4'-H), 7.10 (s, 1H, C3'-H), 6.92 (dd, 1H, *J* = 8.9, 2.4 Hz, C6'-H), 4.81 (t, 1H, *J* = 10.8 Hz, C2-H), 4.63 (dd, 1H, *J* = 10.8, 3.9 Hz, C2-H), 4.23–4.18 (m, 1H, C1-H), 4.16 (dd, 1H, *J* = 10.5, 2.8 Hz, C*H*HCl), 3.92 (dd, 1H, *J* = 10.6, 7.7 Hz, CH*H*Cl), 3.89 (s, 3H, OCH_3), 3.82 (s, 3H, OCH_3); IR (neat) ν_{max} 3322, 2943, 1699, 1602, 1519, 1432, 1218 cm^{-1}; FABHRMS (NBA–CsI) *m/z* 586.0160 (M^+ +

Cs, $C_{23}H_{20}N_3O_5Cl$ requires 586.0146).

(+)-**50**:$[\alpha]_D^{25}$ +10 (*c* 0.11, THF).

ent-(–)-**50**: $[\alpha]_D^{25}$ –11 (*c* 0.10, THF).

Methyl 3-[(Indol-2-yl)carbonyl]-1-(chloromethyl)-5-hydroxy-1,2-dihydro-3*H*-pyrrolo[3,2-*e*]indole-7-carboxylate (49): (78%) as a gray solid: ^{1}H NMR (acetone-d_6, 400 MHz) δ 10.80 (s, 1H, NH), 10.76 (s, 1H, NH), 8.92 (br s, 1H, OH), 7.95 (br s, 1H, C4-H), 7.71 (d, 1H, *J* = 7.9 Hz, C4'-H), 7.58 (d, 1H, *J* = 8.3 Hz, C7'-H), 7.29 (s, 1H, C8-H), 7.26 (dt, 1H, *J* = 7.1, 1.1 Hz, C6'-H), 7.19 (s, 1H, C3'-H), 7.10 (dt, 1H, *J* = 7.1, 0.8 Hz, C5'-H), 4.84 (t, 1H, *J* = 10.6 Hz, C2-H), 4.65 (dd, 1H, *J* = 10.8, 4.0 Hz, C2-H), 4.23–4.19 (m, 1H, C1-H), 4.16 (dd, 1H, *J* = 10.8, 3.3 Hz, C*H*HCl), 3.93 (dd, 1H, *J* = 10.8, 7.8 Hz, CH*H*Cl), 3.89 (s, 3H, OCH_3); IR (neat) ν_{max} 3321, 2932, 1707, 1599, 1436 cm^{-1}; FABHRMS (NBA–CsI) *m/z* 424.1076 (M^+ + H, $C_{22}H_{18}N_3O_4Cl$ requires 424.1064).

Methyl 3-[(6-Methoxyindol-2-yl)carbonyl]-1-(chloromethyl)-5-hydroxy-1,2-dihydro-3*H*-pyrrolo[3,2-*e*]indole-7-carboxylate (51): (79%) as a pale yellow solid: ^{1}H NMR (acetone-d_6, 400 MHz) δ 10.78 (br s, 1H, NH), 10.63 (s, 1H, NH), 8.95 (br s, 1H, OH), 8.01 (s, 1H, C4-H), 7.58 (d, 1H, *J* = 8.7 Hz, C4'-H), 7.27 (s, 1H, C8-H), 7.12 (dd, 1H, *J* = 2.1, 0.6 Hz, C3'-H), 7.06 (d, 1H, *J* = 2.2 Hz, C7'-H), 6.76 (dd, 1H, *J* = 8.7, 2.3 Hz, C5'-H), 4.80 (dd, 1H, *J* = 10.8, 9.4 Hz, C2-H), 4.61 (dd, 1H, *J* = 10.8, 4.0 Hz, C2-H), 4.23–4.14 (m, 2H, C1-H, C*H*HCl), 3.92 (dd, 1H, *J* = 10.7, 7.7 Hz, CH*H*Cl), 3.89 (s, 3H, OCH_3), 3.81 (s, 3H, OCH_3); IR (neat) ν_{max} 3272, 1708, 1610, 1513, 1436, 1303, 1221, 1159, 1013 cm^{-1}; FABHRMS (NBA–CsI) *m/z* 586.0160 (M^+ + Cs, $C_{23}H_{20}N_3O_5Cl$ requires 586.0146).

(1*S*)-**51**: $[\alpha]_D^{25}$ –1.9 (*c* 0.13, THF).

ent-(1*R*)-**51**: $[\alpha]_D^{25}$ +2.3 (*c* 0.11, THF).

Methyl 3-[(7-Methoxyindol-2-yl)carbonyl]-1-(chloromethyl)-5-hydroxy-1,2-dihydro-3*H*-pyrrolo[3,2-*e*]indole-7-carboxylate (52): (81%) as a white solid: ^{1}H NMR (acetone-d_6, 400 MHz) δ 11.22 (br s, 1H, NH), 10.47 (br s, 1H, NH), 9.45 (br s, 1H, OH), 7.91 (br s, 1H, C4-H), 7.28 (d, 1H, *J* = 8.0 Hz, C4'-H), 7.25 (s, 1H, C8-H), 7.12 (s, 1H, C3'-H), 7.02 (t, 1H, *J* = 7.9 Hz, C5'-H), 6.78 (d, 1H, *J* = 7.7 Hz, C6'-H), 4.77 (dd, 1H, *J* = 10.3, 9.8 Hz, C2-H), 4.57 (dd, 1H, *J* = 10.8, 3.9 Hz, C2-H), 4.17–4.09 (m, 2H, C1-H, C*H*HCl), 3.97 (s, 3H, OCH_3), 3.93–3.88 (m, 1H, CH*H*Cl), 3.91 (s, 3H,

OCH_3); IR (neat) ν_{max} 3323, 2933, 1708, 1595, 1436, 1349, 1256, 1159 cm^{-1}; FABHRMS (NBA–CsI) *m/z* 586.0161 (M^+ + Cs, $C_{23}H_{20}N_3O_5Cl$ requires 586.0146).

(1*S*)-**52**: $[\alpha]_D^{25}$ –3.5 (*c* 0.13, THF).

ent-(1*R*)-**52**: $[\alpha]_D^{25}$ +2.7 (*c* 0.12, THF).

General Procedure for the Preparation of 53-56: Methyl 2-[(5-Methoxyindol-2-yl)carbonyl]-1,2,8,8a-tetrahydrocyclopropa[*c*]pyrrolo[3,2-*e*]indol-4-one-6-carboxylate (54). A suspension of NaH (0.4 mg, 60%, 10.5 μmol, 3.0 equiv) in THF (0.12 mL) at 0 °C under Ar was treated with a solution of **50** (1.6 mg, 3.5 μmol, 1.0 equiv) in 50% THF–DMF (0.24 mL), and the reaction mixture was stirred for 30 min at 0 °C. Hexane (0.2 mL) was added, and the mixture was subjected to flash chromatography (0.5 × 7.0 cm SiO_2, 2–3.5% CH_3OH–CH_2Cl_2 gradient elution) to afford **54** (1.4 mg, 96%) as a pale yellow solid: ^1H NMR (acetone-d_6, 400 MHz) δ 11.32 (s, 1H, NH), 10.79 (s, 1H, NH), 7.46 (d, 1H, *J* = 8.9 Hz, C7'-H), 7.13 (s, 1H, C3'-H), 7.13 (s, 1H, C4'-H), 6.96 (dd, 1H, *J* = 7.1, 1.9 Hz, C6'-H), 6.91 (s, 1H, C3-H), 6.75 (s, 1H, C7-H), 4.61 (dd, 1H, *J* = 10.3, 5.0 Hz, C1-H), 4.53 (d, 1H, *J* = 10.3 Hz, C1-H), 3.84 (s, 3H, OCH_3), 3.81 (s, 3H, OCH_3), 3.05 (dt, 1H, *J* = 7.7, 3.9 Hz, C8a-H), 1.81 (dd, 1H, *J* = 7.7, 4.0 Hz, C8-H), 1.62 (t, 1H, *J* = 4.5 Hz, C8-H); IR (neat) ν_{max} 3284, 2934, 1713, 1633, 1607, 1512, 1389, 1257 cm^{-1}; FABHRMS (NBA–CsI) *m/z* 550.0361 (M^+ + Cs, $C_{23}H_{19}N_3O_5$ requires 550.0379).

(+)-**54**: $[\alpha]_D^{25}$ +158 (*c* 0.06, THF).

ent-(–)-**54**: $[\alpha]_D^{25}$ –168 (*c* 0.04, THF).

Methyl 2-[(Indol-2-yl)carbonyl]-1,2,8,8a-tetrahydrocyclopropa[*c*]pyrrolo[3,2-*e*]indol- 4-one-6-carboxylate (53, DSA-indole$_1$): (88%) as a pale yellow solid: ^1H NMR (acetone-d_6, 400 MHz) δ 10.92 (br s, 1H, NH), 7.69 (dd, 1H, *J* = 8.0, 0.8 Hz, C4'-H), 7.57 (dd, 1H, *J* = 8.3, 0.9 Hz, C7'-H), 7.29 (dt, 1H, *J* = 8.2, 1.1 Hz, C6'-H), 7.23 (s, 1H, C3'-H), 7.11 (dt, 1H, *J* = 8.0, 0.9 Hz, C5'-H), 6.93 (s, 1H, C3-H), 6.76 (s, 1H, C7-H), 4.64 (dd, 1H, *J* = 10.3, 5.0 Hz, C1-H), 4.56 (d, 1H, *J* = 10.3 Hz, C1-H), 3.84 (s, 3H, OCH_3), 3.08–3.04 (m, 1H, C8a-H), 1.81 (dd, 1H, *J* = 7.7, 4.0 Hz, C8-H), 1.63 (t, 1H, *J* = 4.5 Hz, C8-H); IR (neat) ν_{max} 3303, 2923, 1708, 1641, 1610, 1390, 1262 cm^{-1}; FABHRMS (NBA–NaI) *m/z* 388.1310 (M^+ + H, $C_{22}H_{17}N_3O_4$ requires 388.1297).

(+)-**53**: $[\alpha]_D^{25}$ +181 (*c* 0.04, CH_3OH).

ent-(–)-**53**: $[\alpha]_D^{25}$ –176 (*c* 0.05, CH_3OH).

Methyl 2-[(6-Methoxyindol-2-yl)carbonyl]-1,2,8,8a-tetrahydrocyclopropa[*c*]-pyrrolo[3,2-*e*]indol-4-one-6-carboxylate (55): (87%) as a pale yellow solid: ^{1}H NMR (acetone-d_6, 400 MHz) δ 11.34 (br s, 1H, NH), 10.71 (br s, 1H, NH), 7.56 (d, 1H, J = 8.7 Hz, C4'-H), 7.17 (s, 1H, C3'-H), 7.04 (d, 1H, J = 2.1 Hz, C7'-H), 6.96 (s, 1H, C3-H), 6.77 (dd, 1H, J = 8.8, 2.3 Hz, C5'-H), 6.75 (s, 1H, C7-H), 4.61 (dd, 1H, J = 10.2, 4.9 Hz, C1-H), 4.53 (d, 1H, J = 10.2 Hz, C1-H), 3.84 (s, 3H, OCH_3), 3.83 (s, 3H, OCH_3), 3.08–3.03 (m, 1H, C8a-H), 1.80 (dd, 1H, J = 7.7, 4.0 Hz, C8-H), 1.61 (t, 1H, J = 4.5 Hz, C8-H); IR (neat) ν_{max} 3261, 2954, 1713, 1634, 1505, 1386, 1260 cm^{-1}; FABHRMS (NBA) *m/z* 418.1403 (M^+ + H, $C_{23}H_{19}N_3O_5$ requires 418.1411).

(+)-**55**: $[\alpha]_D^{25}$ +146 (*c* 0.035, THF).

ent-(–)-**55**: $[\alpha]_D^{25}$ –137 (*c* 0.075, THF).

Methyl 2-[(7-Methoxyindol-2-yl)carbonyl]-1,2,8,8a-tetrahydrocyclopropa[*c*] pyrrolo[3,2-*e*]indol-4-one-6-carboxylate (56): (91%) as a pale yellow solid: ^{1}H NMR (acetone-d_6, 400 MHz) δ 11.21 (br s, 1H, NH), 10.46 (br s, 1H, NH), 7.25 (d, 1H, J = 8.1 Hz, C4'-H), 7.17 (s, 1H, C3'-H), 7.03 (t, 1H, J = 7.9 Hz, C5'-H), 6.80 (d, 1H, J = 7.6 Hz, C6'-H), 6.80 (s, 1H, C3-H), 6.75 (s, 1H, C7-H), 4.59 (dd, 1H, J = 10.4, 5.0 Hz, C1-H), 4.49 (d, 1H, J = 10.4 Hz, C1-H), 3.95 (s, 3H, OCH_3), 3.84 (s, 3H, OCH_3), 3.06–3.02 (m, 1H, C8a-H), 1.82 (dd, 1H, J = 7.6, 4.1 Hz, C8-H), 1.65 (t, 1H, J = 4.5 Hz, C8-H); IR (neat) ν_{max} 3231, 2944, 1708, 1610, 1518, 1390, 1256 cm^{-1}; FABHRMS (NBA–CsI) *m/z* 550.0363 (M^+ + Cs, $C_{23}H_{19}N_3O_5$ requires 550.0379).

(+)-**56**: $[\alpha]_D^{25}$ +166 (*c* 0.08, THF).

ent-(–)-**56**: $[\alpha]_D^{25}$ –172 (*c* 0.06, THF).

Methyl 3-[(3-Carbamoyl-1,2-dihydro-3*H*-pyrrolo[3,2-*e*]indol-7-yl)carbonyl]-1-(chloromethyl)-5-hydroxy-1,2-dihydro-3*H*-pyrrolo[3,2-*e*]indole-7-carboxylate (57): Chromatography (1 × 5 cm SiO_2, 10% CH_3OH–CH_2Cl_2) afforded **57** (1.6 mg, 67%) as an off-white solid: mp >230 °C: ^{1}H NMR (DMSO-d_6, 400 MHz) δ 11.63 (br s, 1H, NH), 11.55 (br s, 1H, NH), 9.82 (br s, 1H, OH), 7.97 (d, 1H, J = 8.9 Hz, C4′-H), 7.79 (br s, 1H), 7.28 (d, 1H, J = 2.1 Hz), 7.21 (d, 1H, J = 9.1 Hz, C5′-H), 6.93 (d, 1H, J = 1.5 Hz), 6.11 (s, 2H, NH_2), 4.75 (t, 1H, J = 10.2 Hz, C2-H), 4.41 (dd, 1H, J = 11.0, 4.1 Hz, C2-H), 4.11–4.06 (m, 2H), 4.02–3.90 (m, 1H), 3.97 (t, 2H, J = 9.2 Hz, C2′-H), 3.86 (s, 3H, OCH_3), 3.33–3.29 (m, 2H, C1′-H, obscured by H_2O); IR (neat) ν_{max} 3347, 2956, 2922, 2854, 1708, 1657, 1602, 1512, 1501, 1433, 1344, 1002 cm^{-1}; FABHRMS

(NBA–CsI) *m/z* 507.1322 ($M^+ + H$, $C_{25}H_{22}N_5O_5Cl$ requires 507.1309).

(1*S*)-**57**: $[\alpha]_D^{23}$ +13 (*c* 0.16, DMF).

ent-(1*R*)-**57**: $[\alpha]_D^{23}$ –14 (*c* 0.2, DMF).

Methyl 3-[(1,2-Dihydro-3-[(1,2-dihydro-3-carbamoyl-3*H*-pyrrolo[3,2-*e*]indol-7-yl)carbonyl]-3*H*-pyrrolo[3,2-*e*]indol-7-yl)carbonyl]-1-(chloromethyl)-5-hydroxy-1,2-dihydro-3*H*-pyrrolo[3,2-*e*]indole-7-carboxylate (58): Chromatography (0.5 × 5 cm SiO_2, 30% DMF–toluene) afforded **58** (2.4 mg, 67%) as a gray solid: mp > 230 °C; ^1H NMR (DMSO-d_6, 400 MHz) δ 11.75 (d, 1H, *J* = 2.0 Hz, NH), 11.64 (s, 1H, NH), 11.55 (d, 1H, *J* = 1.6 Hz, NH), 9.83 (s, 1H, OH), 8.26 (br s, 1H, C4-H), 7.96 (d, 1H, *J* = 8.9 Hz, C4′-H), 7.81 (br s, 1H), 7.36 (d, 1H, *J* = 9.2 Hz, C5′′-H), 7.29 (d, 1H, *J* = 2.1 Hz, C8-H), 7.22 (d, 1H, *J* = 8.4 Hz, C5′-H), 7.10 (s, 1H, C8′′-H), 6.96 (s, 1H, C8′-H), 6.10 (s, 2H, NH_2), 4.78 (t, 1H, *J* = 9.8 Hz, C2-H), 4.65 (t, 2H, *J* = 8.2 Hz, C2′-H), 4.45 (dd, 1H, *J* = 11.0, 3.9 Hz, C2-H), 4.18–3.95 (m, 3H), 3.86 (s, 3H, OCH_3), 3.46 (dd, 2H, *J* = 11.6, 8.3 Hz), 3.40–3.20 (m, 4H, C1′-H and C1′′-H, obscured by H_2O); IR (neat) ν_{max} 3321, 2950, 2924, 2852, 1710, 1657, 1608, 1502, 1432, 1005 cm^{-1}; FABHRMS (NBA) *m/z* 691.1978 ($M^+ + H$, $C_{36}H_{30}N_7O_6Cl$ requires 691.1946).

(1*S*)-**58**: $[\alpha]_D^{23}$ +6 (*c* 0.2 DMF).

ent-(1*R*)-**58**: $[\alpha]_D^{23}$ –8 (*c* 0.1 DMF).

Methyl 2-[(3-Carbamoyl-1,2-dihydro-3*H*-pyrrolo[3,2-*e*]indol-7-yl)carbonyl]-1,2,8,8a-tetrahydrocyclopropa[*c*]pyrrolo[3,2-*e*]indol-4-one-6-carboxylate (60, DSA–CDPI$_1$): Chromatography (1 × 5 cm SiO_2, 15% DMF–toluene) afforded **60** (71–98%) as a pale yellow solid: mp >245 °C; ^1H NMR (DMSO-d_6, 400 MHz) δ 12.64 (br s, 1H, NH), 11.69 (d, 1H, *J* = 1.6 Hz, NH), 8.00 (d, 1H, *J* = 8.9 Hz, C4′-H), 7.20 (d, 1H, *J* = 8.9 Hz, C5′-H), 7.01 (d, 1H, *J* = 1.6 Hz), 6.80 (s, 1H), 6.74 (s, 1H), 6.12 (br s, 2H, NH_2), 4.55 (dd, 1H, *J* = 10.5, 5.1 Hz, C1-H), 4.41 (d, 1H, *J* = 10.5 Hz, C1-H), 3.96 (t, 2H, *J* = 8.8 Hz, C2′-H), 3.78 (s, 3H, OCH_3), 3.34–3.22 (m, 2H, C1′-H, obscured by H_2O), 3.08–3.00 (m, 1H, C8a-H), 1.77 (dd, 1H, *J* = 7.7, 3.8 Hz, C8-H), 1.59 (t, 1H, *J* = 4.4 Hz, C8-H); IR (neat) ν_{max} 3352, 2921, 2849, 1707, 1657, 1602, 1502, 1422, 1390, 1265, 1001 cm^{-1}; FABHRMS (NBA) *m/z* 472.1629 ($M^+ + H$, $C_{25}H_{21}N_5O_5$ requires 472.1621).

(+)-**60**: $[\alpha]_D^{23}$ +71 (*c* 0.1, DMF).

ent-(–)-**60**: $[\alpha]_D^{23}$ –67 (*c* 0.05, DMF).

Methyl 2-[(1,2-Dihydro-3-[(1,2-dihydro-3-carbamoyl-3*H*-pyrrolo[3,2-*e*]indol-7-yl)carbonyl-3*H*-pyrrolo[3,2-*e*]indol-7-yl)carbonyl]-1,2,8,8a-tetrahydrocyclopropa[*c*]-pyrrolo [3,2-*e*]indol -4-one-6-carboxylate (61, DSA–CDPI$_2$): Chromatography (1 × 5 cm SiO_2, 30% DMF–toluene) afforded **61** (87–94%) as a pale yellow solid: mp >230 °C; ^{1}H NMR (DMSO-d_6, 400 MHz) δ 12.63 (s, 1H, NH), 11.87 (s, 1H, NH), 11.55 (s, 1H, NH), 8.27 (br s, 1H, C4′-H), 7.97 (d, 1H, J = 8.9 Hz, C4′′-H), 7.35 (d, 1H, J = 8.8 Hz, C5′′-H), 7.21 (d, 1H, J = 8.8 Hz, C5′-H), 7.17 (s, 1H, C8′′-H), 6.95 (s, 1H, C8′-H), 6.80 (s, 1H), 6.74 (s, 1H), 6.09 (s, 2H, NH_2), 4.64 (t, 2H, J = 8.6 Hz, C2′-H), 4.58 (dd, 1H, J = 10.2, 5.0 Hz, C1-H), 4.47 (d, 1H, J = 10.6 Hz, C1-H), 3.96 (t, 2H, J = 8.8 Hz, C2′′-H), 3.79 (s, 3H, OCH_3), 3.40–3.20 (m, 2H, C1′′-H), 3.39 (t, 2H, J = 8.8 Hz, C1′-H), 3.10–3.00 (m, 1H, C8a-H), 1.79 (dd, 1H, J = 7.7, 3.7 Hz, C8-H), 1.61 (t, 1H, J = 4.5 Hz, C8-H); IR (neat) ν_{max} 3371, 2926, 1710, 1657, 1608, 1501, 1430, 1390, 1265, 1056 cm^{-1}; FABHRMS (NBA) *m/z* 656.2268 (M^+ + H, $C_{36}H_{29}N_7O_6$ requires 656.2258).

(+)-**61**: $[\alpha]_D^{23}$ +43 (*c* 0.04, DMF).

ent-(–)-**61**: $[\alpha]_D^{23}$ –39 (*c* 0.2, DMF).

Acid-Catalyzed Addition of CH_3OH to (±)-*N*-BOC-DSA (39). 25 °C: A solution of (±)-*N*-BOC-DSA (**39**, 2.3 mg, 6.6 μmol) in 0.66 mL of CH_3OH was treated with 0.8 μmol of CF_3SO_3H dissolved in THF (17 μL) and the mixture was stirred for 1 h at 25 °C under Ar. $NaHCO_3$ (2 mg) was added followed by H_2O (2 mL). The mixture was extracted with EtOAc (4 × 1 mL) and the combined organic layers were dried (Na_2SO_4) and concentrated. Chromatography (SiO_2, 20% EtOAc–hexane) afforded **66** (1.9 mg, 75%) and **67** (0.45 mg, 18%).

0 °C: A solution of (±)-*N*-BOC-DSA (**39**, 1.5 mg, 4.4 μmol) in 0.44 mL of CH_3OH was treated with 0.5 μmol of CF_3SO_3H dissolved in THF (3 μL) and the mixture stirred for 3 h at 0 °C under Ar. $NaHCO_3$ (2 mg) was added followed by H_2O (2 mL). The mixture was extracted with EtOAc (4 × 1 mL) and the combined organic layers were dried (Na_2SO_4) and concentrated. Chromatography (SiO_2, 20% EtOAc–hexane) afforded **66** (1.24 mg, 76%) and **67** (0.2 mg, 12%).

For methyl 3-((*tert*-butyloxy)carbonyl)-5-hydroxy-1-(methoxymethyl)-1,2-dihydro-3*H*-pyrrolo[3,2-*e*]indole-7-carboxylate (**66**): ^{1}H NMR (acetone-d_6, 400 MHz) δ 10.47 (s, 1H, NH), 8.60 (s, 1H, OH), 7.61 (s, 1H), 7.11 (s, 1H), 4.06 (m, 2H, NCH_2),

3.87 (s, 3H, CO_2CH_3), 3.78 (d, 2H, J = 4.4 Hz, CH_2OCH_3), 3.40 (m, 1H, ArCH), 3.34 (s, 3H, OCH_3), 1.53 (s, 9H, $C(CH_3)_3$); FABHRMS (NBA–NaI) *m/z* 399.1539 (M^+ + Na, $C_{19}H_{24}N_2O_6$ requires 399.1532).

For methyl 6-((*tert*-butyloxy)carbonyl)-4-hydroxy-8-methoxy-6,7,8,9-tetrahydropyrrolo[3,2-*f*]quinoline-2-carboxylate (**67**): ^{1}H NMR (acetone-d_6, 400 MHz) δ 10.57 (s, 1H, NH), 8.51 (s, 1H, OH), 7.10 (s, 1H), 7.06 (s, 1H), 3.87 (s, 3H, CO_2CH_3), 3.83 (dd, 1H, J = 12.6, 7.2 Hz, NCH), 3.78 (m, 1H, $CHOCH_3$), 3.71 (dd, 1H, J = 12.6, 2.1 Hz, NCH), 3.42 (s, 3H, OCH_3), 3.21 (dd, 1H, J = 17.2, 6.0 Hz, ArCH), 2.85 (dd, 1H, J = 17.2, 4.0 Hz, ArCH), 1.49 (s, 9H, $C(CH_3)_3$); FABHRMS (NBA–NaI) *m/z* 399.1547 (M^+ + Na, $C_{19}H_{24}N_2O_6$ requires 399.1532).

Acid-Catalyzed Addition of CH_3OH to (+)-*N*-BOC-DSA (39). A solution of (+)-*N*-BOC-DSA (**39**, 1.9 mg, 5.5 μmol) in 0.55 mL of CH_3OH was treated with 0.66 μmol of CF_3SO_3H dissolved in THF (6 μL) and the mixture was stirred for 1 h at 25 °C under Ar. $NaHCO_3$ (2 mg) was added followed by H_2O (2 mL). The mixture was extracted with EtOAc (4 ×1 mL) and the combined organic layers were dried (Na_2SO_4), concentrated, and passed through a short plug of SiO_2. Samples of the reaction mixture were dissolved in *i*-PrOH and eluted on a Daicel ChiralCel AD analytical HPLC column (0.46 × 25 cm) with 15% *i*-PrOH–hexanes at a flow rate of 0.75 mL/min. Authentic samples of (±)-**66** eluted with a t_R = 8.09 and 9.03 min and those of (±)-**67** eluted with t_R = 16.55 and 25.99 min. Only one enantiomer of **66** (t_R = 8.98 min) and **67** (t_R = 16.55 min) were detected in the acid-cataylzed addition of CH_3OH to (+)-**39**.

Acid-Catalyzed Addition of H_2O to *N*-BOC-DSA (39). A solution of *N*-BOC-DSA (**39**, 3.6 mg, 10 μmol) in 1.0 mL of THF–H_2O (4:1) was treated with 2.4 μmol of CF_3SO_3H dissolved in THF (10 μL) and the mixture was stirred for 48 h at 25 °C under Ar. $NaHCO_3$ (2 mg) was added followed by H_2O (2 mL). The mixture was extracted with EtOAc (4 ×1 mL) and the combined organic layers were dried (Na_2SO_4) and concentrated. Chromatography (SiO_2, 20% EtOAc–hexane) afforded **35** (2.9 mg, 81%) identical in all respects with that previously described[17] and **68** (0.5 mg, 14%).

For methyl 6-((*tert*-butyloxy)carbonyl)-4,8-dihydroxy-6,7,8,9-tetrahydropyrrolo[3,2-*f*]quinoline-2-carboxylate (**68**): ^{1}H NMR ($CDCl_3$, 400 MHz) δ 9.19 (s, 1H, NH), 7.24 (s, 1H), 7.04 (d, 1H, J = 2.2 Hz), 5.93 (s, 1H, OH), 4.35 (m, 1H, $CHOH$), 3.95 (s, 3H, OCH_3), 3.88 (dd, 1H, J = 12.9, 5.6 Hz, NCH), 3.71 (dd, 1H, J =

13.2, 2.5 Hz, NCH), 3.20 (dd, 1H, J = 17.2, 5.8 Hz, ArCH), 2.85 (dd, 1H, J = 17.3, 4.6 Hz, ArCH), 1.54 (s, 9H, $C(CH_3)_3$); FABHRMS (NBA–NaI) *m/z* 385.1382 (M^+ + Na, $C_{18}H_{22}N_2O_6$ requires 385.1376).

4-(Benzyloxy)-*N*-(*tert*-butyloxycarbonyl)-1-iodo-*N*-(4-penten-1-yl)-2-naphthylamine (81). A solution of **80** (1.00 g, 2.11 mmol, 1 equiv) in benzene (100 mL) was treated with 50% w/v aqueous NaOH (20 mL). Benzyltributylammonium chloride (1.32 g, 4.22 mmol, 2 equiv) was added followed by 5-[(methanesulfonyl) oxy]-1-pentene (1.73 g, 10.53 mmol, 5 equiv). The resulting biphasic mixture was stirred vigorously at 25 °C for 12 h. The layers were allowed to separate and the aqueous portion was extracted with EtOAc (2 × 30 mL). The combined organic portions were washed with H_2O (2 × 100 mL) and saturated aqueous NaCl (50 mL). Drying ($MgSO_4$), filtration, and concentration was followed by flash chromatography (SiO_2, 3.5 × 14 cm, 5% EtOAc-hexane) to furnish **81** (0.975 g, 1.15 g theoretical, 85%) as a pale yellow solid: mp 69–71 °C; ^{1}H NMR (500 MHz, $CDCl_3$) major rotamer δ 8.34–8.32 (m, 1H), 8.23–8.21 (m, 1H), 7.62–7.49 (m, 4H), 7.42–733 (m, 3H), 6.70 (s, 1H), 5.81–5.71 (m, 1H), 5.34–5.18 (m, 2H), 5.01–4.93 (m, 2H), 3.84 (ddd, J = 17.5, 12.6, 7.6 Hz, 1H), 3.37–3.31 (m, 1H), 2.07–2.02 (m, 2H), 1.74–1.65 (m, 2H), 1.31 (s, 9H); ^{13}C NMR (125 MHz, $CDCl_3$) major rotamer δ 155.1, 154.0, 143.2, 137.9, 136.4, 135.4, 132.8, 128.7 (2C), 128.5, 128.2 (2C), 127.2, 126.2, 122.5, 115.0, 107.8, 95.1, 80.1, 70.3, 49.1, 31.3, 28.6, 28.3 (3C), 27.5; IR (film) ν_{max} 3067, 3036, 2974, 2923, 1697, 1615, 1590 cm^{-1}; FABHRMS (NBA–NaI) *m/z* 544.1337 (M + Na^+, $C_{27}H_{30}INO_3$ requires 544.1349).

Anal. Calcd for Calcd for $C_{27}H_{30}INO_3$: C, 59.65; H, 5.57; N, 2.58. Found C, 60.02; H, 5.27; N, 2.54.

7-(Benzyloxy)-5-(*tert*-butyloxycarbonyl)-1-methylidene-1,2,3,4-tetrahydro-5*H*-naphtho[1,2-*b*]azepine (82). A solution of **81** (0.503 g, 0.926 mmol, 1 equiv) in CH_3CN (18 mL, 0.051 M, degassed and purged with Ar) in a thick-walled reaction tube was treated with Et_3N (0.257 mL, 1.85 mmol, 2 equiv) followed by $(Ph_3P)_4Pd$ (0.032 g, 0.0277 mmol, 0.03 equiv). The reaction vessel was sealed and the mixture was warmed at 130 °C for 14 h. Concentration gave a yellow semisolid that was suspended in 5% EtOAc–hexanes. The precipitated salts were removed by filtration and thoroughly rinsed with the solvent mixture. Concentration of the filtrate and radial chromatography

(SiO_2, 2 mm plate, 5% EtOAc–hexane) afforded **82** as a colorless oil (0.343 g, 0.384 g theoretical, 89%) which slowly crystallized upon storage: mp 99–100 °C; ^{1}H NMR (400 MHz, $CDCl_3$) major rotamer δ 8.37–8.35 (m, 1H), 8.13–8.11 (m, 1H), 7.54–7.34 (m, 7H), 6.72 (s, 1H), 5.52 (s, 1H), 5.24 (s, 2H), 4.94 (s, 1H), 4.50–4.10 (m, 1H), 3.70–3.30 (m, 1H), 2.95–1.70 (m, 4H), 1.26 (s, 9H); ^{13}C NMR (100 MHz, $CDCl_3$) major rotamer δ 153.1, 145.3, 137.2, 137.0, 132.2, 129.8, 128.7 (3C), 128.0 (2C), 127.7, 127.2, 126.6, 126.1, 124.9, 122.1, 117.3, 106.5, 79.7, 70.2, 47.4, 35.1, 29.8, 28.3 (3C); IR (film) ν_{max} 3071, 3031, 2971, 2931, 2852, 1694, 1590 cm^{-1}; FABHRMS (NBA–NaI) *m/z* 438.2065 (M + Na$^+$, $C_{27}H_{29}NO_3$ requires 438.2045).

7-(Benzyloxy)-5-(*tert*-butyloxycarbonyl)-1-(hydroxymethyl)-1,2,3,4-tetrahydro-5*H*-naphtho[1,2-*b*]azepine (83). A solution of **82** (0.209 g, 0.504 mmol, 1 equiv) in THF (5 mL) was cooled to 0 °C prior to dropwise addition of BH_3•SMe_2 (0.151 mL, 10 M, 3(9) equiv). The cooling bath was removed after 5 min and the mixture was stirred at 25 °C for 12 h. The excess borane was quenched with slow addition of H_2O (0.6 mL). Oxidative workup was accomplished by the addition of 2.5 M aqueous NaOH (0.605 mL, 3 equiv) followed by 30% H_2O_2 (0.514 mL, 9 equiv) and the resulting heterogeneous solution was stirred rapidly at 25 °C (1 h) and 50 °C (1 h). The cooled reaction mixture was treated with saturated aqueous NaCl (0.5 mL) and the layers separated. The aqueous portion was extracted with EtOAc (2 × 5 mL) and the combined organic portions were dried ($MgSO_4$), filtered, and concentrated. Radial chromatography (SiO_2, 2 mm plate, 30% EtOAc–hexane) provided **83** as a colorless oil (0.179 g, 0.218 g theoretical, 82%) which slowly crystallized upon storage: mp 108–110 °C; ^{1}H NMR (400 MHz, $CDCl_3$) major rotamer δ 8.40 (d, *J* = 8.3 Hz, 1H), 8.18 (d, *J* = 8.6 Hz, 1H), 7.57–7.34 (m, 7H), 6.62 (s, 1H), 5.28 (d, *J* = 12.1 Hz, 1H), 5.17 (d, *J* = 12.0 Hz, 1H), 4.41–4.37 (m, 1H), 4.09–4.06 (m, 1H), 3.88–3.86 (m, 2H), 2.81–2.75 (m, 1H), 2.23–2.03 (m, 2H), 1.71–1.48 (m, 3H), 1.29 (s, 9H); ^{13}C NMR (100 MHz, $CDCl_3$) major rotamer δ 154.0, 153.2, 139.9, 136.9, 133.6, 128.7 (2C), 128.0 (2C), 127.7 127.0 (2C), 125.4, 125.0, 123.7, 122.7, 107.3, 80.2, 70.1, 63.3, 47.5, 39.1, 28.3 (3C), 26.3, 24.1; IR (film) ν_{max} 3429, 3067, 3037, 2967, 2926, 2866, 1694, 1674, 1619, 1594 cm^{-1}; FABHRMS (NBA–CsI) *m/z* 566.1333 (M + Cs$^+$, $C_{27}H_{31}NO_4$ requires 566.1307).

Anal. Calcd for $C_{27}H_{31}NO_4$: C, 74.79; H, 7.21; N, 3.23. Found: C, 74.49; H, 7.37;

N, 3.44.

7-(Benzyloxy)-5-(*tert*-butyloxycarbonyl)-1-[((methanesulfonyl)oxy)methyl]-1,2,3,4-tetrahydro-5*H*-naphtho[1,2-*b*]azepine (84). A solution of **83** (0.138 g, 0.319 mmol, 1 equiv) in CH_2Cl_2 (3 mL) was cooled to 0 °C prior to sequential addition of Et_3N (0.222 mL, 1.59 mmol, 5 equiv) and CH_3SO_2Cl (0.049 mL, 0.637 mmol, 2 equiv). The cooling bath was removed after 5 min and the mixture was stirred at 25 °C for 1 h. The reaction was quenched with the addition of saturated aqueous $NaHCO_3$ (0.5 mL) and the layers were separated. The aqueous portion was extracted with EtOAc (2 × 5 mL) and the combined organic portions were dried ($MgSO_4$), filtered, and concentrated. Radial chromatography (SiO_2, 2 mm plate, 30% EtOAc–hexane) furnished **84** (0.143 g, 0.163 g theoretical, 89%) as a white solid: mp 134–135 °C; ^{1}H NMR (400 MHz, $CDCl_3$) major rotamer δ 8.40 (d, J = 8.2 Hz, 1H), 8.13 (d, J = 8.6 Hz, 1H), 7.60–7.35 (m, 7H), 6.63 (s, 1H), 5.26 (d, J = 11.7 Hz, 1H), 5.17 (d, J = 11.6 Hz, 1H), 4.49–4.44 (m, 2H), 4.38–4.30 (m, 2H), 2.69–2.64 (m, 4H), 2.26–2.05 (m, 2H), 1.73–1.70 (m, 2H), 1.32 (s, 9H); ^{13}C NMR (100 MHz, $CDCl_3$) major rotamer δ 153.8, 153.6, 140.5, 136.7, 133.0, 128.8 (2C), 128.6, 128.1 (2C), 127.7, 127.6, 127.1, 125.2, 123.3, 122.8, 107.1, 80.8, 71.4, 70.2, 47.7, 37.1, 36.1, 28.3 (3C), 26.5, 24.4; IR (film) ν_{max} 3056, 2974, 2933, 2862, 1692, 1615, 1590 cm^{-1}; FABHRMS (NBA–NaI) *m/z* 534.1914 (M + Na$^+$, $C_{28}H_{33}NO_6S$ requires 534.1926).

Anal. Calcd for $C_{28}H_{33}NO_6S$: C, 65.73; H, 6.51; N, 2.74; S, 6.25. Found: C, 65.68; H, 6.59; N, 2.55; S, 6.31.

A solution of **84** (0.055 g) in 50% *i*-PrOH–hexane was resolved on a semipreparative Diacel Chiracel OD column (10 μm, 2 × 25 cm) using 10% *i*-PrOH–hexane as eluent (7 mL/min). The effluent was monitored at 254 nm and the enantiomers eluted with retention times of 38.0 and 45.0 min, respectively (α = 1.18). The fractions were collected and concentrated to afford *ent*-(+)-(1*S*)-**84** (t_R = 38.0 min, 0.0251 g) and (–)-(1*R*)-**77** (t_R = 45.0 min, 0.0248 g) with a 91% recovery (> 99.9% ee).

(–)-(1*R*)-**84**: $[\alpha]_D^{25}$ –41 (*c* 0.12, $CHCl_3$).

ent-(+)-(1*S*)-**84** : $[\alpha]_D^{25}$ +46 (*c* 0.13, $CHCl_3$).

5-(*tert*-Butyloxycarbonyl)-7-hydroxy-1-[((methanesulfonyl)oxy)methyl]-1,2,3,4-tetrahydro-5*H*-naphtho[1,2-*b*]azepine (85). A solution of **84** (0.096 g, 0.188 mmol, 1 equiv) in THF (3.0 mL) was treated with 10% Pd-C (0.042 g, 0.04 mmol, 0.2

equiv) followed by aqueous HCO_2NH_4 (1.0 mL, 25% w/v, 21 equiv) and the resulting mixture was stirred at 25 °C for 2.5 h. The mixture was filtered through Celite to afford a biphasic filtrate which was partitioned. The aqueous phase was extracted with EtOAc (2 × 2 mL) and the combined organic portions were dried ($MgSO_4$), filtered, and concentrated to give **85** as an analytically pure white solid (0.072 g, 0.079 g theoretical, 91%): mp 141–142 °C; ^{1}H NMR (400 MHz, DMF-d_7) major rotamer δ 8.29 (d, J = 8.2 Hz, 1H), 8.26 (d, J = 8.7 Hz, 1H), 7.62–7.59 (m, 1H), 7.54–7.50 (m, 1H), 6.82 (s, 1H), 4.59–4.47 (m, 1H), 4.43–4.25 (m, 3H), 3.02 (s, 3H), 2.98–2.76 (m, 1H), 2.35–2.20 (m, 1H), 2.13–1.95 (m, 1H), 1.71–1.67 (m, 2H), 1.39 (s, 9H); ^{13}C NMR (100 MHz, DMF-d_7) major rotamer δ 154.0, 153.5, 141.8, 134.0, 127.7, 125.2, 125.1, 124.3, 123.3, 123.0, 110.3, 80.4, 71.4, 48.2, 36.8, 36.4, 28.2 (3C), 27.2, 25.0; IR (film) ν_{max} 3262, 2974, 2933, 2872, 1692, 1662, 1594 cm^{-1}; FABHRMS (NBA–NaI) *m/z* 444.1468 (M + Na$^+$, $C_{21}H_{27}NO_6S$ requires 444.1457).

(–)-(1*R*)-**85**: $[\alpha]_D^{25}$ –63 (*c* 0.084, THF).

ent-(+)-(1*S*)-**85**: $[\alpha]_D^{25}$ +58 (*c* 0.084, THF).

7-(Benzyloxy)-5-(*tert*-butyloxycarbonyl)-1-(chloromethyl)-1,2,3,4-tetrahydro-5*H*-naphtho[1,2-*b*]azepine (86). A solution of **83** (0.105 g, 0.24 mmol, 1 equiv) in CH_2Cl_2 (2 mL) was treated with CCl_4 (0.225 mL, 2.33 mmol, 9.7 equiv) followed by Ph_3P (0.212 g, 0.81 mmol, 3.3 equiv) and the mixture was stirred at 25 °C for 2.5 h. The crude reaction solution was passed through a plug of silica gel and concentrated. Radial chromatography (SiO_2, 1 mm plate, 5% EtOAc–hexane) provided **86** as a pale yellow oil (0.048 g, 0.108 g theoretical, 44%) : ^{1}H NMR (250 MHz, $CDCl_3$) major rotamer δ 8.44–8.36 (m, 1H), 8.15–7.12 (m, 1H), 7.62–7.33 (m, 7H), 6.64 (s, 1H), 5.31–5.15 (m, 2H), 4.46–4.41 (m, 1H), 4.17–4.08 (m, 1H), 3.92–3.81 (m, 1H), 3.74–3.63 (m, 1H), 2.78–2.69 (m, 1H), 2.41–2.35 (m, 1H), 2.17–2.05 (m, 1H), 1.72–1.67 (m, 2H), 1.30 (s, 9H); IR (film) ν_{max} 2971, 2930, 2859, 1693, 1617, 1592 cm^{-1}; FABHRMS (NBA–NaI) *m/z* 451.1933 (M$^+$, $C_{27}H_{30}ClNO_3$ requires 451.1914).

5-(*tert*-Butyloxycarbonyl)-1-(chloromethyl)-7-hydroxy-1,2,3,4-tetrahydro-5*H*-naphtho[1,2-*b*]azepine (87). A solution of **86** (0.043 g, 0.095 mmol, 1 equiv) in THF (1.5 mL) was treated with 10% Pd–C (0.020 g, 0.019 mmol, 0.2 equiv) followed by aqueous HCO_2NH_4 (0.5 mL, 25% w/v, 1.98 mmol, 21 equiv) and the resulting black suspension was stirred rapidly at 25 °C for 2.5 h. The crude mixture was filtered

through a plug of Celite to afford a biphasic filtrate which was partitioned. The aqueous portion was extracted with EtOAc (2 × 1 mL) and the combined organic portions were dried ($MgSO_4$), filtered, and concentrated to provide **87** as an analytically pure white solid (0.032 g, 0.034 g theoretical, 94%). Recrystallization from 10% EtOAc–hexane gave colorless plates suitable for X-ray analysis:[24] mp 157–159 °C; ^{1}H NMR (400 MHz, $CDCl_3$) major rotamer δ 7.98–7.94 (m, 1H), 7.37–7.32 (m, 1H), 7.22–7.19 (m, 1H), 6.96–6.90 (m, 1H), 6.47 (s, 1H), 4.41–4.26 (m, 1H), 4.19–4.07 (m, 1H), 3.89–3.81 (m, 2H), 2.88–2.78 (m, 1H), 2.51–2.46 (m, 1H), 2.18–2.05 (m, 1H), 1.71–1.67 (m, 2H), 1.40 (s, 9H); ^{1}H NMR (400 MHz, acetone-d_6) major rotamer δ 9.17 (s, 1H), 8.27 (d, J = 8.1 Hz, 1H), 8.19–8.17 (m, 1H), 7.59–7.54 (m, 1H), 7.50–7.46 (m, 1H), 6.75 (s, 1H), 4.39–4.36 (m, 1H), 4.19–4.15 (m, 1H), 3.92–3.87 (m, 1H), 3.75–3.63 (m, 1H), 2.75–2.68 (m, 1H), 2.37–2.33 (m, 1H), 2.06–2.04 (m, 1H), 1.69–1.67 (m, 2H), 1.40 (s, 9H); ^{13}C NMR (100 MHz, $CDCl_3$) major rotamer δ 155.8, 152.9, 151.6, 139.3, 132.3, 126.5, 124.9, 124.7, 123.5, 122.4, 109.4, 81.5, 48.9, 44.6, 38.6, 28.4 (3C), 26.3, 24.2; IR (film) ν_{max} 3287, 2965, 2915, 2844, 1693, 1663 cm^{-1}; FABHRMS (NBA–NaI) *m/z* 384.1352 (M + Na$^+$, $C_{20}H_{24}ClNO_3$ requires 384.1342).

A solution of **87** (0.0096 g) in 50% *i*-PrOH–hexane was resolved on a semipreparative Diacel Chiracel OD column (10 μm, 2 × 25 cm) using 6% *i*-PrOH–hexane as eluent (6 mL/min). The effluent was monitored at 254 nm and the enantiomers eluted with retention times of 22.6 and 26.8 min, respectively (α = 1.19). The fractions were collected and concentrated to afford (–)-(1*R*)-**87** (t_R = 22.6 min, 0.0033 g) and *ent*-(+)-(1*S*)-**87** (t_R = 26.8 min, 0.0031 g) with a 67% recovery (>99.9% ee). The absolute configuration of (–)-(1*R*)-**80** was established by X-ray analysis.[24]

(–)-(1*R*)-**87**: $[\alpha]_D^{25}$ –67 (*c* 0.017, THF).

ent-(+)-(1*S*)-**87**: $[\alpha]_D^{25}$ +67 (*c* 0.016, THF).

***N*-(*tert*-Butyloxycarbonyl)-1,2,3,4,11,11a-hexahydrocyclopropa[*c*]naphtho[2,1-*b*]azepin-6-one (*N*-BOC-CNA, 78).** A sample of **85** (0.025 g, 0.059 mmol, 1 equiv) was suspended in CH_3CN (1.0 mL) and treated with DBU (0.027 mL, 0.178 mmol, 3 equiv) at 25 °C to instantly afforded a homogeneous pale yellow solution. The solvent was removed with a gentle stream of N_2 after 5 min. Flash chromatography (SiO_2, 1 × 7 cm, 30% EtOAc–hexane with 5% Et_3N) furnished **78** as a colorless oil (0.017 g, 0.019 g theoretical, 87%): ^{1}H NMR (400

MHz, CD_3CN) δ 8.12 (dd, J = 7.9, 1.5 Hz, 1H), 7.61 (ddd, J = 8.3, 7.1, 1.5 Hz, 1H), 7.41 (ddd, J = 8.0, 7.2, 1.0 Hz, 1H), 7.14 (d, J = 8.1 Hz, 1H), 6.48 (s, 1H), 4.09–4.02 (m, 1H), 2.69–2.54 (m, 1H), 2.28–2.22 (m, 1H), 2.10–2.07 (m, 2H), 1.95–1.91 (m, 2H overlapping with solvent), 1.75–1.72 (m, 1H), 1.62–1.57 (m, 1H), 1.26 (broad s, 9H); ^{13}C NMR (100 MHz, CD_3CN) δ 186.4, 162.1, 146.8, 133.7, 132.8, 129.3, 126.8, 126.6, 123.3, 81.0, 47.8, 40.2, 33.8, 28.4, 28.3, 26.8 (3C), 26.0, 25.9; IR (film) ν_{max} 2923, 2852, 1698, 1647, 1596 cm^{-1}; UV (THF) λ_{max} 304 (ε 8600), 258 (ε 11100), 220 (ε 15500) nm; FABHRMS (NBA–NaI) *m/z* 326.1766 (M + H^+, $C_{20}H_{24}NO_3$ requires 326.1756).

(+)-**78**: $[\alpha]_D^{25}$ +36 (*c* 0.009, EtOAc).

ent-(–)-**78**: $[\alpha]_D^{25}$ –36 (*c* 0.016, EtOAc).

1,2,3,4,11,11a-Hexahydrocyclopropa[*c*]naphtho[2,1-*b*]azepin-6-one (CNA, 79). A sample of **85** (0.030 g, 0.07 mmol, 1 equiv) was suspended in 3.9 M HCl–EtOAc (1.5 mL). After 40 min, the volatiles were removed with a gentle stream of N_2 followed by high vacuum. The resulting white foam was dissolved in CH_3CN containing DBU (0.105 mL, 0.70 mmol, 10 equiv in 1 mL of CH_3CN). The solvent was removed with a gentle stream of N_2 after 5 min. Radial chromatography (SiO_2, 1 mm plate, 95% CH_2Cl_2–CH_3OH) furnished **79** as a pale yellow solid (0.012 g, 0.016 g theoretical, 77%). Recrystallization from 10% CH_3OH–CH_3CN gave pale yellow plates suitable for X-ray analysis:[24] mp 180–183 °C with decomposition; ^1H NMR (400 MHz, CD_3OD) δ 8.07 (dd, J = 7.8, 1.5 Hz, 1H), 7.50 (ddd, J = 8.7, 7.2, 1.6 Hz, 1H), 7.33 (ddd, J = 8.0, 7.2, 1.0 Hz, 1H), 7.13 (d, J = 8.1 Hz, 1H), 6.00 (s, 1H), 3.54–3.48 (m, 1H), 3.00–2.90 (m, 1H), 2.78–2.74 (m, 1H), 2.50 (dd, J = 8.7, 5.0 Hz, 1H), 2.41–2.36 (m, 1H), 2.24–2.15 (m, 1H), 1.92–1.79 (m, 3H); ^{13}C NMR (150 MHz, CD_3OD) δ 184.6, 175.0, 146.3, 133.0, 132.7, 126.6, 126.1, 122.4, 107.9, 45.4, 38.2, 31.0 (2C), 26.4, 26.1; IR (film) ν_{max} 3285, 2924, 2855, 1608, 1584 cm^{-1}; UV (CH_3OH) λ_{max} 342 (ε 11900), 308 (ε 8300), 245 (ε 17100) nm; FABHRMS (NBA–NaI) *m/z* 226.1238 (M + H^+, $C_{15}H_{16}NO$ requires 226.1232).

7-(Benzyloxy)-1-methylidene-1,2,3,4-tetrahydro-5*H*-naphthol[1,2-*b*]azepine Hydrochloride (88). A solution of **82** (0.226 g, 0.55 mmol, 1 equiv) was dissolved in 3.9 M HCl–EtOAc (7.0 mL). After 40 min, the volatiles were removed with a gentle stream of N_2 followed by high vacuum. The resulting crude pale green solid was used

directly for the synthesis of **89** and **90** without further characterization.

7-(Benzyloxy)-5-(methoxycarbonyl)-1-methylidene-1,2,3,4-tetrahydro-5*H*-naphtho-[1,2-*b*]azepine (89). A solution of **88** (0.049 g, 0.14 mmol, 1 equiv) in THF (1.5 mL) was treated with $NaHCO_3$ (0.026 g, 0.31 mmol, 2.2 equiv) followed by methyl chloroformate (0.022 ml, 0.28 mmol, 2.0 equiv) and the mixture was stirred at 25 °C for 5 h. The reaction was quenched with the addition of saturated aqueous $NaHCO_3$ (0.5 mL) and the resulting layers were separated. The aqueous portion was extracted with EtOAc (2 × 2 mL) and the combined organic portions were dried ($MgSO_4$), filtered, and concentrated. Trituration with 10% EtOAc–hexane furnished **89** as a white solid (0.049 g, 0.052 g theoretical, 94%): mp 99–100 °C; ^{1}H NMR (500 MHz, $CDCl_3$) major rotamer δ 8.38–8.36 (m, 1H), 8.14–8.13 (m, 1H), 7.54–7.36 (m, 7H), 6.73 (s, 1H), 5.56 (s, 1H), 5.25 (s, 2H), 4.99 (s, 1H), 4.50–4.20 (m, 1H), 3.59 (s, 3H), 3.10–2.35 (m, 1H), 2.22–1.70 (m, 4H); ^{13}C NMR (125 MHz, $CDCl_3$) major rotamer δ 155.5, 153.4, 144.7, 136.8, 136.2, 132.2, 129.9, 128.6 (2C), 127.9, 127.3 (2C), 126.8, 126.1, 125.2 (2C), 122.2, 118.0, 105.8, 70.2, 52.8, 48.1, 35.0, 29.7; IR (film) ν_{max} 3067, 2923, 2862, 1703, 1590, 1508 cm^{-1}; FABHRMS (NBA–NaI) *m/z* 373.1688 (M^+, $C_{24}H_{23}NO_3$ requires 373.1678).

7-(Benzyloxy)-1-(hydroxymethyl)-5-(methoxycarbonyl)-1,2,3,4-tetrahydro-5*H*-naphtho[1,2-*b*]azepine (91). Following the general procedure detailed for **83**, **89** (0.049 g, 0.013 mmol, 1 equiv) was treated with BH_3•SMe_2 (0.039 mL, 10 M, 3(9) equiv), quenched with H_2O (0.16 mL), and oxidized with aqueous 2.5 M NaOH (0.16 mL, 0.39 mmol, 3 equiv) and 30% aqueous H_2O_2 (0.134 mL, 9 equiv). Radial chromatography (SiO_2, 1 mm plate, 50% EtOAc–hexane) provided **91** as a white solid (0.033 g, 0.051g theoretical, 64%): mp 90–92 °C; ^{1}H NMR (500 MHz, $CDCl_3$) major rotamer δ 8.41 (d, J = 8.5 Hz, 1H), 8.18 (d, J = 8.5 Hz, 1H), 7.57–7.35 (m, 7H), 6.63 (s, 1H), 5.25–5.17 (m, 2H), 4.46–4.43 (m, 1H), 4.09–4.07 (m, 1H), 3.87–3.76 (m, 2H), 3.59 (s, 3H), 2.93–2.83 (m, 1H), 2.21–2.08 (m, 2H), 1.70–1.64 (m, 3H); ^{13}C NMR (125 MHz, $CDCl_3$) major rotamer δ 155.6, 153.4, 139.0, 136.7, 133.5, 128.6 (2C), 128.0 (2C), 127.6, 127.3 (3C), 125.2, 123.7, 122.8, 106.9, 70.1, 63.4, 52.9, 48.3, 39.1, 26.4, 24.1; IR (film) ν_{max} 3453, 3063, 3032, 2940, 2868, 1696, 1593 cm^{-1}; FABHRMS (NBA–NaI) *m/z* 392.1871 ($M + H^+$, $C_{24}H_{25}NO_4$ requires 392.1862).

7-(Benzyloxy)-1-[((methanesulfonyl)oxy)methyl]-5-(methoxycarbonyl)-

1,2,3,4-tetrahydro-5*H*-naphtho[1,2-*b*]azepine (93). Following the general procedure detailed for **84**, **91** (0.029 g, 0.074 mmol, 1 equiv) was treated with Et_3N (0.052 mL, 0.371 mmol, 5 equiv) and CH_3SO_2Cl (0.017 mL, 0.148 mmol, 2 equiv). Radial chromatography (SiO_2, 1 mm plate, 50% EtOAc–hexane) furnished **93** (0.032 g, 0.035 g theoretical, 91%) as a white solid: mp 130–132 °C; ^{1}H NMR (500 MHz, $CDCl_3$) major rotamer δ 8.40 (d, J = 8.5 Hz, 1H), 8.13 (d, J = 8.5 Hz, 1H), 7.61–7.35 (m, 7H), 6.63 (s, 1H), 5.27–5.17 (m, 2H), 4.51–4.33 (m, 4H), 3.60 (s, 3H), 2.86–2.81 (m, 1H), 2.54 (s, 3H), 2.32–2.23 (m, 1H), 2.07–2.04 (m, 1H), 1.76–1.70 (m, 2H); ^{13}C NMR (125 MHz, $CDCl_3$) major rotamer δ 155.3, 153.7, 139.5, 136.6, 133.1, 128.6 (2C), 128.0 (2C), 127.7, 127.6, 127.3, 125.4, 124.3, 123.4, 122.8, 106.9, 71.1, 70.1, 53.0, 48.3, 36.8, 36.2, 26.7, 24.5 ; IR (film) ν_{max} 3063, 3022, 2938, 2858, 1701, 1593 cm^{-1}; FABHRMS (NBA) *m/z* 470.1648 (M + H$^+$, $C_{25}H_{27}NO_6S$ requires 470.1637).

7-Hydroxy-1-[((methanesulfonyl)oxy)methyl]-5-(methoxycarbonyl)-1,2,3,4-tetrahydro-5*H*-naphtho[1,2-*b*]azepine (95). Following the general procedure detailed for **85**, **93** (0.028 g, 0.060 mmol, 1 equiv) was treated with 10% Pd-C (0.010 g, 0.009 mmol, 0.16 equiv) followed by aqueous HCO_2NH_4 (0.265 mL, 25% w/v, 18 equiv). Filtration and concentration gave **95** as an analytically pure white solid (0.0204 g, 0.0225 g theoretical, 91%): mp 113–115 °C; ^{1}H NMR (500 MHz, CD_3OD) major rotamer δ 8.25 (d, J = 7.5 Hz, 1H), 8.14 (d, J = 8.5 Hz, 1H), 7.55–7.45 (m, 2H), 6.60 (s, 1H), 4.41–4.33 (m, 4H), 3.66 (s, 3H), 2.85–2.79 (m, 1H), 2.64 (s, 3H), 2.35–2.20 (m, 1H), 2.13–1.95 (m, 1H), 1.71–1.67 (m, 2H); ^{13}C NMR (125 MHz, CD_3OD) major rotamer δ 157.2, 154.4, 140.9, 134.8, 128.3, 126.2, 125.8 (2C), 124.5, 124.3, 123.9, 72.5, 53.6, 49.9, 37.3, 36.9, 27.9, 25.5; IR (film) ν_{max} 3283, 2938, 2857, 1672, 1621, 1591 cm^{-1}; FABHRMS (NBA–NaI) *m/z* 379.1081 (M$^+$, $C_{18}H_{21}NO_6S$ requires 379.1090).

***N*-(Methoxycarbonyl)-1,2,3,4,11,11a-hexahydrocyclopropa[*c*]naphtho[2,1-*b*]azepin-6-one (*N*-CO$_2$Me-CNA, 97).** Following the general procedure detailed for **78**, **95** (0.0071 g, 0.019 mmol, 1 equiv) was treated with DBU (0.008 mL, 0.057 mmol, 3 equiv). Flash chromatography (SiO_2, 1 × 7 cm, 50% EtOAc–hexane with 5% Et_3N) furnished **97** as a colorless oil (0.0048 g, 0.0052 g theoretical, 90%). Recrystallization from 10% EtOAc–hexane gave colorless plates suitable for X-ray analysis:[24] mp 259–261 °C ; ^{1}H NMR (500 MHz, acetone-d_6) δ 8.13 (dd, J = 8.0, 1.5 Hz, 1H), 7.63

(ddd, J = 8.5, 7.5, 1.5 Hz, 1H), 7.42 (ddd, J = 8.0, 7.2, 1.5 Hz, 1H), 7.20 (d, J = 8.5 Hz, 1H), 6.52 (s, 1H), 4.26–4.15 (m, 1H), 3.61 (s, 3H), 2.79–2.73 (m, 1H), 2.32–2.28 (m, 1H), 2.18–2.09 (m, 3H), 1.96–1.94 (m, 1H), 1.80–1.78 (m, 1H), 1.69–1.65 (m, 1H); ^{13}C NMR (125 MHz, acetone-d_6) δ 185.6, 155.2, 146.5 (2C), 133.6, 132.9, 129.7, 126.7, 126.5, 123.2, 53.1, 48.6, 39.8, 33.5, 26.8, 25.8, 25.5; IR (film) ν_{max} 3067, 2923, 2851, 1708, 1646, 1600, 1446 cm^{-1}; FABHRMS (NBA–NaI) *m/z* 284.1281 (M + H$^+$, $C_{17}H_{17}NO_3$ requires 284.1287).

7-(Benzyloxy)-5-[(5,6,7-trimethoxyindol-2-yl)carbonyl]-1-methylidene-1,2,3,4-tetrahydro-5*H*-naphtho[1,2-*b*]azepine (90). A solution of **88** (0.142 g, 0.405 mmol, 1 equiv) in DMF (3 mL) was treated with [[3-(dimethylamino)propyl]ethyl]carbodiimide hydrochloride (EDCI, 0.233 g, 1.22 mmol, 3 equiv) followed by 5,6,7-trimethoxyindole-2-carboxylic acid (0.122 g, 0.486 mmol, 1.2 equiv) and the reaction mixture was stirred at 25 °C for 4.5 h. The crude reaction mixture was diluted with EtOAc (4 mL) and extracted with H_2O (2 mL). The aqueous portion was extracted with EtOAc (2 × 1 mL). The combined organic portions were dried ($MgSO_4$), filtered, and concentrated. Radial chromatography (SiO_2, 2 mm plate, 50% EtOAc–hexane) furnished **90** (0.177 g, 0.222 g theoretical, 80%) as a pale yellow solid: mp 88–90 °C; ^{1}H NMR (500 MHz, $CDCl_3$) major rotamer δ 9.30 (s, 1H), 8.47–8.44 (m, 1H), 7.98–7.97 (m, 1H), 7.63–7.57 (m, 2H), 7.39–7.36 (m, 2H), 7.26–7.18 (m, 3H), 6.72 (s, 1H), 6.46 (s, 1H), 6.23–6.18 (m, 1H), 5.31–5.27 (m, 1H), 5.19–5.14 (m, 1H), 5.09–5.04 (m, 1H), 4.94–4.89 (m, 1H), 4.02 (s, 3H), 3.88 (s, 3H), 3.75 (s, 3H), 3.67–3.61 (m, 1H), 3.00–2.91 (m, 1H), 2.18–2.10 (m, 4H); ^{13}C NMR (125 MHz, $CDCl_3$) major rotamer δ 162.1, 154.5, 149.4, 144.3, 139.8, 138.6, 137.3, 136.5, 136.4, 136.3 , 132.0, 129.5, 128.4 (2C), 127.9, 127.1 (2C), 126.9, 126.3, 125.7, 123.4, 122.9, 118.2, 107.3, 106.9, 97.8, 70.2, 61.4, 56.0, 54.7, 47.3, 34.7, 25.2, 22.9; IR (film) ν_{max} 3448, 3235, 3062, 2930, 1607, 1581, 1495 cm^{-1}; FABHRMS (NBA–CsI) *m/z* 681.1378 (M + Cs$^+$, $C_{34}H_{32}N_2O_5$ requires 681.1366).

7-(Benzyloxy)-1-(hydroxymethyl)-5-[(5,6,7-trimethoxyindol-2-yl)carbonyl]-1,2,3,4-tetrahydro-5*H*-naphtho[1,2-*b*]azepine (92). Following the general procedure detailed for **83, 90** (0.200 g, 0.365 mmol, 1 equiv) was treated with BH_3•SMe_2 (0.110 mL, 10 M, 9 equiv), quenched with H_2O (0.44 mL), and oxidized with aqueous 2.5 M NaOH (0.44 mL, 1.10 mmol, 3 equiv) and 30% aqueous H_2O_2 (0.373 mL, 9 equiv).

Radial chromatography (SiO_2, 2 mm plate, 70% EtOAc–hexane) provided **92** (0.107 g, 0.207 g theoretical, 52%) as an amber oil. Recrystallization from EtOAc gave a white microcrystalline solid: mp 178–180 °C with decomposition; ^{1}H NMR (500 MHz, $CDCl_3$) major rotamer δ 9.26 (s, 1H), 8.48 (d, J = 10.4 Hz, 1H), 8.28 (d, J = 10.8 Hz, 1H), 7.68–7.65 (m, 1H), 7.60–7.57 (m, 1H), 7.35–7.33 (m, 2H), 7.22–7.13 (m, 3H), 6.66 (s, 1H), 6.43 (s, 1H), 5.23–5.21 (m, 1H), 5.13–5.10 (m, 1H), 5.03–4.99 (m, 1H), 4.95–4.90 (m, 1H), 4.24–4.21 (m, 2H), 4.03 (s, 3H), 3.87 (s, 3H), 3.73 (s, 3H), 3.26–3.20 (m, 1H), 2.46–2.40 (m, 1H), 1.95–1.92 (m, 1H), 1.30–1.23 (m, 3H); ^{13}C NMR (125 MHz, $CDCl_3$) major rotamer δ 160.7, 153.9, 149.5, 140.0, 139.8, 138.6, 136.3, 134.3, 129.0, 128.4 (2C), 127.8, 127.7, 127.1 (2C), 126.2, 125.9, 125.6, 124.8, 123.7, 123.3, 123.2, 108.4, 107.6, 97.9, 70.6, 70.2, 61.4, 61.1, 56.1, 41.3, 38.8, 31.8, 17.3; IR (film) 3446, 3290, 3062, 2927, 1732, 1608, 1587 cm^{-1}; FABHRMS (NBA–CsI) *m/z* 699.1482 (M + Cs^+, $C_{34}H_{34}N_2O_6$ requires 699.1471).

A solution of **92** (0.025 g) in 50% *i*-PrOH–hexane was resolved on a semipreparative Diacel Chiracel OD column (10 μm, 2 × 25 cm) using 30% *i*-PrOH–hexane as eluent (8 mL/min). The effluent was monitored at 254 nm and the enantiomers eluted with retention times of 20.9 and 24.0 min, respectively (α = 1.15). The fractions were collected and concentrated to afford (+)-(1*R*)-**92** (t_R = 20.9 min, 0.0088 g) and *ent*-(–)-(1*S*)-**92** (t_R = 45 min, 0.0093 g) with a 72% recovery (> 99.9% ee).

(+)-(1*R*)-**92**: $[\alpha]_D^{25}$ +58 (*c* 0.044, EtOAc).[38]

ent-(–)-(1*S*)-**92**: $[\alpha]_D^{25}$ –56 (*c* 0.047, EtOAc).

7-(Benzyloxy)-1-[((methanesulfonyl)oxy)methyl]-5-[(5,6,7-trimethoxyindol-2-yl)carbonyl]-1,2,3,4-tetrahydro-5*H*-naphtho[1,2-*b*]azepine (94). Following the general procedure detailed for **84**, **92** (0.040 g, 0.071 mmol, 1 equiv) was treated with Et_3N (0.049 mL, 0.354 mmol, 5 equiv) and CH_3SO_2Cl (0.011 mL, 0.141 mmol, 2 equiv). Radial chromatography (SiO_2, 1 mm plate, 70% EtOAc–hexane) furnished **94** (0.034 g, 0.046 g theoretical, 75%) as a white solid: mp 175–177 °C with decomposition; ^{1}H NMR (500 MHz, $CDCl_3$) major rotamer δ 9.30 (s, 1H), 8.49 (dd, J = 8.0, 1.0 Hz, 1H), 8.25 (d, J = 9.0 Hz, 1H), 7.68 (ddd, J = 8.0, 6.5, 1.0 Hz 1H), 7.61–7.58 (m, 1H), 7.36-7.34 (m, 2H), 7.22–7.16 (m, 3H), 6.69 (s, 1H), 6.43 (s, 1H), 5.28 (d, J = 2.0 Hz, 1H), 5.27–5.26 (m, 1H), 5.14 (d, J = 11.5 Hz, 1H), 5.03–4.99 (m,

2H), 4.52–4.49 (m, 1H), 4.04 (s, 3H), 3.88 (s, 3H), 3.74 (s, 3H), 3.21–3.17 (m, 1H), 2.78 (s, 3H), 2.60–2.59 (m, 1H), 2.20–2.18 (m, 1H), 1.34–1.32 (m, 3H); ^{13}C NMR (125 MHz, $CDCl_3$) major rotamer δ 160.7, 154.0, 149.6, 140.1, 139.9, 138.6, 136.2, 133.8, 128.7, 128.4 (2C), 127.9, 127.8, 127.1 (2C), 125.9, 125.7, 125.1, 124.9, 123.5, 123.3, 123.2, 108.6, 107.4, 97.8, 79.9, 70.2, 61.4, 61.1, 56.0, 41.4, 38.4, 36.7, 30.5, 16.9; IR (film) ν_{max} 3453, 3299, 3001, 2929, 2827, 1608, 1588 cm^{-1}; FABHRMS (NBA–CsI) *m/z* 777.1267 (M + Cs$^+$, $C_{35}H_{36}N_2O_6$ requires 777.1247).

(+)-(1*R*)-**94**: $[\alpha]_D^{25}$ +26 (*c* 0.044, EtOAc).[38]

ent-(–)-(1*S*)-**94**: $[\alpha]_D^{25}$ –28 (*c* 0.042, EtOAc).

7-Hydroxy-1-[((methanesulfonyl)oxy)methyl]-5-[(5,6,7-trimethoxyindol-2-yl)carbonyl]-1,2,3,4-tetrahydro-5*H*-naphtho[1,2-*b*]azepine (96). Following the general procedure detailed for **85**, **94** (0.024 g, 0.037 mmol, 1 equiv) was treated 10% Pd-C (0.006 g, 0.15 equiv) followed by aqueous HCO_2NH_4 (0.165 mL, 25 % w/v, 18 equiv). Filtration and concentration gave **96** as an analytically pure colorless oil in quantitative yield (0.020 g, 0.020 g theoretical): ^{1}H NMR (500 MHz, acetone-d_6) major rotamer δ 10.17 (s, 1H), 9.20 (s, 1H), 8.37–8.34 (m, 2H), 7.68–7.56 (m, 2H), 6.66 (s, 1H), 6.51 (s, 1H), 5.42 (s, 1H), 5.23–5.22 (m, 1H), 4.95–4.92 (m, 1H), 4.60–4.59 (m, 1H), 3.98 (s, 3H), 3.79 (s, 3H), 3.68 (s, 3H), 3.21–3.13 (m, 1H), 3.05 (s, 3H), 2.55–2.43 (m, 1H), 2.19–2.16 (m, 1H), 1.40–1.37 (m, 3H); ^{13}C NMR (125 MHz, acetone-d_6) major rotamer δ 161.1, 153.4, 150.8, 141.3, 141.1, 139.8, 135.1, 130.6, 128.3, 126.0, 125.8 (2C), 125.0, 124.6, 124.3, 123.8, 110.7, 108.8, 98.7, 81.6, 61.4, 61.3, 56.3, 41.8, 38.1, 37.5, 31.2, 17.4; IR (film) ν_{max} 3313, 2936, 2836, 1731, 1592, 1584 cm^{-1}; FABHRMS (NBA–CsI) *m/z* 687.0751 (M + Cs$^+$, $C_{28}H_{30}N_2O_8S$ requires 687.0774).

(+)-(1*R*)-**96**: $[\alpha]_D^{25}$ +143 (*c* 0.036, THF).[38]

ent-(–)-(1*S*)-**96**: $[\alpha]_D^{25}$ –147 (*c* 0.036, THF).

***N*-[(5,6,7-Trimethoxyindol-2-yl)carbonyl]-1,2,3,4,11,11a-hexahydrocyclopropa-[*c*]naphtho[2,1-*b*]azepin-6-one (98, CNA-TMI).** Following the general procedure detailed for **78**, **97** (0.0054 g, 0.001 mmol, 1 equiv) was treated with DBU (0.004 mL, 0.030 mmol, 3 equiv). Flash chromatography (SiO_2, 1 × 7 cm, 50% EtOAc–hexane with 5% Et_3N) furnished **98** as a yellow solid (0.0022 g, 0.0046 g theoretical, 48%). Recrystallization from EtOAc gave yellow needles: mp 222–227 °C; ^{1}H NMR (CD_3CN, 400 MHz) major rotamer δ 9.67 (br s, 1H), 8.15 (dd, *J* = 7.8, 1.3 Hz,

1H), 7.65–7.61 (m, 1H), 7.49–7.31 (m, 1H), 7.32 (d, J = 8.1 Hz, 1H), 6.77 (s, 1H), 6.63 (s, 1H), 6.12 (s, 1H), 4.29 (ddd, J = 12.0, 6.3, 5.3 Hz, 1H), 3.99 (s, 3H), 3.83 (s, 3H), 3.76 (s, 3H), 3.37 (ddd, J = 13.0, 8.5, 7.0 Hz, 1H), 2.86–2.83 (m, 1H), 2.54–2.48 (m, 1H), 2.32–2.27 (m, 2H), 1.31–1.26 (m, 3H); IR (film) ν_{max} 3292, 2923, 2841, 1626, 1600, 1523, 1456 cm^{-1}; FABHRMS (NBA–CsI) *m/z* 459.1934 (M + H^+, $C_{27}H_{26}N_2O_5$ requires 459.1920).

(–)-**98**: $[\alpha]_D^{25}$ –146 (*c* 0.004, THF).[38]

ent-(+)-**98**: $[\alpha]_D^{25}$ +146 (*c* 0.004, THF).

Acid-Catalyzed Addition of H_2O to 10: 6-(*tert*-Butyloxycarbonyl)-2,8-dihydroxy-1,2,3,4,5-pentahydro-6*H*-naphtho[1,2-*b*]azocine (99). A solution of **78** (0.0074 g, 0.022 mmol, 1 equiv) in THF (0.75 mL) was treated with H_2O (0.25 mL) followed by CF_3SO_3H (0.027 mL, 0.1 M in THF, 0.12 equiv) at 25 °C and the mixture was stirred for 5 min. The reaction mixture was treated with $NaHCO_3$ (0.01 g) followed by H_2O (1.0 mL). The aqueous portion was extracted with EtOAc (2 × 1 mL) and the combined organic portions were dried ($MgSO_4$), filtered, and concentrated to a colorless oil. ^1H NMR analysis of the crude mixture and comparison with **101** indicated the presence of the ring expansion solvolysis product exclusively (≥ 40–20:1). Radial chromatography (SiO_2, 1 mm plate, 50% EtOAc–hexane) provided **99** as a colorless oil (0.0077 g, 0.0078 g theoretical, 99%) which slowly crystallized upon storage: mp 235–237 °C; ^1H NMR (400 MHz, acetone-d_6) major rotamer δ 9.08 (s, 1H), 8.26 (d, J = 8.3 Hz, 1H), 8.11 (d, J = 8.5 Hz, 1H), 7.57–7.54 (m, 1H), 7.49–7.44 (m, 1H), 6.68 (s, 1H), 4.38–4.35 (m, 1H), 4.07–3.95 (m, 1H), 3.40–3.35 (m, 1H), 3.02–2.80 (m, 2H), 2.01–1.93 (m, 1H), 1.71–1.63 (m, 1H), 1.52–1.44 (m, 1H), 1.28 (s, 9H), 1.20–1.17 (m, 2H); IR (film) ν_{max} 3309, 2977, 2927, 2867, 1689, 1664, 1619, 1589 cm^{-1}; FABHRMS (NBA–CsI) *m/z* 476.0848 (M + Cs^+, $C_{20}H_{25}NO_4$ requires 476.0838).

Acid-Catalyzed Addition of H_2O to (+)-78: (–)-6-(*tert*-Butyloxycarbonyl)-2,8-dihydroxy-1,2,3,4,5-pentahydro-6*H*-naphtho[1,2-*b*]azocine (99). A solution of (+)-**78** (0.0030 g, 0.009 mmol, 1 equiv) in THF (0.38 mL) was treated with H_2O (0.13 mL) followed by CF_3SO_3H (0.011 mL, 0.1 M in THF, 0.12 equiv) at 25 °C and the mixture was stirred for 5 min. Workup as described for racemic **99** and radial chromatography (SiO_2, 1 mm plate, 50% EtOAc–hexane) provided (–)-**99** as a colorless oil (0.0032 g, 0.0032 g theoretical, 99%) which slowly crystallized upon storage. This material was

identical with racemic **99** in all respects. The solvolysis of (+)-**78** provided a single enantiomer established by chiral phase HPLC separation on a ChiralCel OG column (10 μm, 0.46 × 25 cm, 5% *i*-PrOH–hexane, 1 mL/min).

(–)-(2*R*)-**99**: $[\alpha]_D^{25}$ –9 (*c* 0.009, THF).

5-(*tert*-Butyloxycarbonyl)-7-hydroxy-1-(hydroxymethyl)-1,2,3,4-tetrahydro-5*H*-naphtho[1,2-*b*]azepine (101). Following the general procedure detailed for **86, 84** (0.015 g, 0.035 mmol, 1 equiv) was treated with 10% Pd-C (0.001 g, 0.3 equiv) followed by aqueous HCO_2NH_4 (0.2 mL, 25 % w/v, 23 equiv). Filtration and concentration gave **101** as an analytically pure colorless oil in quantitative yield (0.012 g, 0.012 g theoretical) which crystallized upon storage: mp 202–203 °C; ^{1}H NMR (400 MHz, $CDCl_3$) major rotamer δ 9.19 (s, 1H), 8.07–8.05 (m, 1H), 7.26–7.22 (m, 1H), 6.81–6.75 (m, 2H), 6.50 (s, 1H), 4.28–4.24 (m, 1H), 4.18–4.08 (m, 2H), 3.89–3.86 (m, 1H), 2.85–2.79 (m, 1H), 2.11–2.07 (m, 1H), 1.94–1.91 (m, 1H), 1.70–1.67 (m, 2H), 1.62 (s, 9H); ^{1}H NMR (400 MHz, acetone-d_6) major rotamer 9.03 (s, 1H), 8.26 (d, J = 8.2 Hz, 1H), 8.07 (d, J = 8.6 Hz, 1H), 7.55–7.51 (m, 1H), 7.46–7.43 (m, 1H), 6.74 (s, 1H), 4.37–4.33 (m, 1H), 4.03–3.99 (m, 1H), 3.91–3.80 (m, 1H), 3.61–3.52 (m, 2H), 2.73–2.66 (m, 1H), 2.36–2.32 (m, 1H), 2.20–2.10 (m, 1H), 1.60–1.55 (m, 1H), 1.33 (s, 9H); IR (film) ν_{max} 3272, 2976, 2925, 1662, 1621, 1596 cm^{-1}; FABHRMS (NBA–NaI) *m/z* 344.1855 (M + H$^+$, $C_{20}H_{25}NO_4$ requires 344.1862).

Acid-Catalyzed Addition of CH_3OH to 78: 6-(*tert*-Butyloxycarbonyl)-8-hydroxy-2-methoxy-1,2,3,4,5-pentahydro-6*H*-naphtho[1,2-*b*]azocine (100). A solution of **78** (0.0069 g, 0.021 mmol, 1 equiv) in freshly distilled CH_3OH (1.0 mL) was treated with CF_3SO_3H (0.027 mL, 0.1 M in CH_3OH, 0.12 equiv) at 25 °C for 5 min. Workup as described for **101** and radial chromatography (SiO_2, 1 mm plate, 50% EtOAc–hexane) provided **100** as a colorless oil (0.0070 g, 0.0076 g theoretical, 92%) which slowly crystallized upon storage: mp 199–200 °C with decomposition; ^{1}H NMR (500 MHz, acetone-d_6) major rotamer δ 9.09 (s, 1H), 8.27 (d, J = 8.5 Hz, 1H), 8.11 (d, J = 8.5 Hz, 1H), 7.59–7.56 (m, 1H), 7.49–7.47 (m, 1H), 6.69 (s, 1H), 4.37–4.29 (m, 1H), 3.57–3.56 (m, 1H), 3.49–3.46 (m, 1H), 3.43 (s, 3H), 2.85–2.79 (m, 2H), 1.99–1.90 (m, 1H), 1.81–1.75 (m, 1H), 1.28 (s, 9H overlapping with m, 2H); IR (film) ν_{max} 3268, 2971, 2868, 1695, 1664, 1587 cm^{-1}; FABHRMS (NBA–CsI) *m/z* 357.1951 (M + Cs$^+$, $C_{21}H_{27}NO_4$ requires 357.1940).

Addition of HCl to 78: 6-(*tert*-Butyloxycarbonyl)-2-chloro-8-hydroxy-1,2,3,4,5-pentahydro-6*H*-naphthol[1,2-*b*]azocine (102). A solution of **78** (0.0031 g, 0.0095 mmol, 1 equiv) in THF (0.31 mL) was treated with 3.3 M HCl–THF (0.0043 mL, 1.5 equiv) at –78 °C for 5 min. Evaporation of the volatiles and chromatography (SiO_2 1 × 7 cm, 30% EtOAc–hexane) furnished **102** as a pure white foam (0.0034 g, 0.0034 g theoretical, 100%): ^{1}H NMR (400 MHz, acetone-d_6) major rotamer δ 9.27 (br s, 1H), 8.27 (d, J = 8.5 Hz, 1H), 8.06 (d, J = 8.5 Hz, 1H), 7.63–7.59 (m, 1H), 7.57–7.49 (m, 1H), 6.72 (s, 1H), 4.49–4.43 (m, 1H), 3.67–3.63 (m, 1H), 3.24–3.21 (m, 1H), 2.88–2.82 (m, 2H), 2.02–1.90 (m, 1H), 1.81–1.75 (m, 1H), 1.68–1.67 (m, 1H), 1.43–1.41 (m, 1H), 1.29 (s, 9H); IR (film) ν_{max} 3251, 2974, 2933, 1692, 1662, 1621, 1585 cm^{-1}; FABHRMS (NBA–NaI) *m/z* 384.1333 (M + Na$^+$, $C_{20}H_{24}ClNO_3$ requires 384.1342).

4-(Benzyloxy)-1-bromo-*N*-(*tert*-butyloxycarbonyl)-*N*-(4-penten-1-yl)naphthylamine (103). A solution of the carbamate **102** (500 mg, 1.17 mmol) in benzene (25 mL) was added to a mixture of 50% aqueous NaOH (5 g) and benzyltributylammonium chloride (720 mg, 2.30 mmol, 2 equiv). The mixture was stirred vigorously for 15 min and 1-((methanesulfonyl)oxy)-4-pentene (1.91 g, 11.6 mmol, 10 equiv) was added. The mixture was stirred vigorously for 24 h at 25 °C. Ice-cold H_2O (200 mL), and EtOAc (50 mL) were added. The aqueous layer was extracted with EtOAc (50 mL), the combined organic layers were dried (Na_2SO_4) and the solvent was removed under vacuum. Chromatography (SiO_2, 4 × 20 cm, 15% EtOAc–hexane gradient elution) afforded **103** (272 mg, 581 mg theoretical, 47%) as an oil: ^{1}H NMR ($CDCl_3$, 400 MHz) δ 8.34 (d, J = 8.3 Hz, 1H), 8.27 (d, J = 8.6 Hz, 1H), 7.63 (t, J = 7.3 Hz, 1H), 7.55–7.49 (m, 3H), 7.42–7.33 (m, 3H), 6.77 and 6.68 (two s, 1H), 5.85 (m, 1H), 5.32–5.25 (m, 2H), 5.92 (m, 2H), 3.78 (m, 1H), 3.48 (m, 1H), 2.03 (m, 2H), 2.85–1.54 (m, 2H), 1.31 (s, 9H); IR (film) ν_{max} 2975, 2947, 1717, 1701, 1624, 1486 cm^{-1}; FABHRMS (NBA–CsI) *m/z* 628.0439 (M + Cs$^+$, $C_{27}H_{30}BrNO_3$ requires 628.0463).

Anal. Calcd for $C_{27}H_{30}BrNO_3$: C, 65.32; H, 6.09; N, 2.82. Found: C, 65.42; H, 5.90; N, 2.97.

5-((*tert*-Butyldimethylsilyl)oxy)-1-((tetrahydropyranyl)oxy)-1-pentene (105). A suspension of triphenyl[(2-tetrahydropyranyloxy)methyl]phosphonium chloride (6.12

g, 14.8 mmol, 3 equiv) in THF (50 mL) at –78 °C was treated dropwise with a solution of *n*-BuLi (5.7 mL, 2.5 M in hexane, 14.3 mmol, 2.9 equiv). The reaction mixture was stirred for 5 min at –78 °C, the cooling bath was removed and the mixture allowed to warm until it reached 0 °C. The mixture was recooled to –78 °C, and HMPA (21.5 mL, 123 mmol, 24.9 equiv) and **104** (1 g, 4.9 mmol) were added sequentially. The reaction mixture was stirred for 1.5 h at –78 °C and 24 h at 25 °C before it was quenched by the addition of phosphate buffer (500 mL, pH 7). The mixture was extracted with EtOAc (3 × 100 mL), and the combined organic phase was dried (Na_2SO_4) and the solvent removed under vacuum. Chromatography (SiO_2, 4 × 25 cm, 10% EtOAc–hexane containing 1% Et_3N) afforded **105** (1.37 g, 1.48 g theoretical, 92%) as a colorless oil as a mixture of *E*- and *Z*-olefin isomers (50:50): ^1H NMR ($CDCl_3$, 400 MHz) δ 6.24 (dt, *J* = 12.3, 1.3 Hz, 0.5H), 6.14 (dt, *J* = 6.3, 1.4 Hz, 0.5H), 5.09 (dt, *J* = 12.3, 7.5 Hz, 0.5H), 4.88 and 4.85 (two t, *J* = 3.1, 3.4 Hz, 1H), 4.47 (m, 0.5H), 3.83 and 3.54 (two m, 2H), 3.62 and 3.59 (two t, *J* = 6.4 Hz, 6.6 Hz, 2H), 2.17 and 1.98 (two m, 2H), 1.85–1.49 (m, 8H), 0.883 and 0.877 (two s, 9H), 0.04 and 0.03 (two s, 6H); IR (film) ν_{max} 2929, 2856, 1673, 1472 cm^{-1}; FABMS (NBA–NaI) *m/z* 301 ($M + H^+$).

Anal. Calcd for $C_{16}H_{32}O_3Si$: C, 63.95; H, 10.73. Found: C, 64.02; H, 10.43.

1-((Tetrahydropyranyl)oxy)-1-penten-5-ol (106). A solution of **105** (900 mg, 3 mmol) in THF (20 mL) was treated with Bu_4NF (1 M in THF, 3 mL, 3 mmol, 1 equiv) at 0 °C. The reaction mixture was stirred at 0 °C for 1 h and at 25 °C for 2 h. Phosphate buffer (100 mL, pH 7) was added and the mixture was extracted with EtOAc–hexane (2:1, 3 × 30 mL). The combined organic phase was dried (Na_2SO_4) and the solvent removed under vacuum. Chromatography (SiO_2, 4 × 25 cm, 30% EtOAc–hexane containing 2% Et_3N) afforded **106** (445 mg, 557 mg theoretical, 80%) as a colorless oil as a mixture of *E*- and *Z*-olefin isomers (50:50). Careful rechromatography of this material (SiO_2, 4 × 25 cm, 10–30% EtOAc–hexane containing 2% Et_3N gradient elution) enabled the partial separation of the two isomers.

E-isomer: ^1H NMR ($CDCl_3$, 400 MHz) δ 6.26 (m, 1H), 5.07 (dt, *J* = 12.3, 7.5 Hz, 1H), 4.86 (t, *J* = 3.1 Hz, 1H), 3.83 and 3.54 (two m, 2H), 3.62 (t, *J* = 6.4 Hz, 1H), 2.01 (m, 2H), 1.89–1.50 (m, 8H); IR (film) ν_{max} 3395, 2938, 2853, 1674, 1202 cm^{-1}.

Anal. Calcd for $C_{10}H_{18}O_3$: C, 64.49; H, 9.74. Found: C, 64.76; H, 9.58.

Z-isomer: ^1H NMR ($CDCl_3$, 400 MHz) δ 6.17 (dt, *J* = 6.3, 1.2 Hz, 1H), 4.84 (t, *J*

= 3.3 Hz, 1H), 4.45 (dt, J = 6.3, 7.6 Hz, 1H), 3.79 and 3.52 (two m, 2H), 3.59 (t, J = 6.3 Hz, 1H), 2.23 (br s, 1H), 2.18 (m, 2H), 1.85–1.46 (m, 8H); IR (film) ν_{max} 3404, 2941, 2870, 1669, 1356, 1254 cm^{-1}.

5-((Methanesulfonyl)oxy)-1-((tetrahydropyranyl)oxy)-1-pentene (107). The alcohol **106** (147 mg, 0.791 mmol) was added to a suspension of NaH (60% in oil, 38 mg, 0.95 mmol, 1.2 equiv) in THF (5 mL). The resulting mixture was stirred at 25 °C for 30 min and cooled to 0 °C before CH_3SO_2Cl was added dropwise. The reaction mixture was stirred 15 min at 0 °C and 15 min at 25 °C. Phosphate buffer (100 mL, pH 7) was added and the mixture extracted with CH_2Cl_2 (2 × 50 mL). The combined organic phase was dried (Na_2SO_4) and the solvent was removed under vacuum. Chromatography (SiO_2, 2 × 25 cm, 30% EtOAc–hexane containing 2% Et_3N) afforded **107** (205 mg, 208 mg theoretical, 98%) as a colorless oil as a mixture of *E*- and *Z*-olefin isomers (50:50): ^1H NMR ($CDCl_3$, 400 MHz) δ 6.24 (dt, J = 12.3, 1.3 Hz, 0.5 H), 6.14 (dt, J = 6.3, 1.4 Hz, 0.5H), 5.05 (dt, J = 12.3, 7.5 Hz, 0.5H), 4.88 and 4.85 (two t, J = 3.1, 3.4 Hz, 1H), 4.43 (m, 0.5H), 4.15 (m, 1H), 3.83 and 3.54 (two m, 2H), 3.05 (s, 3H), 2.17 and 1.98 (two m, 2H), 1.85–1.49 (m, 8H).

4-(Benzyloxy)-*N*-(*tert*-butyloxycarbonyl)-1-iodo-*N*-[5-((tetrahydropyranyl)oxy)-4-penten-1-yl]naphthylamine (108). A solution of **80** (53 mg, 112 μmol) in benzene (5 mL) was added to a mixture of 50% aqueous NaOH (0.5 g) and benzyltributylammonium chloride (70 mg, 224 μmol, 2 equiv). The mixture was stirred vigorously for 15 min and **100** (147 mg, 556 μmol, 5 equiv) was added. The mixture was stirred vigorously for 12 h at 25 °C. Ice-cold H_2O (50 mL), and EtOAc (10 mL) were added. The aqueous layer was extracted with EtOAc (10 mL), the combined organic layers were dried (Na_2SO_4) and the solvent was removed under vacuum. Chromatography (SiO_2, 2 × 20 cm, 10–25% EtOAc–hexane gradient elution) afforded **108** (58 mg, 72 mg theoretical, 80%) as an oil: ^1H NMR ($CDCl_3$, 400 MHz) δ 8.31 and 8.27 (two d, J = 8.3, 8.8 Hz, 1H), 8.21 (d, J = 8.2 Hz, 1H), 7.61–7.49 (m, 4H), 7.42–7.33 (m, 3H), 6.82–6.69 (m, 1H), 6.21 (m, 0.5H), 6.13 (d, 0.5H), 5.32–5.17 (m, 2H), 5.01 (dt, J = 12.2, 7.5 Hz, 0.5H), 4.86 and 4.82 (two m, 1H), 4.41 (m, 0.5H), 3.81 (m, 2H), 3.51 (m, 1H), 3.36–3.21 (m, 1H), 2.12 and 1.92 (two m, 2H), 1.83–1.49 (m, 8H), 1.29 (s, 9H); IR (film) ν_{max} 2940, 1699, 1591, 1407, 1366, 1338, 1158, 1099, 1037 cm^{-1}.

4-(Benzyloxy)-1-bromo-*N*-(*tert*-butyloxycarbonyl)-*N*-[5-((tetrahydropyranyl)oxy)-4-penten-1-yl]naphthylamine (109). A solution of **102** (37 mg, 86 μmol) in benzene (2 mL) was added to a mixture of 50% aqueous NaOH (0.5 g) and benzyltributylammonium chloride (54 mg, 172 μmol, 2 equiv). The mixture was stirred vigorously for 15 min and **107** (122 mg, 461 μmol, 7.7 equiv) was added. The mixture was stirred vigorously for 12 h at 25 °C. Ice-cold H_2O (50 mL), and EtOAc (10 mL) were added. The aqueous layer was extracted with EtOAc (10 mL), the combined organic layers were dried (Na_2SO_4), and the solvent was removed under vacuum. Chromatography (SiO_2, 2 × 20 cm, 10–25% EtOAc–hexane gradient elution) afforded **109** (40 mg, 51 mg theoretical, 80%) as an oil: ^{1}H NMR ($CDCl_3$, 400 MHz) δ 8.34 (d, J = 8.3 Hz, 1H), 8.27 (d, J = 8.6 Hz, 1H), 7.62 (t, J = 7.3 Hz, 1H), 7.55–7.49 (m, 3H), 7.42–7.33 (m, 3H), 6.80–6.68 (m, 1H), 6.18 (d, J = 12.0 Hz, 0.5H), 6.12 (d, J = 6.3 Hz, 0.5H), 5.30–5.16 (m, 2H), 5.00 (dt, J = 12.2, 7.4 Hz, 0.5H), 4.84 and 4.80 (two m, 1H), 4.40 (m, 0.5H), 3.83–3.72 and 3.51–3.31 (two m, 4H), 2.12 and 1.91 (two m, 2H), 1.82–1.49 (m, 8H), 1.29 (s, 9H), IR (film) ν_{max} 2945, 2937, 1703, 1591, 1405, 1370, 1163, 1100 cm^{-1}.

4-(Benzyloxy)-*N*-(*tert*-butyloxycarbonyl)-1-iodo-*N*-(4-oxobut-1-yl)naphthylamine (110). A solution of **81** (44 mg, 81 μmol) in THF (3 mL) was treated sequentially with a solution of $NaIO_4$ (35 mg, 162 μmol, 2 equiv) in 0.5 mL H_2O and a solution of OsO_4 (7.5 mM in THF, 0.53 mL, 4 μmol, 0.05 equiv). The reaction mixture was stirred for 6 h at 25 °C. EtOAc (20 mL) was added and the organic layer was dried (Na_2SO_4), filtered through Celite, and the solvent removed under vacuum. Chromatography (SiO_2, 1 × 15 cm, 15% EtOAc–hexane) afforded **110** (35 mg, 80%) as an oil: ^{1}H NMR ($CDCl_3$, 400 MHz) δ 9.73 (t, J = 1.3 Hz, 1H), 8.32 (d, J = 8.2 Hz, 1H), 8.20 (d, J = 8.4 Hz, 1H), 7.61–7.49 (m, 4H), 7.42–7.32 (m, 3H), 6.77 and 6.72 (two s, 1H), 5.32–5.25 (m, 2H), 3.86 (ddd, J = 14.0, 8.6 Hz, 6.7 Hz, 1H), 3.47 (m, 1H), 2.48 (m, 2H), 1.93–1.75 (m, 2H), 1.29 and 1.23 (two s, 9H); IR (film) ν_{max} 3064, 3032, 2975, 2930, 2722, 1638, 1616, 1590, 1407, 1160 cm^{-1}; FABHRMS (NBA–CsI) *m/z* 678.0095 (M + Cs$^+$, $C_{26}H_{28}INO_4$ requires 678.0117).

4-(Benzyloxy)-1-bromo-*N*-(*tert*-butyloxycarbonyl)-*N*-(4-oxobut-1-yl)naphthylamine (111). A solution of **102** (115 mg, 0.23 mmol) in THF (8 mL) was treated sequentially with a solution of $NaIO_4$ (110 mg, 514 μmol, 2 equiv) in 1.5 mL

H_2O and a solution of OsO_4 (7.5 mM in THF, 1.5 mL, 11.2 μmol, 0.05 equiv). The reaction mixture was stirred for 6 h at 25 °C. EtOAc (20 mL) was added and the organic layer was dried (Na_2SO_4), filtered through Celite, and the solvent removed under vacuum. Chromatography (SiO_2, 2 × 15 cm, 15% EtOAc–hexane) afforded **111** (75 mg, 65%) as an oil: ^{1}H NMR ($CDCl_3$, 400 MHz) δ 9.73 (t, J = 1.3 Hz, 1H), 8.35 (d, J = 8.2 Hz, 1H), 8.27 (d, J = 8.4 Hz, 1H), 7.62 (t, J = 7.3 Hz, 1H), 7.56–7.49 (m, 3H), 7.42–7.32 (m, 3H), 6.75 and 6.70 (two s, 1H), 5.33–5.23 (m, 2H), 3.87 (m, 1H), 3.48 (m, 1H), 2.48 (2H), 1.92–1.77 (m, 2H), 1.29 and 1.23 (two s, 9H); IR (film) ν_{max} 3064, 3032, 2975, 2930, 2722, 1638, 1616, 1590, 1407, 1160 cm^{-1}; FABHRMS (NBA–CsI) *m/z* 630.0262 (M + Cs$^+$, $C_{26}H_{28}BrNO_4$ requires 630.0253).

(*E*)-4-(Benzyloxy)-*N*-(*tert*-butyloxycarbonyl)-1-iodo-*N*-[5-(methoxycarbonyl)-4-penten-1-yl]naphthylamine (112). A solution of **110** (13.3 mg, 24.4 μmol) in THF (0.3 mL) was treated with methyl (triphenylphosphoranylidene)acetate (23.9 mg, 71.5 μmol, 3 equiv). The reaction mixture was stirred for 48 h at 25 °C and the solvent removed under vacuum. Chromatography (SiO_2, 10–25% EtOAc–hexane gradient elution) afforded **112** (9 mg, 14 mg theoretical, 63%) as an oil: ^{1}H NMR ($CDCl_3$, 400 MHz) δ 8.32 (d, J = 8.2 Hz, 1H), 8.20 (d, J = 8.2 Hz, 1H), 7.61–7.48 (m, 5H), 7.42–7.32 (m, 2H), 6.91 (m, 1H), 6.74 and 6.64 (two s, 1H), 5.79 (d, J = 15.5 Hz, 1H), 5.31–5.23 (m, 2H), 3.81 (ddd, J = 14.0, 9.6, 3.6 Hz, 1H), 3.70 (s, 3H), 3.35 (m, 1H), 2.18 (m, 2H), 1.75–1.55 (m, 2H), 1.29 and 1.24 (two s, 9H); IR (film) ν_{max} 2975, 2947, 1702, 1658, 1471, 1391, 1366, 1307, 1272, 1162 cm^{-1}.

(*E*)-4-(Benzyloxy)-1-bromo-*N*-(*tert*-butyloxycarbonyl)-*N*-[5-(methoxycarbonyl)-4-penten-1-yl]naphthylamine (113). A solution of **111** (50.0 mg, 100 μmol) in THF (3 mL) was treated by methyl (triphenylphosphoranylidene)acetate (100 mg, 301 μmol, 3 equiv). The reaction mixture was stirred for 48 h at 25 °C and the solvent removed under vacuum. Chromatography (SiO_2, 10–40% EtOAc–hexane gradient elution) afforded **113** (52 mg, 55 mg theoretical, 94%) as an oil: ^{1}H NMR ($CDCl_3$, 400 MHz) δ 8.35 (d, J = 8.2 Hz, 1H), 8.27 (d, J = 8.2 Hz, 1H), 7.64–7.48 (m, 5H), 7.42–7.35 (m, 2H), 6.90 (m, 1H), 6.74 and 6.65 (two s, 1H), 5.81 (d, J = 15.5 Hz, 1H), 5.32–5.16 (m, 2H), 3.81–3.65 (m, 1H, partially obscured), 3.69 (s, 3H), 3.48 (m, 1H), 2.19 (m, 2H), 1.75–1.55 (m, 2H), 1.29 and 1.24 (two s, 9H); IR (film) ν_{max} 2976, 2945, 1698, 1657, 1394, 1367, 1311, 1272, 1163 cm^{-1}.

Anal. Calcd for $C_{29}H_{32}BrNO_5$: C, 62.82; H, 5.82; N, 2.53. Found: C, 62.80; H, 5.60; N, 2.52.

114. A sample of **112** (31.5 mg, 0.05 mmol) in a thick-walled reaction vessel and $(Ph_3P)_4Pd$ (2 mg, 0.001 mmol) was placed under Ar. To the reaction vessel was added CH_3CN (1.14 mL) and Et_3N (16 μL, 0.1 mmol). The mixture was heated at 115 °C for 24 h. The reaction mixture was cooled and was concentrated under a stream of N_2. Chromatography (SiO_2 20% EtOAc–hexane) gave 24.3 mg (90%) of **112** as a yellow oil: ^1H NMR ($CDCl_3$, 400 MHz) δ 6.80 (br s, 1H), 7.88 (d, J = 6.8 Hz, 1H), 7.52–7.32 (m, 7H), 6.68 (s, 1H), 5.78 (s, 1H), 5.22 (br s, 2H), 4.26 (br s, 1H), 3.82 (br s, 1H), 3.74 (s, 3H), 1.55–1.39 (m, 4H), 1.23 (br s, 9H); ^{13}C NMR δ 166.5, 158.5, 154.0, 136.7, 136.2, 131.1, 128.6, 128.0, 127.3, 127.1, 125.2, 122.3, 120.7, 120.4, 106.3, 105.8, 70.2, 51.1, 48.8, 47.3, 30.4, 30.1, 28.2, 27.2; IR ν_{max} 3070, 2975, 1715, 1694 cm^{-1}; FABHRMS *m/z* 606.1257 ($M + Cs^+$, $C_{29}H_{31}NO_5$ requires 606.1283).

Throughout this specification and the claims which follow, unless the context requires otherwise, the word "comprise", and variations such as "comprises" and "comprising", will be understood to imply the inclusion of a stated integer or step or group of integers or steps but not the exclusion of any other integer or step or group of integers or steps.

The reference to any prior art in this specification is not, and should not be taken as, an acknowledgment or any form of suggestion that that prior art forms part of the common general knowledge in Australia.

THE CLAIMS DEFINING THE INVENTION ARE AS FOLLOWS:

1. A compound selected from the group consisting of:

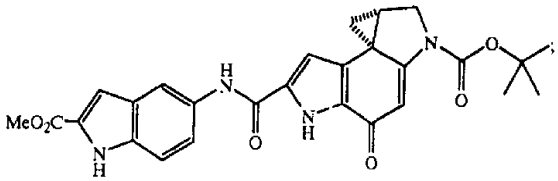

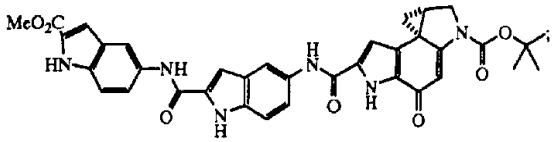

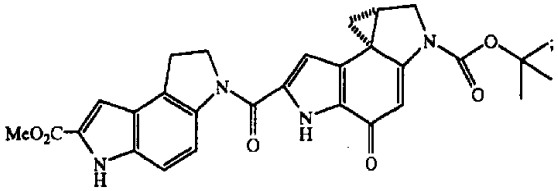

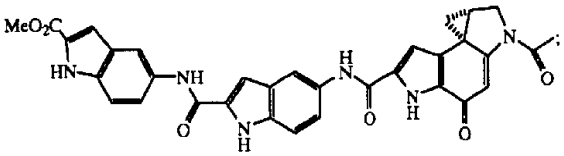

and

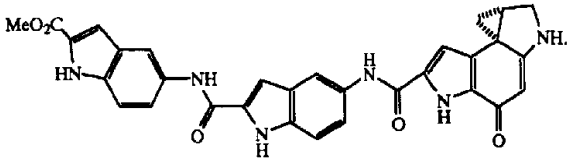

2. A compound selected from the group consisting of:

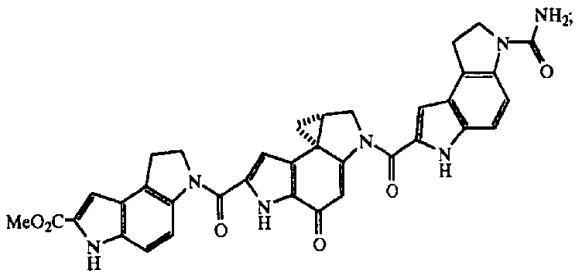

and

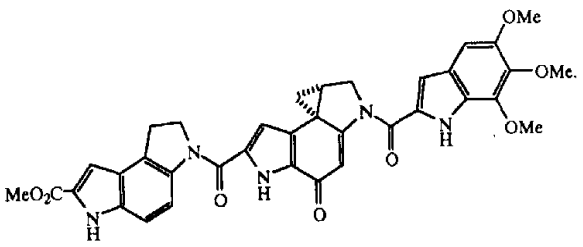

3. A compound selected from the group consisting of:

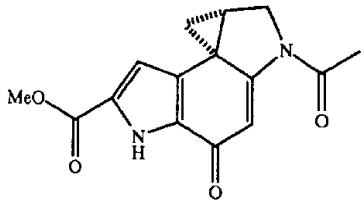

and

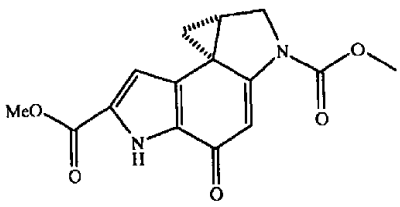

4. A compound selected from the group consisting of:

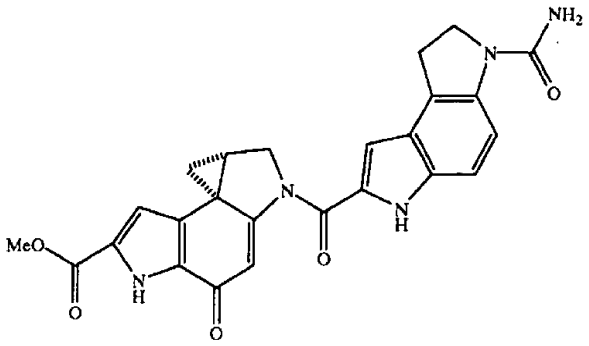

and

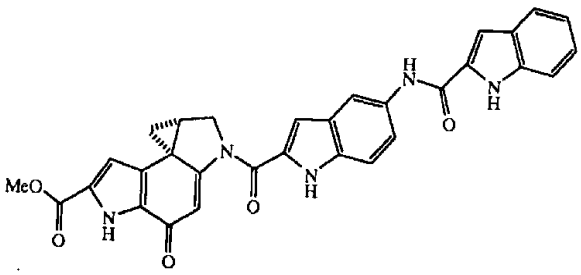

5. A compound selected from the group consisting of:

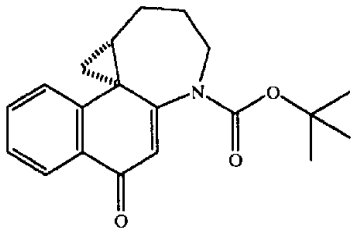

;

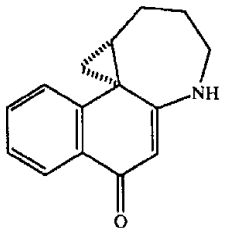

;

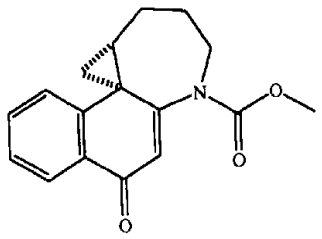

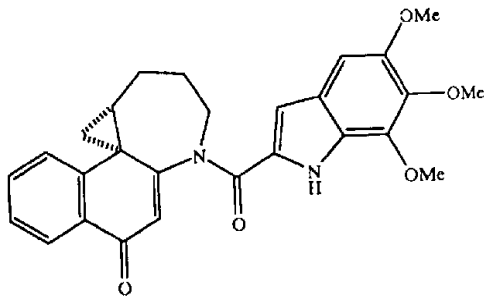

; and

DATED this 16th day of September, 2002

The Scripps Research Institute
by its Patent Attorneys
DAVIES COLLISON CAVE

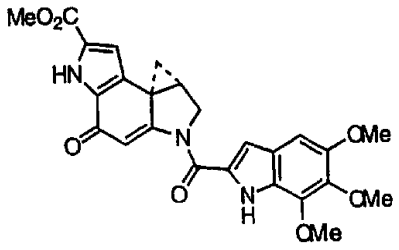

1, (+)-duocarmycin SA

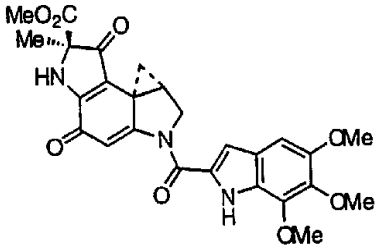

2, (+)-duocarmycin A

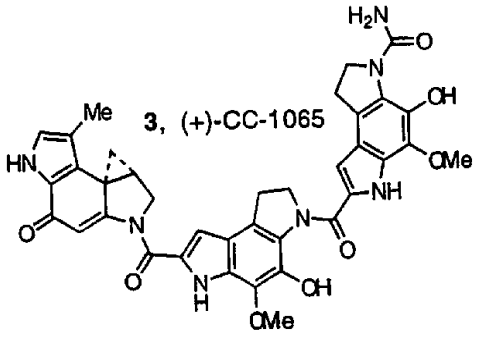

3, (+)-CC-1065

FIG. 1

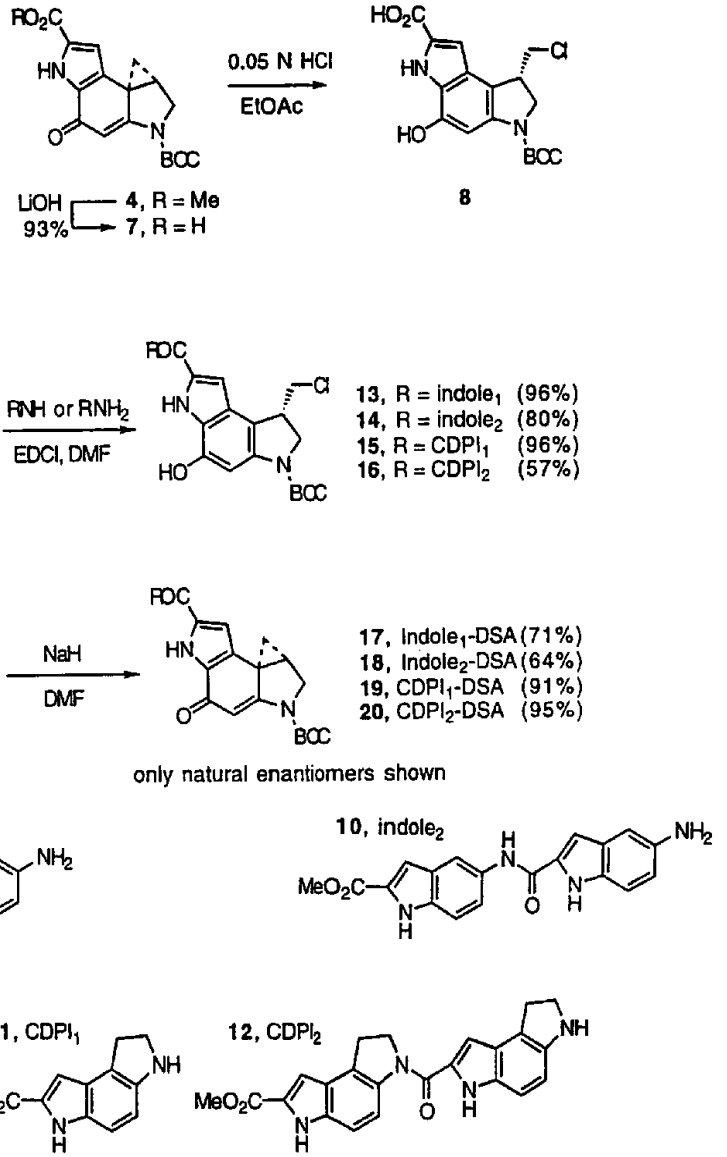
RO2C
HN
O
N
BOC
0.05 N HCl
EtOAc
HO2C
Cl
HO
LiOH
93%
4, R = Me
7, R = H
8
RNH or RNH2
EDCI, DMF
ROC
13, R = indole1 (96%)
14, R = indole2 (80%)
15, R = CDPI1 (96%)
16, R = CDPI2 (57%)
NaH
DMF
17, Indole1-DSA (71%)
18, Indole2-DSA (64%)
19, CDPI1-DSA (91%)
20, CDPI2-DSA (95%)
only natural enantiomers shown
9, indole1
NH2
MeO2C
10, indole2
11, CDPI1
12, CDPI2
NH

FIG. 2

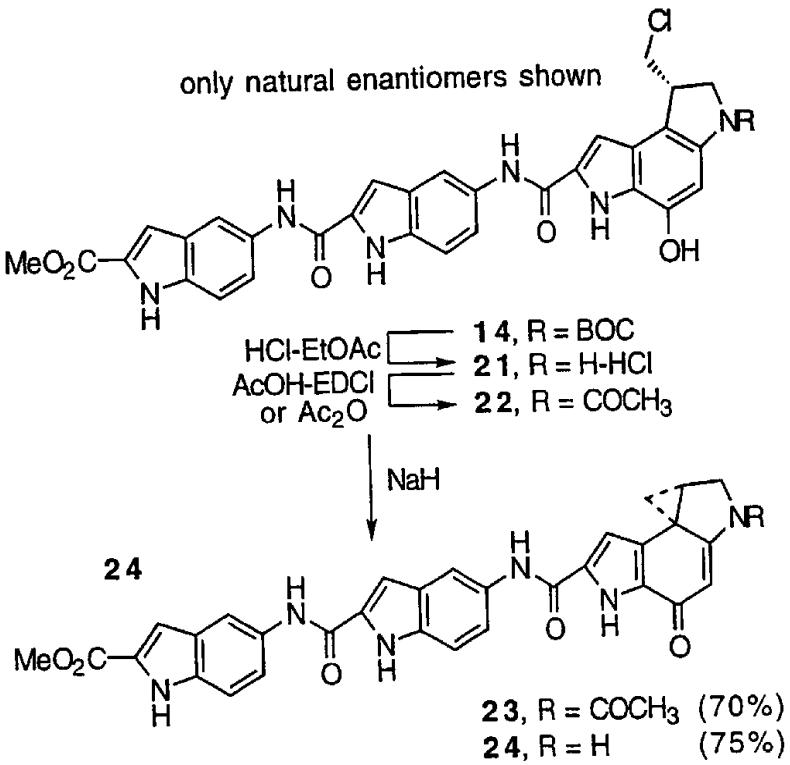
only natural enantiomers shown
Cl
NR
OH
MeO_2C
HCl-EtOAc
AcOH-EDCl
or Ac_2O
14, R = BOC
21, R = H-HCl
22, R = $COCH_3$
NaH
24
23, R = $COCH_3$ (70%)
24, R = H (75%)

FIG. 3

only natural enantiomers shown

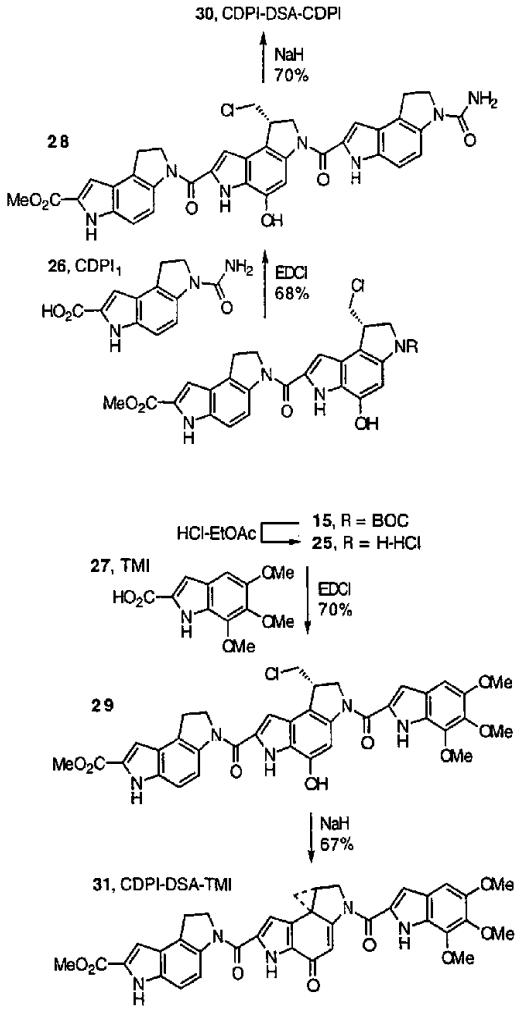

Figure 4

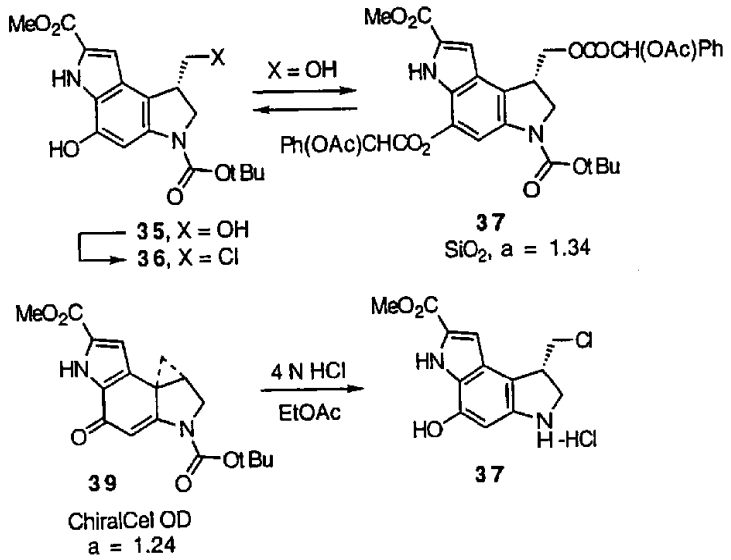
MeO2C
HN
HO
X
X = OH
Ph(OAc)CHCO2
OCOCH(OAc)Ph
OtBu
35, X = OH
36, X = Cl
37
SiO2, a = 1.34
4 N HCl
EtOAc
Cl
H -HCl
39
ChiralCel OD
a = 1.24

FIG. 5

only natural enantiomers shown

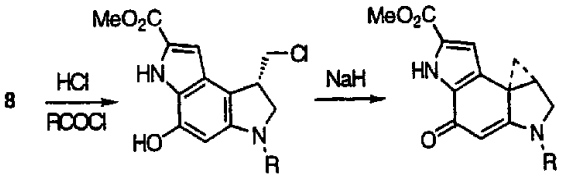

97% **11**, R = $COCH_3$
46% **12**, R = CO_2CH_3

73% **9**, R = $COCH_3$
92% **10**, R = CO_2CH_3
13, R = H

FIG. 6

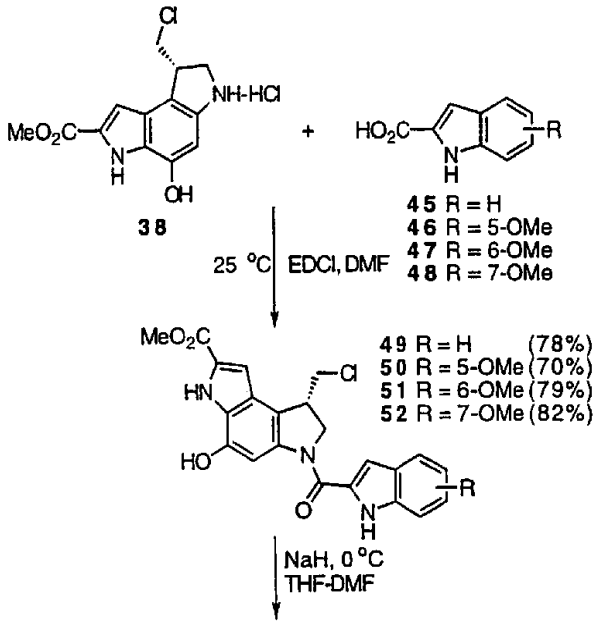

only natural enantiomers shown

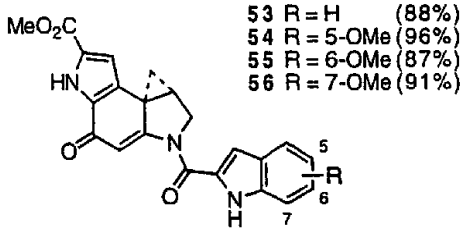

FIG. 7

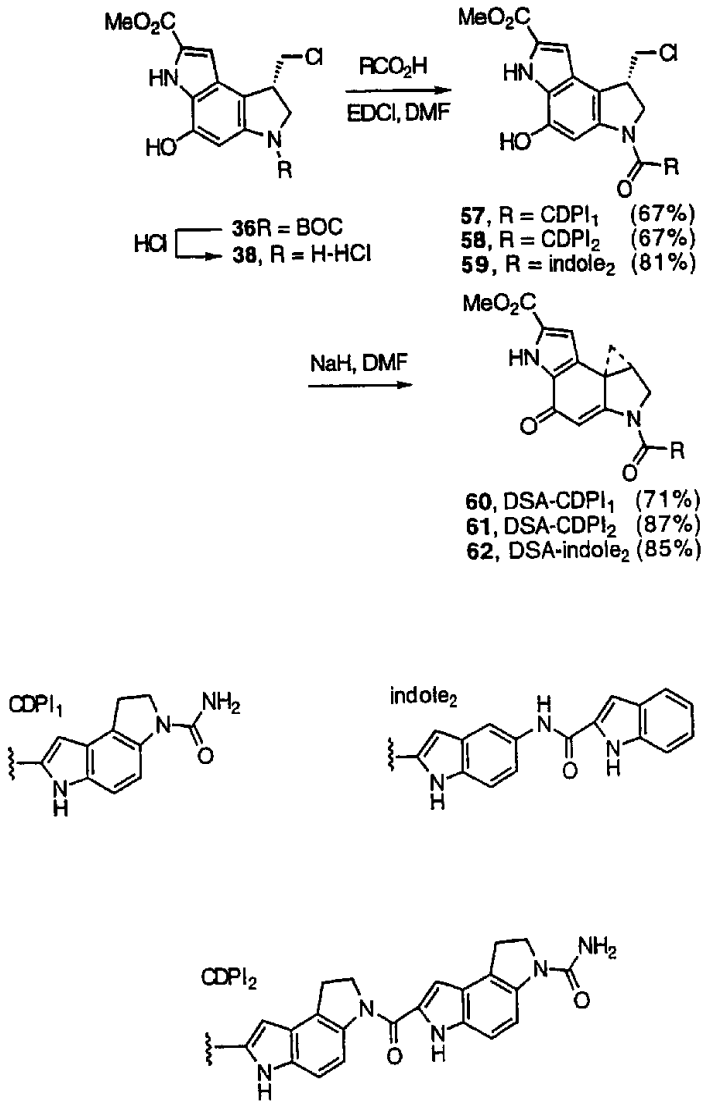
MeO2C
HN
HO
N
R
Cl
RCO2H
EDCI, DMF
HCl
36R = BOC
38, R = H-HCl
57, R = CDPI1 (67%)
58, R = CDPI2 (67%)
59, R = indole2 (81%)
NaH, DMF
60, DSA-CDPI1 (71%)
61, DSA-CDPI2 (87%)
62, DSA-indole2 (85%)
CDPI1
NH2
indole2
CDPI2

FIG. 8

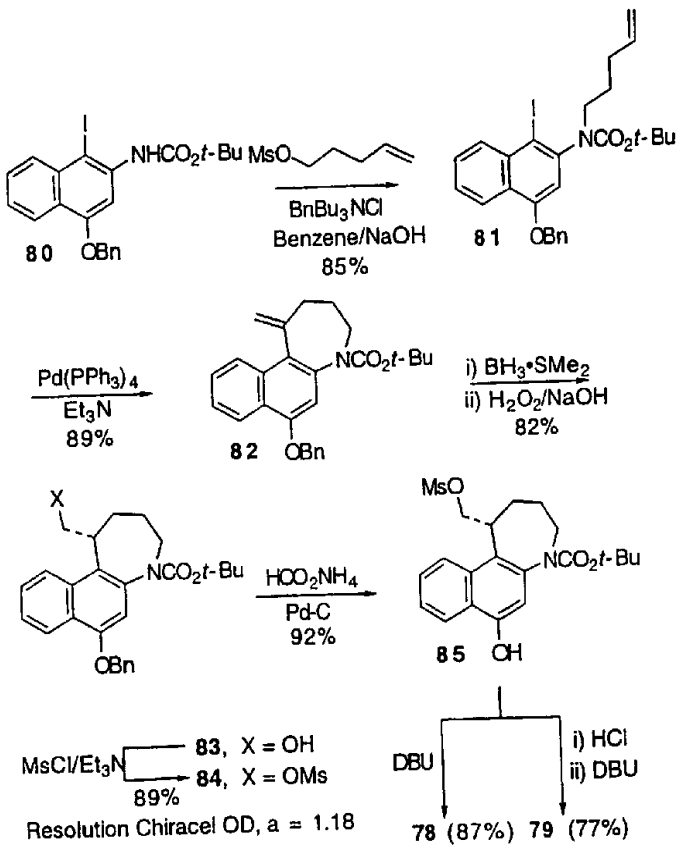
NHCO2t-Bu
MsO
BnBu3NCl
Benzene/NaOH
85%
80
OBn
81
NCO2t-Bu
Pd(PPh3)4
Et3N
89%
82
i) BH3•SMe2
ii) H2O2/NaOH
82%
X
HCO2NH4
Pd-C
92%
85
OH
MsCl/Et3N
83, X = OH
84, X = OMs
89%
Resolution Chiracel OD, a = 1.18
DBU
i) HCl
ii) DBU
78 (87%) 79 (77%)

FIG. 9

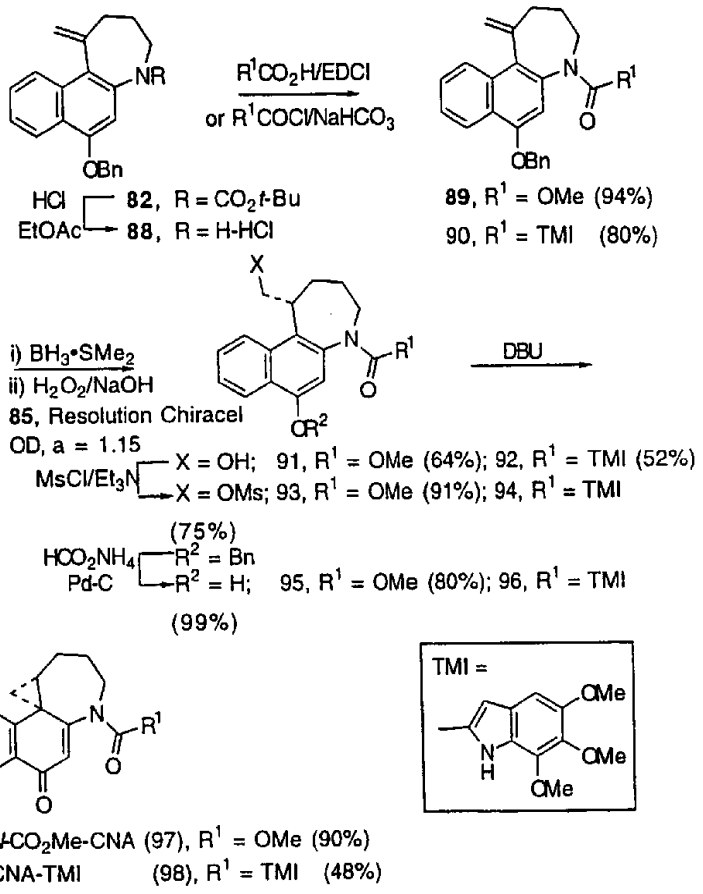
NR
OBn
R1CO2H/EDCI
or R1COCl/NaHCO3
N
R1
O
OBn
HCl
EtOAc
82, R = CO2t-Bu
88, R = H-HCl
89, R1 = OMe (94%)
90, R1 = TMI (80%)
X
i) BH3•SMe2
ii) H2O2/NaOH
85, Resolution Chiracel
OD, a = 1.15
OR2
DBU
MsCl/Et3N
X = OH; 91, R1 = OMe (64%); 92, R1 = TMI (52%)
X = OMs; 93, R1 = OMe (91%); 94, R1 = TMI
(75%)
HCO2NH4
Pd-C
R2 = Bn
R2 = H; 95, R1 = OMe (80%); 96, R1 = TMI
(99%)
TMI =
OMe
OMe
OMe
N
H
N-CO2Me-CNA (97), R1 = OMe (90%)
CNA-TMI (98), R1 = TMI (48%)

FIG. 10

Consensus DNA Alkylation Sequences

Agent	base[a]	5′	4	3	2	1	0	−1	−2	−3	−4	3′
Typical Agents: Natural Enantiomers												
(+)-CC-1065 (3)	A/T (56)[b]		67	78	94	98	100	55	--	--	--	
	Consensus		A/T>G/C	A/T>G/C	A/T	A/T	A	Pu≥Py				
(+)-DSA-$CDPI_2$	A/T (56)		71	85	100	100	100	63	--	--	--	
	Consensus		A/T > G/C	A/T>G/C	A/T	A/T	A	Pu>Py				
(+)-DSA-$CDPI_1$	A/T (56)			65	100	100	100	58			--	
	Consensus			A/T≥G/C	A/T	A/T	A	Pu≥Py				
(+)-duocarmycin SA (1)	A/T (56)		--	79	100	100	100	69	--	--		
	Consensus			A/T>G/C	A/T	A/T	A	Pu>Py				
(+)-*N*-BOC-DSA (4)	A/T (56)		--	--	--	95	100	65	--	--	--	
	Consensus					A/T	A	Pu>Py				
Typical Agents: Unnatural Enantiomers												
(−)-*N*-BOC-DSA (4)	A/T (56)		--	--	--	95	100	65	--	--	--	
	Consensus					A/T	A	Pu>Py				
(−)-duocarmycin SA (1)	A/T (56)		--	--	--	93	100	96	73	56	--	
	Consensus					A/T	A	A/T	A/T>G/C	N		
(−)-DSA-$CDPI_2$	A/T (56)		--	--	--	100	100	100	90	73	58	
	Consensus					A/T	A	A/T	A/T>G/C	A/T>G/C	N	
(−)-CC-1065 (3)	A/T (56)		--	--	--	88	100	93	82	73	56	
	Consensus					A/T	A	A/T	A/T>G/C	A/T>G/C	N	

FIG. 11a

Reversed Analogs: Natural Enantiomers										
(+)-CDPI$_2$-DSA (20)	A/T (56) Consensus	--	--	--	95 A/T	100 A	98 A/T	85 A/T>G/C	70 A/T>G/C	55 N
(+)-CDPI$_1$-DSA (19)	A/T (56) Consensus	--	--	--	92 A/T	100 A	94 A/T	73 A/T>G/C	60 N	--
Reversed Analogs: Unnatural Enantiomers										
(-)-CDPI$_1$-DSA (19)	A/T (56) Consensus	--	70 A/T>G/C	98 A/T	98 A/T	100 A	53 Pu>Py	--	--	--
(-)-CDPI$_2$-DSA (20)	A/T (56) Consensus	69 A/T>G/C	81 A/T>G/C	98 A/T	98 A/T	100 A	59 Pu>Py	--	--	--
Sandwiched Analogs: Natural Enantiomers										
(+)-CDPI-DSA-CDPI (30)	A/T (56) Consensus	--	68	87 A/T>G/C	95 A/T	100 A	95 A/T	74 A/T>G/C	68	--
Sandwiched Analogs: Unnatural Enantiomers										
(-)-CDPI-DSA-CDPI (30)	A/T (56) Consensus	--	64	86 A/T>G/C	94 A/T	100 A	94 A/T	78 A/T>G/C	68	--

a Percentage of the indicated base located at the designated position relative to the adenine-N3 alkylation site.

b Percentage composition within the DNA examined.

FIG. 11b

Detailed summary of the Consensus Alkylation Sequence of (+)- and *ent*-(–)-CDPI-DSA-CDPI.

base[a]	+2	+1	A	–1	–2	3′
(+)-CDPI-DSA-CDPI (natural enantiomer)						
A (30)[b]	66	84	100	74	53	
T (26)[b]	21	11	0	21	21	
G (21)[b]	11	3	0	5	21	
C (23)[b]	3	3	0	0	5	
A/T (56)[b]	87	95	100	95	74	
composite	A/T > G/C	A/T	A	A/T	A/T > G/C	
ent-(–)-CDPI-DSA-CDPI (unnatural enantiomer)						
A (30)[b]	64	83	100	78	56	
T (26)[b]	23	11	0	17	23	
G (21)[b]	11	3	0	6	19	
C (23)[b]	3	3	0	0	3	
A/T (56)[b]	86	94	100	94	78	
composite	A/T > G/C	A/T	A	A/T	A/T > G/C	

[a] Percentage of the indicated base at the designated position at the adenine N3 alkylation sites.

[b] Percentage composition in the DNA examined.

FIG. 12

Sequence Preferences

(+)- and *ent*-(–) *N*-BOC-DSA	(+)-DSA-CDPI$_2$ and *ent*-(–)-CDPI$_2$-DSA	*ent*-(–)-DSA-CDPI$_2$ and (+)-CDPI$_2$-DSA	(+)-CDPI-DSA-CDPI and *ent*-(–)-CDPI-DSA-CDPI
5′-AA (75%)[a]	5′-AAA (62%, 74%)	5′-AAA (72%, 67%)	5′-AAA (59%, 59%)
5′-TA (40%)	5′-TTA (53%, 21%)	5′-AAT (40%, 28%)	5′-AAT (43%, 38%)
	5′-TAA (22%, 39%)	5′-TAA (39%, 33%)	5′-TAA (28%, 28%)
	5′-ATA (22%, 06%)	5′-TAT (13%, 13%)	5′-TAT (00%, 00%)

[a]% Frequency of alkylation, *e.g.* 75% of all available 5′-AA sites were alkylated by (+)- and *ent*-(–)-*N*-BOC-DSA.

FIG. 13

***In vitro* cytotoxic activity of indole$_2$ derivatives.**

Agent	Configuration	IC$_{50}$(pM, L1210)
(+)-DSA-indole$_2$	natural	3
(+)-CCBI-indole$_2$	natural	7
(+)-CBI-indole$_2$	natural	10
(+)-MCBI-indole$_2$	natural	10
(+)-CPI-indole$_2$	natural	40
(±)-CBQ-indole$_2$	racemic	4000
(–)-DSA-indole$_2$	unnatural	150
(–)-CCBI-indole$_2$	unnatural	400
(–)-CBI-indole$_2$	unnatural	3900
(–)-MCBI-indole$_2$	unnatural	30

FIG. 14

Agent	IC_{50}(pM, L1210)	Rel. DNA Alkyl. Efficiency[a]	Agent	IC_{50}(pM, L1210)	Rel. DNA Alkyl. Efficiency[a]
natural enantiomers			unnatural enantiomers		
(+)-**1**	10	1.0	(−)-**1**	100	0.1 (1.0)[a]
(+)-**54**	10–12	1.0	(−)-**54**	200	0.07 (0.7)
(+)-**55**	25	0.2	(−)-**55**	1300	0.04 (0.4)
(+)-**56**	60	0.1	(−)-**56**	1800	0.05 (0.5)
(+)-**57**	65	0.05	(−)-**57**	1700	0.03 (0.3)

[a]Within w794 DNA, 25 °C. The values in parenthesis are relative to *ent*-(−)-duocarmycin SA.

FIG. 15

Consensus Sequences for DNA Alkylation by Key Substructures and Analogs of Duocarmycin SA.[a]

Agent	base[b]	5′	4	3	2	1	0	-1	-2	-3	-4	3′
Natural Enantiomers												
(+)-CC-1065	A/T (56) Consensus		67 A/T≥G/C	78 A/T>G/C	94 A/T	98 A/T	100 A	55 Pu≥Py	--	--	--	
(+)-DSA-CDPI$_2$	A/T (56) Consensus		71 A/T > G/C	85 A/T>G/C	100 A/T	100 A/T	100 A	63 Pu≥Py	--	--	--	
(+)-duocarmycin SA	A/T (56) Consensus		--	79 A/T>G/C	100 A/T	100 A/T	100 A	69 Pu>Py	--	--	--	
(+)-*N*-BOC-DSA	A/T (56) Consensus		--	--	--	95 A/T	100 A	65 Pu>Py	--	--	--	
Unnatural Enantiomers												
(-)-*N*-BOC-DSA	A/T (56) Consensus		--	--	--	95 A/T	100 A	65 Pu>Py	--	--	--	
(-)-duocarmycin SA	A/T (56) Consensus		--	--	--	93 A/T	100 A	96 A/T	73 A/T>G/C	56 N	--	
(–)-DSA-CDPI$_2$	A/T (56) Consensus		--	--	--	100 A/T	100 A	100 A/T	90 A/T>G/C	73 A/T>G/C	58 N	
(–)-CC-1065	A/T (56) Consensus		--	--	--	88 A/T	100 A	93 A/T	82 A/T>G/C	73 A/T>G/C	56 N	

[a] Percentage of the indicated base located at the designated position relative to the adenine-N3 alkylation site. [b] Percentage composition within the DNA examined

FIG. 16

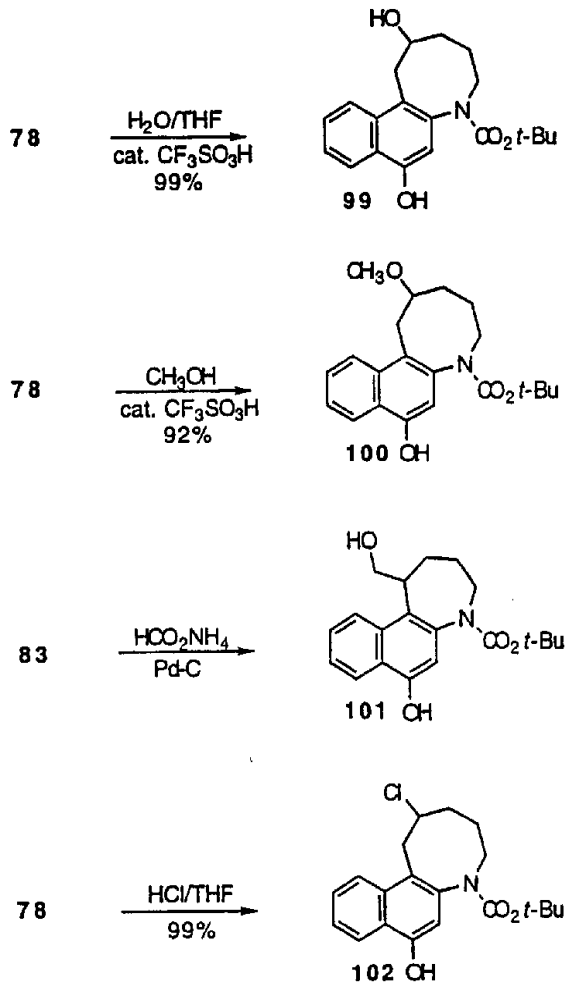
78
H2O/THF
cat. CF3SO3H
99%
HO
N
CO2 t-Bu
99 OH
78
CH3OH
cat. CF3SO3H
92%
CH3O
N
CO2 t-Bu
100 OH
83
HCO2NH4
Pd-C
HO
N
CO2 t-Bu
101 OH
78
HCl/THF
99%
Cl
N
CO2 t-Bu
102 OH

FIG. 17

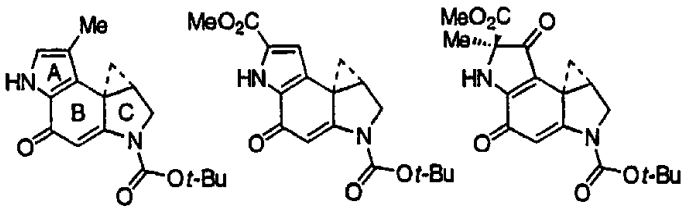

(+)-*N*-BOC-CPI (72) (+)-*N*-BOC-DSA (73) (+)-*N*-BOC-DA (74)

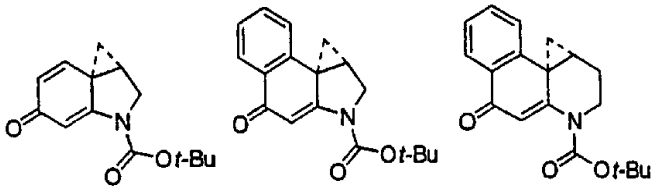

(+)-*N*-BOC-CI (75) (+)-*N*-BOC-CBI (76) (-)-*N*-BOC-CBQ (77)

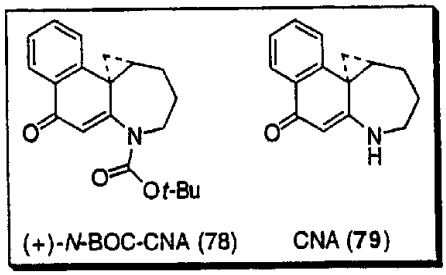

(+)-*N*-BOC-CNA (78) CNA (79)

FIG. 18

***In vitro* cytotoxic activitiy of BOC derivatives.**

Agent	Configuration	IC_{50} (μM, L1210)
(+)-*N*-BOC-DSA	natural	0.006
(+)-*N*-BOC-CCBI	natural	0.02
(+)-*N*-BOC-CBI	natural	0.08
(+)-*N*-BOC-MCBI	natural	0.09
(+)-*N*-BOC-CPI	natural	0.3
(+)-*N*-BOC-DA	natural	2
epi-(+)-*N*-BOC-DA	natural	9
(−)-*N*-BOC-CBQ	natural	2
(±)-*N*-BOC-F_2CBI	racemic	110
(+)-*N*-BOC-CI	natural	18
(−)-*N*-BOC-DSA	unnatural	0.06
(−)-*N*-BOC-CCBI	unnatural	0.08
(−)-*N*-BOC-CBI	unnatural	0.9
(−)-*N*-BOC-MCBI	unnatural	0.2
(−)-*N*-BOC-DA	unnatural	100
epi-(−)-*N*-BOC-DA	unnatural	>100
(+)-*N*-BOC-CBQ	unnatural	11
(−)-*N*-BOC-CI	unnatural	18

FIG. 19

***In vitro* cytotoxic activity of TMI (trimethyloxyindole) derivatives.**

Agent	Configuration	IC_{50} (pM, L1210)
(+)-duocarmycin SA	natural	10
(+)-CCBI-TMI	natural	7
(+)-CBI-TMI	natural	30
(+)-MCBI-TMI	natural	200
(+)-duocarmycin A	natural	1600
epi-(+)-duocarmycin A	natural	4000
(–)-CBQ-TMI	natural	36000
(±)-F_2CBI-TMI	racemic	26000
(+)-CI-TMI	natural	
(–)-duocarmycin SA	unnatural	100
(–)-CCBI-TMI	unnatural	450
(–)-CBI-TMI	unnatural	2000
(–)-MCBI-TMI	unnatural	400
(–)-duocarmycin A	unnatural	23000
epi-(–)-duocarmycin A	unnatural	14000
(+)-CBQ-TMI	unnatural	35000
(–)-CI-TMI	unnatural	26000

FIG. 20